INSTITUTO
UNIVERSITÁRIO
DE LISBOA

Healthcare Status and Behavior Monitoring based on Smart Tailored Environments

Mariana Catela Jacob Rodrigues

PhD in Information Science and Technology

Supervisor:
Prof. Dr. Octavian Adrian Postolache, Full Professor,
Iscte - Instituto Universitário de Lisboa

Co-Supervisor:
Prof. Dr. Francisco Cercas, Full Professor,
Iscte - Instituto Universitário de Lisboa

November, 2023

TECNOLOGIAS
E ARQUITETURA

Department of Information Science and Technology

Healthcare Status and Behavior Monitoring based on Smart Tailored Environments

Mariana Catela Jacob Rodrigues

PhD in Information Science and Technology

Jury:
Prof. Dr. Luís Ducla Soares, Associate Professor with Aggregation,
Iscte - Instituto Universitário de Lisboa (President)

Prof. Dr. Joaquim Mendes, Full Professor,
Faculdade de Engenharia da Universidade do Porto

Prof. Dr. José Miguel Dias Pereira, Main Coordinator Professor,
Instituto Politécnico de Setúbal

Prof. Dr. Pedro Sebastião, Assistant Professor,
Iscte - Instituto Universitário de Lisboa

Prof. Dr. Octavian Adrian Postolache, Full Professor,
Iscte - Instituto Universitário de Lisboa

November, 2023

Acknowledgments

My deepest heartfelt appreciation goes to Professor Octavian Postolache. It is not possible to express in words the sincere gratitude I have for this invaluable friendship. Throughout this journey, Professor Octavian has been a constant and caring presence who has always supported me and believed in my potential. His valuable advice and guidance, along with his willingness and patience to listen to me, have helped me getting through the most difficult and challenging times over the past years and have inspired me and contributed to my growth as a professional, and especially, as a person. To Professor Octavian, I would like to express my profound thanks for all the knowledge I have acquired from you.

To Professor Francisco Cercas, I would like to express my deepest gratitude for his guidance and support. It was also his precious advice and friendship that helped me continue this life's journey with strength and motivation. His teachings were very precious to me, as they gave me a new perspective on how to approach certain professional and personal challenges. For this, I am eternally grateful.

It was a great honor to work under both your supervision. All your transmitted knowledge makes me aspire and motivates me to continue my career in research and academia.

I'm also very grateful for my friends and colleagues who have supported me and accompanied me throughout this journey. Your valuable companionship is what also helped me get motivated. The long days spent working at the university and the exchange of ideas made these years an incredibly enriching and positive experience for me.

I wish to express my appreciation to all the university staff members whom I've encountered throughout the years, for their kindest assistance.

My deepest gratitude goes to my loving parents, for their unconditional support. My entire journey and everything I have achieved so far has been thanks to their teachings, education and moral values that have been passed on to me since my first day. Their patience and valuable recommendations are what kept me motivated and confident even during the most difficult times. I extend my gratitude to my grandmother, who no matter what circumstances life brings us, will always be there for me. To the rest of my family, thank you for all your support and affection.

The work was supported by Fundação para a Ciência e Tecnologia, UIDB/50008/2020, UI/BD/151127/2021 and B-0045-21 UIDB/50008/2020 projects, ISCTE- Instituto Universitário de Lisboa and Instituto de Telecomunicações, Lisbon, Portugal.

Resumo

Com o aumento da taxa de envelhecimento na Europa, têm sido adotadas estratégias que procuram prestar auxílio a esta faixa etária, tal como a melhoraria da sua qualidade de vida e otimização dos custos associados à saúde. Tais estratégias são baseadas na implementação de sistemas inteligentes, nomeadamente ambientes de vida assistida (AVA). Estes são um tipo de ambientes inteligentes adaptáveis que permitem prestar cuidados de saúde pessoais a qualquer indivíduo, monitorizando os seus hábitos diários, o seu estado de saúde e bem-estar, enquanto vive de forma independente no seu ambiente familiar, como a sua casa. Este sistema de monitorização destina-se a apoiar a população idosa, que, com o aumento da esperança média de vida, poderá desenvolver doenças mentais e físicas. Além disso, durante a pandemia de COVID-19, a maioria dos países adotou medidas de confinamento rigorosas, incluindo a necessidade de autoisolamento no ambiente doméstico. Idosos e indivíduos com determinadas condições médicas subjacentes foram particularmente afetados pela COVID-19, pelo que a implementação de tecnologias eficazes de monitorização da saúde e de ferramentas de assistência foi de extrema relevância. Nesta tese, é proposta uma solução AVA inovadora, baseada no desenvolvimento de nós de sensores inteligentes e algoritmos que permitem a análise não intrusiva de sinais vitais, do reconhecimento das atividades da vida diária e da monitorização da qualidade ambiental. Os dados fisiológicos foram adquiridos por sensores biomédicos inteligentes caracterizados por dispositivos *wearable* e não intrusivos. As condições de saúde física e cognitiva foram avaliadas através da monitorização das atividades básicas da vida diária através da implementação de tecnologias de localização *indoor*. O sistema proposto integra também soluções de monitorização da qualidade ambiental interior, que desempenha um papel importante na saúde e no bem-estar. Além disso, a investigação desta tese centrou-se na avaliação do impacto dos jogos sérios de realidade virtual no sistema nervoso autónomo, com o objetivo de identificar a viabilidade de integração destes sistemas virtuais num sistema AVA para estimular o estado físico e cognitivo. Por fim, foram integrados classificadores automáticos baseados em inteligência artificial nesta solução AVA, desempenhando um papel importante na classificação das atividades da vida diária e do comportamento humano, na deteção de níveis de stress e na estimativa do conforto térmico humano. O objetivo final deste sistema foi permitir a criação de uma solução AVA que integra uma variedade de sistemas de monitorização essenciais para o bem-estar e qualidade de vida. Os elementos-chave desta solução incluem a adaptação do ambiente inteligente às necessidades específicas dos indivíduos, garantindo cuidados de saúde personalizados nos seus ambientes de vida preferidos.

Palavras-Chave: Ambientes de Vida Assistida; Ambientes Adaptáveis; Monitorização de Saúde; Monitorização da Qualidade Ambiental; Sensores Biomédicos Inteligentes; Inteligência Artificial; Monitorização das Atividades Diárias; Localização *Indoor*.

Abstract

With the increase in the ageing rate in Europe, strategies have been adopted to help this demographic, aiming to enhance their quality of life while helping the optimization of healthcare associated costs. These strategies are based on the implementation of sophisticated systems, namely Ambient Assisted Living (AAL) systems. Ambient Assisted Living is expressed by a type of smart tailored environments that help to assure personal healthcare to any individual by monitoring their daily habits, health status, and well-being in a non-intrusive way, while living independently in a preferred environment, such as home. Such monitoring system is meant to support the elderly population, that with the increasing of life expectancy may develop mental and physical illnesses. Moreover, during COVID-19 pandemic, strict containment measures were adopted by most countries, including the need of self-isolation in the home environment. Older adults and individuals with certain underlying medical conditions were particularly affected by COVID-19, and therefore, the implementation of effective health monitoring technologies and assistive tools were of extreme relevance.

An innovative AAL solution is proposed in this thesis, based on the development of smart sensor nodes and algorithms that enable a non-intrusive analysis of vital signs, recognition of daily life activities, and environmental quality monitoring. Physiological data was acquired by smart biomedical sensors expressed by wearable and non-obtrusive devices. Physical and cognitive health conditions were evaluated by monitoring the basic activities of daily living (ADL) through the implementation of indoor localization technologies. The proposed system also integrated indoor environmental quality (IEQ) monitoring solutions, particularly indoor air quality (IAQ), which play major roles in human health and well-being.

Furthermore, this thesis research work focused on evaluating the impact of virtual reality serious games on the autonomic nervous system, aiming to identify the feasibility of integrating these virtual systems into an AAL system to stimulate both physical and cognitive state.

Finally, artificial intelligence classifiers were integrated in this AAL solution, playing a major role on classifying daily life activities and human behavior, detecting stress levels, and estimating human thermal comfort based on the information provided by the developed sensor nodes.

The final purpose of this system was to allow the creation of an AAL solution that integrates a variety of monitoring systems that are essential to human well-being and quality of life. Key elements of this solution include the adaptation of the smart environment to the specific needs of individuals, guaranteeing personalized healthcare within their preferred living environments.

Keywords: Ambient Assisted Living; Smart Tailored Environment; Healthcare Monitoring; Environmental Quality Monitoring; Smart Biomedical Sensors; Artificial Intelligence; Activities of Daily Living Monitoring; Indoor Localization.

Acronyms

ADC – Analog to Digital Converter

AAL – Ambient Assisted Living

ADL – Activities of Daily Living

ANN – Artificial Neural Network

ANS – Autonomic Nervous System

Apen – Approximate Entropy

AR – Augmented Reality

ASMR – Autonomous Sensory Meridian Response

BLE – Bluetooth Low Energy

BCG – Ballistocardiogram

BS – Body Sensor Network

COPD – Chronic Obstructive Pulmonary Disease

CFD – Computational Fluid Dynamics

CNN – Convolutional Neural Networks

CRF – Conditional Random Fields

DFA – Detrended Fluctuation

DT – Decision Trees

DWT – Discrete Wavelet Transform

ECG – Electrocardiogram

EDA – Electrodermal Activity

EEG – Electroencephalograms

Emfi – Electromechanical Film Sensor

EMG – Electromyogram

EOG – Electrooculograms

FFT – Fast Fourier Transform

FKL – Fisher Kernel Learning

GAN – Generative Adversarial Network

GRU – Gate Recurrent Units

HF – High Frequency

HR – Heart Rate

HRV – Heart Rate Variability

IAQ – Indoor Air Quality

IEQ – Indoor Environmental Quality

ILQ – Indoor Lighting Quality

IMU – Inertial Measurement Unit

IoT – Internet of Things

KNN – K- Nearest Neighbours

LED – Light Emitting Diode

LF – Low Frequency

LSTM- Long Short-Term Memory

LPF – Low-Pass Filter

LR – Logistic Regression

ML – Machine Learning

MQTT – Message Queuing Telemetry Transport

MLP – Multilayer Perceptron

NN50 – Number of Successive Intervals Differing More Than 50 Ms

PM – Particulate Matter

PPG – Photoplethysmogram

PRV – Pulse Rate Variability

PVDF – Polyvinylidene Fluoride

RF – Random Forest

RFID – Radio Frequency Identification Devices

RF – Radio Frequency

RMSSD – Root Mean Square of Successive NN Interval Differences

RNN – Recurrent Neural Network

RSSI – Received Signal Strength Indicator

SCG – Seismocardiogram

SVM – Support Vector Machines

Sampen – Sample Entropy

SNR – Signal-To-Noise Ratio

SVM – Support Vector Machines

Sampen – Sample Entropy

SNR – Signal-To-Noise Ratio

SpO2 – Oxygen Saturation

STFT – Short-Time Fourier Transform

TCN – Temporal Convolutional Networks

Tof – Time of Flight

UHF – Ultra High Frequency

UWB – Ultra-Wideband

VLF – Very Low Frequency

VOC – Volatile Organic Compounds

VR – Virtual Reality

WSN – Wireless Sensor Network

WSAN – Wireless Sensor and Actuator Networks

Contents

List of Figures

List of Tables

CHAPTER 1

Introduction

The development of smart environments, especially those tailored to the specific needs of individuals, has gained growing importance in recent years. This is motivated by the fact that there is a growing availability of technologies that allow the collection of sensitive data about the health status of an individual without requiring the intervention of health professionals. Furthermore, with the increase of life expectancy, permanent care and assistance for elderly people is an ever more necessary requirement.

To meet these needs, the development of healthcare systems based on the Internet of Things (IoT) has been an important contributor to improving human quality of life, health, and life expectancy. These systems can rely on the acquisition of environmental data, as well as the acquisition of physiological and behavioral information from an individual, through the distribution of smart sensors, both in the environment and on the human body. These smart sensors can be expressed by wearable biomedical devices or sensing units embedded in daily used objects (e.g., chair, wheelchair), that can provide real-time information about the health status of an individual. Other environmental sensing systems can also capture indoor environmental parameters, such as air quality, noise levels, and lighting quality.

The IoT architecture for healthcare purposes has been one of the industry's expanding sectors; therefore, it has been widely explored by academia [1], with a special focus on creating personalized and effective health-monitoring systems for monitoring patients. In this context, smart homes or environments are technologies that provide fundamental services that help improve the quality of life of its inhabitants. Normally, these services are common automated mechanisms that provide the ability to monitor and control several home appliances, doors, windows, and even air conditioning systems. In this matter, many factors and services differentiate the types of smart home environments according to their final purpose. For instance, assistive services are specially tailored to the individual's preference and basic needs and are part of what is designated as an assisted living environment. These services are based on acquiring high-level information from individuals by monitoring their physiological health and cognitive behavior.

The ambient assisted living (AAL) concept precisely supports the inclusion of these assistive services in a certain environment. These environments include private homes, workplaces, assisted living facilities as well as healthcare facilities. AAL has the responsibility of deploying more sophisticated technologies for monitoring a person's health status, as well as assistive tools and devices, being specially designed to support elderly and chronically ill patients in their daily routine [2].

Therefore, the main objective of AAL is to improve the quality of life of their inhabitants and help extend the time they can still live independently in their preferred environments. This can be achieved by deploying an ecosystem of wearable and non-wearable biomedical devices, as well as wireless sensor and actuator networks (WSANs). With the integration of web or mobile applications that allow the visualization of data collected by sensors and processed by computation platforms, these systems provide a complete overview of the patient's health under specific environmental conditions. In this way, information regarding the patient's health is presented in an accessible format for better understanding and decision making by healthcare entities, such as medical doctors, caregivers, physiotherapists, and family members, while the patients live in their preferred environments. This is quite advantageous since hospital bills can be greatly reduced and better treatment is guaranteed if medical diagnostics are taken directly from the patient's home [3]. Most patients and elderly people prefer to stay at their private home, rather than going to long-term care facilities or residential homes. Although these care services help stimulate social activities among the care community, it is also possible to achieve these results by enabling social interactions and physical activities associated with active aging in their own home, by monitoring their daily life activities and notify family members or caregivers whenever there might be social isolation or lack of mobility.

1.1. Research Challenges

As technology advances, there are always innovative solutions for assisted living systems and healthcare assessment. The implementation of healthcare monitoring systems based on the IoT concept has been a widely explored theme in recent years, as it helps prevent and diagnose possible health impairments in people, especially in the elderly population. Medical diagnostics taken directly from the patient's home can greatly reduce hospital bills and allow better treatment. In this way, the proposal of new architectures for AAL systems is essential to improve quality of life and reach healthy, elderly, or disabled individuals.

A great variety of AAL systems have been proposed in the literature for the last decade [4], with most projects providing efficient solutions to improve the patient's quality of life and active life by monitoring of activities of daily living and their physiological status. Most projects are effective in monitoring human physiological status with the use of body sensor networks and others to monitor the activities of daily living using indoor localization techniques and machine learning algorithms. However, few or non-existent, consider the creation of smart assistive environments that consider the integration of various important assistive services into a single, fully implemented AAL system. These various assistive services include the assessment of physiological parameters, indoor environmental conditions, daily life activities and behavior, as well as physical and cognitive stimulation based on VR/AR implementations. Moreover, most healthcare assessment and indoor air quality (IAQ)

monitoring solutions available in the market do not offer open access to the collected data and do not support mobile compatibility.

This thesis aims to address this gap by outlining the contributions detailed in the following subsection 1.2.

1.2. Contributions

This thesis's main contributions are related to the research problems that were stated above. Hence, the development of a new solution for AAL environments that is meant to integrate the most important healthcare services that were not included in previous works found in the literature, is addressed.

The proposed system is based on the implementation of four different assistive services:

- Physiological parameters assessment: this is performed by the study of Photoplethysmogram (PPG) and Ballistocardiogram (BCG) signals collected from both developed wearable and non-wearable biomedical sensors.
- Activity recognition and behavior monitoring: information of the user's cognitive health status was determined by monitoring their behavior and the activities of daily living (ADL). This was achieved based on indoor localization mechanisms, as well as the implementation of machine learning and data analysis algorithms.
- Indoor environmental quality assessment: the integration of wireless sensor nodes to monitor indoor environments, namely the assessment and analysis of indoor air quality in real-time, was considered.
- Physical and cognitive stimulation: the inclusion of VR serious games for physical rehabilitation and an analysis on how these systems can help improve physical, cognitive, and psychological conditions of the users (e.g., elderly and people with chronical diseases) was addressed. This contribution stands as a valuable proposition for their integration into AAL environments.
- For system validation, this thesis includes the study of the influence of external or environmental *stimuli* on human physiological status and the autonomous nervous system, using the developed physiological and environmental sensor nodes.

1.3. Scientific Outputs

Throughout the preparation of this thesis, several scientific studies were produced as a result of the new AAL solution developed in this project. A total of 10 publications were made - first authorship of 3 scientific journals (Q1), first authorship of 2 book chapters (Q2), first authorship of 3 international

conference papers and co-authorship of 1 conference paper. The scientific publications are listed below:

Scientific Journals

- **M. Jacob Rodrigues**, O. Postolache, F. Cercas, (2020). "Physiological and Behavior Monitoring Systems for Smart Healthcare Environments: A Review". Sensors 20 8 (2020): 2186-2186.
  Published • https://doi.org/10.3390/s20082186
- **M. Jacob Rodrigues**, O. Postolache, F. Cercas, (2022) "Unobtrusive Cardio-Respiratory Assessment for Different Indoor Environmental Conditions," in IEEE Sensors Journal, vol. 22, no. 23, pp. 23243-23257, 1 Dec.1, 2022
  Published • https://doi.org/10.1109/JSEN.2022.3207522
- **M. Jacob Rodrigues**, O. Postolache and F. Cercas, (2023) "The Influence of Stress Noise and Music Stimulation on the Autonomous Nervous System," in IEEE Transactions on Instrumentation and Measurement, vol. 72, pp. 1-19, 2023, Art no. 4006819
  Published • https://doi.org/10.1109/TIM.2023.3279881

Book Chapters

- **M. Jacob Rodrigues**, O. Postolache, F. Cercas, (2021). Autonomic Nervous System Assessment Based on HRV Analysis During Virtual Reality Serious Games. In N. T. Nguyen, L. Iliadis, I. Maglogiannis, & B. Trawiński (Eds.), Computational Collective Intelligence (pp. 756–768). Springer International Publishing.
  Published • https://doi.org/10.1007/978-3-030-88081-1_57

- **M. Jacob Rodrigues**, O. Postolache, F. Cercas, (2023). Wearable Tag for Indoor Localization in the Context of Ambient Assisted Living. In: Nguyen, N.T., et al. Computational Collective Intelligence. ICCCI 2023. Lecture Notes in Computer Science(), vol 14162. Springer International Publishing.
  Published • https://doi.org/10.1007/978-3-031-41456-5_32

International Conferences with peer review

- J. Araujo, **M. J. Rodrigues**, O. Postolache, F. Cercas, F. F. Martín and A. L. Martínez, "Heart Rate Variability Analysis in Healthy Subjects Under Different Colored Lighting Conditions," 2020 IEEE International Instrumentation and Measurement Technology Conference (I2MTC), Dubrovnik, Croatia, 2020, pp. 1-5
  Published • https://doi.org/10.1109/I2MTC43012.2020.9129619

- **M. J. Rodrigues**, O. Postolache and F. Cercas, "Autonomic Nervous System Assessment During Physical Rehabilitation Serious Game," 2021 IEEE International Symposium on Medical Measurements and Applications (MeMeA), Lausanne, Switzerland, 2021, pp. 1-5
  Published • https://doi.org/10.1109/MeMeA52024.2021.9478742
- **M. J. Rodrigues**, O. Postolache and F. Cercas, "The Influence of Music Stimulation on Heart Rate Variability: Preliminary Results," 2022 IEEE International Symposium on Medical Measurements and Applications (MeMeA), Messina, Italy, 2022, pp. 1-6
  Published • https://doi.org/10.1109/MeMeA54994.2022.9856561
- **M. J. Rodrigues**, O. Postolache and F. Cercas, " Wearable Smart Sensing and UWB System for Fall Detection in AAL Environments ", 2023 IEEE Sensor Applications Symposium, Ottawa, Canada, 2023.
  Published • https://doi.org/10.1109/SAS58821.2023.10254065

Other publications

1. M. L. Lima et al. 2020. Saúde Societal: Uma abordagem inclusiva do conhecimento em saúde. https://www.iscte-iul.pt/conteudos/iscte-saude/2080/saude-societal.

1.4. Structure of the Thesis

This thesis is organized in 6 Chapters:

- Chapter 2 presents the state of the art of the current AAL solutions presented in the literature, characterized by vital signs monitoring systems. It identifies the most relevant physiological parameters that need to be considered in order to provide viable health diagnostics. Indoor localization technologies for user location and daily activities' recognition are also addressed, as well as the most suitable machine learning and signal processing algorithms for activity recognition and pattern classification. Additionally, various monitoring solutions for indoor environmental quality assessment and cognitive and physical stimulation based on immersive environments are included in this chapter respectively.
- Chapter 3 makes a description of the proposed smart tailored environment system for an AAL implementation, which follows a healthcare-focused IoT architecture. Its hardware and software components are described.
- Chapter 4 addresses three different studies that made use of the developed physiological and environmental sensor nodes to perceive how environmental factors and other external *stimuli*, such as music and stress noise, as well as the practice of virtual reality serious games, may affect our physiological status and nervous system. A validation of the developed sensor nodes

is presented using biomedical reference systems, and the use of machine learning models is explored to estimate human thermal comfort and stress levels based on the acquired physiological data.

- Chapter 5 focuses on the indoor localization and behavior monitoring component of the proposed system. Machine learning algorithms were used to perform activity recognition, namely the most performed daily activities. Moreover, the chapter shows the system' capability on detecting fall events, highlighting its potential for guaranteeing user safety and well-being.
- Chapter 6 summarizes the results reported in this thesis and delineates the future directions of this research.

CHAPTER 2

State of the Art

The adaptation of the surrounding environment to the physiological needs of its inhabitants has been one of the key objectives of smart tailored environments. These environments are built around a sensor network that provides real-time data about the health-status of an individual, as well as key environmental quality indicators. The ability to process this data and help improve quality of life is what makes these solutions so indispensable, especially when considering their integration in ambient assisted living (AAL) environments [5]. This chapter encompasses a concise literature review on all the necessary components for the implementation of a smart tailored environment, specially an AAL environment.

2.1. Health Status Assessment Systems

2.1.1 Cardiovascular Monitoring

The monitoring of physiological parameters and daily activities of patients is the main objective of healthcare services related to the implementation of assisted living systems. Wearable medical sensors are essential components, as they collect health-related information that can be used to elaborate real-time diagnostics of human health conditions [6]. As noted earlier, an AAL system may be based on medical sensors that, when connected to home gateways, send medical data to health monitoring systems in real-time. Wireless sensor networks (WSNs), an integral part of IoT architectures, are used to connect sensors to smart gateways and healthcare applications, thus allowing caregivers or physicians to monitor patients remotely, commonly represented by the architecture depicted in Figure 2.1.

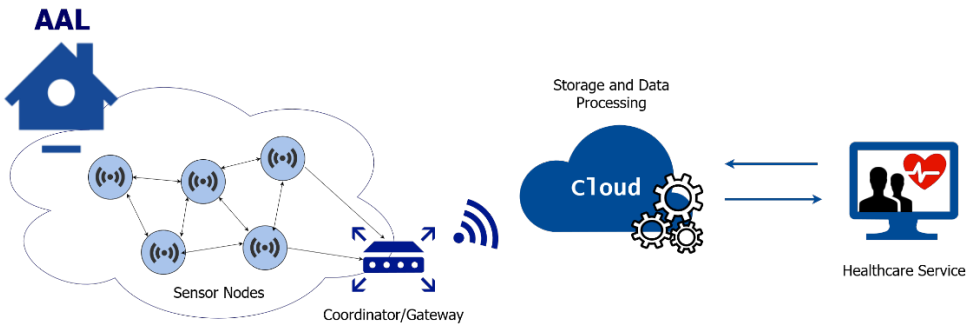

FIGURE 2.1. Overview of a wireless sensor network architecture for healthcare systems

To assess an individual's health and their response to external factors, it is essential to monitor various physiological parameters that are relevant. Over the years, the following five vital signs have been examined: temperature, heart rate, blood pressure, respiratory rate, and blood oxygen saturation [7]. These can be obtained through non-invasive and non-intrusive sensors, which can be included in long-term health monitoring systems [8]. Such sensors are mostly referred to as wearable sensors. They can monitor and record real time information concerning an individual's physiological condition and motor activities, without causing discomfort nor interrupting the practice of their daily activities. These biomedical sensors measure physiological signs that can be used to obtain electrocardiograms (ECGs), electromyograms (EMGs), photoplethysmograms (PPGs), seismocardiograms (SCGs), ballistocardiograms (BCGs), blood pressure and body temperature and determine the heart rate (HR), oxygen saturation (SpO2), respiration rate (RespR) and many other parameters. These sensors are generally connected in a wireless body area network (WBAN) or body sensor network (BSN) and can be placed directly on top of the skin, over clothes or even implanted in the person's tissue.

A. Electrocardiography

There are several methods to record and monitor cardiac activity using non-invasive techniques. The most widely used technique and diagnostic tool for healthcare environments and considered the "gold standard" technique for monitoring cardiovascular activity is the ECG, which measures the electrical activity of the heart. An ECG is visualized by the formation of a waveform characterized by five peaks and valleys named P, Q, R, S and T, respectively, as demonstrated in Figure 2.2. Each one reflects the physiological conditions of the patient's heart and its main blood vessels. The QRS complex indicates ventricular depolarization and has a short duration if the heart is working efficiently. The R wave, or peak, is the first positive wave of the complex and it is used to determine the patient's HR and heart rate variability (HRV), regarding the time between its occurrences (called RR intervals) [9], [10].

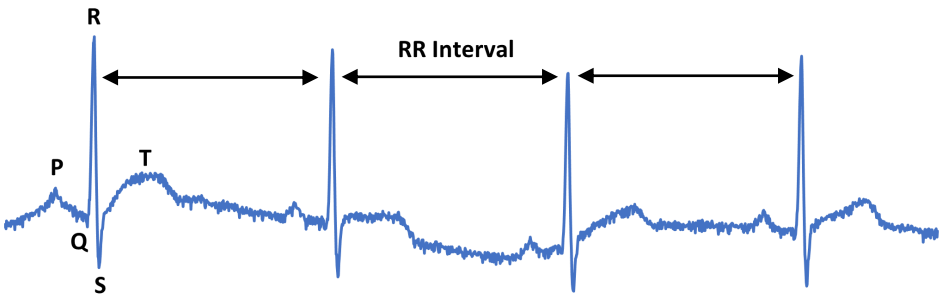

FIGURE 2.2. ECG signal with representation of the QRS complex and R-R intervals

The electrocardiography method uses Ag-AgCl electrodes (wet electrodes) that must be affixed in specific areas of the body. However, the electrode has a conducting gel that surrounds it, which serves as a conduction medium between the skin and the electrode. This gel can cause irritant effects on the skin when used continuously for longer periods. Another potential drawback associated with long-term use is the surface degradation of electrodes, which leads to the deterioration of signal quality [11]. For this reason, ECG monitoring based on wet electrodes is less reliable when considering long term monitoring of cardiac activity and it cannot be used without affecting the individual's daily activities.

Several alternatives for replacing these traditional electrodes have been suggested in the literature. Dry textile electrodes can be embedded in custom clothes, such as undershirts and bras, for ECG recording. This method proved to be usable for continuous ECG monitoring as stated in [12] and [13]. The characteristics of hydrophilic and flexible material such as the hitoe® textile electrode (Toray Industries Inc., Tokyo, Japan)[14], allows an easy adaptation to the human's skin surface, while it is highly conductive and allows a non-invasive and continuous ECG recording. Other authors [15] designed textile electrodes that combine a motion sensor with a textile-based electrode. The synchronism between the two signals is beneficial for the diagnosis of heart diseases, since variations in heart rate may occur during or following certain behaviors, such as changes in posture or gait patterns. Also, the association of daily physical activity derived from motion data with an ECG is very useful for cardiologists as it can help them determine the cause of a certain heart disease, e.g., abnormal ECG caused by over-exercising. Based on the numerous advantages of e-textile electrodes, many other researchers reported the use of such technology and materials for wearable ECG monitoring systems [16]–[19]. Smart textile systems based on fiber optic sensors have also shown to be a viable method to monitor respiratory and cardiac activity, as the system proposed in [20], which implements a smart textile based on a fiber Bragg grating (FBG) to detect small chest motions induced by the heartbeat.

B. Photoplethysmography

The photoplethysmography (PPG) technique has proven to be a great alternative over the ECG [21], [22], especially for HRV, HR and SpO2 measurements. It is considered a non-invasive and unobtrusive method. It uses a light source and a photodetector placed in contact with the skin's surface to measure volumetric variations of blood circulation in veins and arteries [23].

Optical absorption or reflection of the light is associated with the amount of blood flow that is present in the optical path. Changes in blood volume are synchronous with the heartbeat. A PPG sensor is usually placed at peripheral body sites, to measure the volumetric variations in the microvascular beds [24]. Parts of the human peripheral vascular system that can be used to place the sensor's coverage area include the finger, earlobe, and forehead.

The PPG optical sensors are either based on transmission or reflection mode measurements (Figure 2.3 a). In the transmission measurement mode, the infra-red LED is placed on the human tissue on the opposite side of the photodetector, to detect the residual light from the LED after being absorbed by the tissue. In the reflective PPG, the light source and photodetector are placed side by side, thus measuring the intensity of light that is reflected from the skin (Figure 2.3 b). The choice of each technique will depend on the body area where the sensors are to be placed.

The PPG waveform is characterized by a systolic peak, dicrotic notch and a diastolic peak. The systolic peak amplitude indicates the change in blood volume after an increase of arterial blood flow that is preceded by the heartbeat. The distance in time between two consecutive systolic peaks represents the completion of a heart cycle, and thus, similarly to the R-R interval of the ECG signal, it is used to measure the HR and HRV.

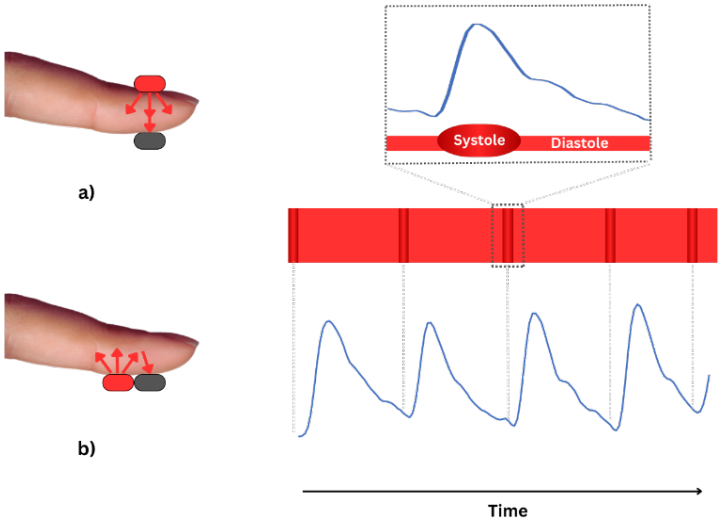

FIGURE 2.3. Working principle of the PPG sensor: a) transmission, b) reflection modes. Representation of the PPG signal and the systole and diastole cardiac cycle events.

Many researchers have relied on the PPG method to monitor cardiac activity. Most systems are designed wearable solutions that do not offer any constraints when in use, thus helping maintain the normal execution of the daily tasks of their users, as demonstrated in [25]. Thinking on multi-sensory devices, the authors in [26] designed a wrist worn device that included a channel for cardiac activity monitoring based on PPG and a body kinematics measurement channel for daily motor activities assessment, therefore enabling multiparametric monitoring in non-invasive and non-obtrusive ways.

Mary et al. [27] reported the development of a physiological parameter measurement system based on wearable devices to monitor human body temperature, heart rate and oxygen saturation using PPG signal.

PPG also poses as a great solution for real-time and continuous detection of atrial fibrillation (AF), one of the most common types of arrhythmias. The detection of this cardiac rhythm disturbance can be based on the implementation of statistical analysis, machine learning and deep learning approaches. Pereira et al. [28] reviewed different studies based on these algorithms for AF detection through the evaluation of PPG signals. The authors highlight the main challenges that PPG-based AF detection comprises in clinical applications and how the different classification approaches address those limitations.

C. Ballistocardiography

Additional unobtrusive techniques include ballistocardiography (BCG), which is used to measure repetitive motions of the human body, associated with cardiac cycles. The BCG signal is demonstrated in Figure 2.4. It is one of the oldest non-invasive methods for cardiac–respiratory monitoring and can be used to get information about the activity of the heart, its condition and breathing patterns. Its graphical representation consists of the action–reaction force caused by the heartbeat and the pump of blood through the aorta [29]. The IJK wave complex from the BCG represents the ejection phase of the cardiac cycle. These main waves and time intervals between them reflect the physiological condition of the subject's heart and its main blood vessels. BCG systems can either require mechanical connection between the subject's body and the sensor or can be performed by contactless devices, which are, for example, ultrasonic sensors [30] and the microwave Doppler radar [31]. The main devices requiring mechanical contact are piezoelectric sensors, load cells, sternal accelerometers, and electromechanical film sensors (EMFi). The robustness of BCG monitoring systems based on EMFi sensors has been evidenced in its large number of implementations [29], [32]–[34]. However, the adoption of this solution in medical facilities is still limited in present days.

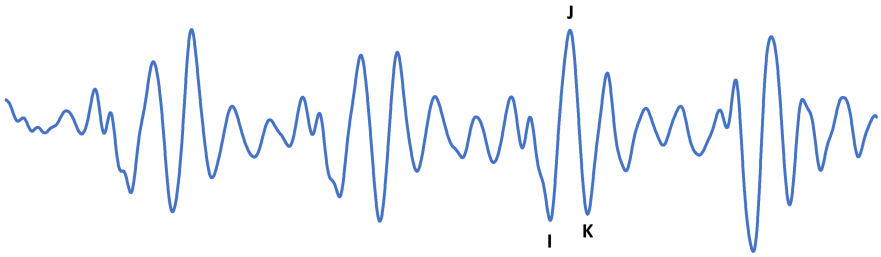

FIGURE 2.4. BCG signal with representation of the IJK complex

Innovative solutions that have been emerging in the literature have a new way to provide advanced and continuous physiological signal acquisition rely on the development of soft electronic circuits and highly stretchable systems. Electronic systems that can be attached to the epidermis allow a more comfortable and accurate measurement of human physiological conditions, when compared to the traditional systems. The physical properties of such devices offer levels of stretchability and

thickness that are compliant to those of the skin, allowing a more precise and noninvasive mechanical connection with its surface, and therefore reduce motion artifacts and other limitations usually offered by common wearable systems.

Different studies have reported the development of multifunctional sensing platforms based on epidermal electronic system of ultrathin and soft stretchable electronic layouts [35]–[37]. These systems can acquire ECG, EMG, electrooculograms (EOGs) and electroencephalograms (EEGs), while allowing long-term human health monitoring without constraining body movements and affecting the person's daily activity. These systems may incorporate microfluidic constructions to allow elastic stretchability and flexibility and at the same time, mechanically isolate rigid electronic materials [36]. Another innovative solution based on a stretchable and lightweight wearable device was presented by Ha et al. [38]. An electronic tattoo (e-tattoo) was developed for both ECG and SCG measurement. The authors relied on a piezoelectric polymer, polyvinylidene fluoride (PVDF), to construct a stretchable vibration sensor capable of acquiring SCG signals. The synchronous collection of data from both ECG and SCG techniques increased the system's efficiency on determining cardiac health conditions.

The novel characteristics of these new wearable technologies are very promising for the future implementation of healthcare monitoring systems related to ambient assisted living. A selection of the available techniques for vital signs monitoring reported in the literature is presented in Table 2.1.

TABLE 2.1. Vital signs monitoring techniques

Method	Working Principle/Application	Monitored Signals	Reviewed Works
Electrocardiography (ECG)	Measurement of electrical activity of the heart.	HR, RR	[12], [15]–[19], [35], [36], [38]
Photoplethysmography (PPG)	Optical measurement of blood volume changes in microvascular bed	HR, SPO_2, RR, Blood pressure	[25]–[27]
Seismocardiography (SCG)	Measurement of micro-vibrations of the chest wall produced by the heart contraction and blood flow	HR, RR	[20], [38]
Ballistocardiography (BCG)	Measurement of hole-body micro-vibrations associated with the cardiac cycle	HR, RR, Blood pressure	[29]–[34]
Contact thermometry	Temperature measurement based on conductive heat changes between the surface of skin and a temperature sensor	Skin temperature	[39]–[43]

D. Autonomous Nervous System Assessment

In addition to monitoring cardiovascular status, these methods can also be used to measure the autonomic nervous system (ANS) response and the person's emotional state. This is done through HRV analysis, which is based on the study of the variation of the time interval between consecutive heart beats (RR intervals or peak to peak intervals). This analysis can quantify the sympathetic and parasympathetic nervous system to understand the overall status of the ANS (Figure 2.5). Its clinical importance includes the possibility of predicting mortality after the occurrence of an acute myocardial infarction, diabetic neuropathy, and other neurologic disorders [9], [10]. Both branches of the ANS are involved in the regulation of HR, with the sympathetic activity having a tendency of increasing the HR and decreasing HRV, whereas the parasympathetic activity decreasing the HR and increasing HRV [44].

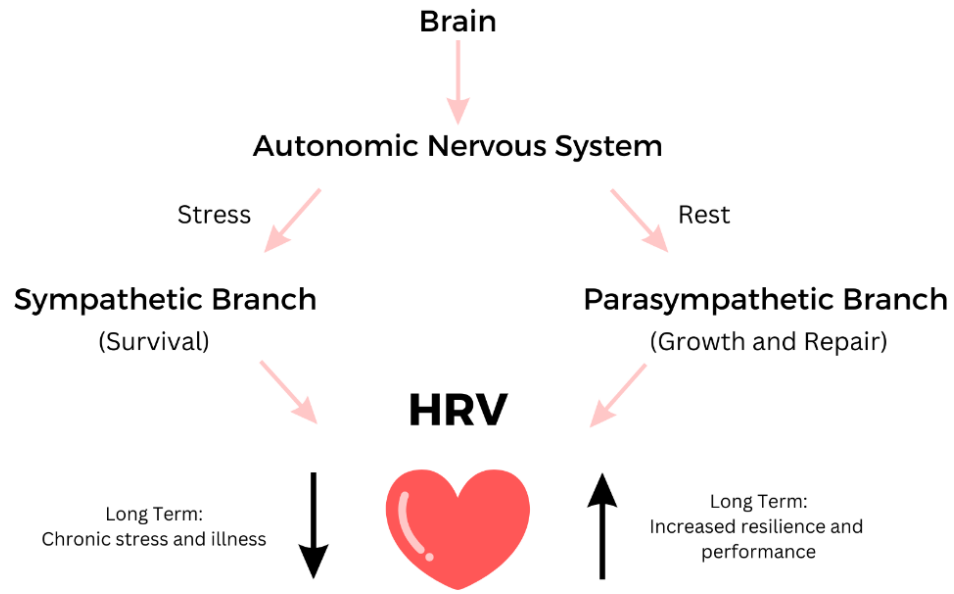

FIGURE 2.5. The autonomic system and its influence in heart rate variability

HRV can be evaluated by three different methods [9], [10]: time-domain, frequency-domain, and non-linear methods. The simplest to implement is the time domain measurement, in which the time interval between successive heart beats is determined. The most common time-domain variables for statistical measurements include the mean RR interval, mean HR, the difference between the shortest and longest NN interval (where NN corresponds to time intervals between normal pulse peaks), standard deviation of the NN intervals (SDNN), root mean square of successive NN interval differences (RMSSD), standard deviation of successive NN interval differences (SDSD) and the number of successive intervals differing more than 50 ms (NN50). Frequency domain methods are better to discriminate between sympathetic and parasympathetic activities of the HRV. The power spectrum density (PSD) is estimated, in most cases, using a Fast Fourier transform (FFT) and provides basic information about the distribution of power (i.e., variance) over frequency. For short term recording periods, whose standard is 5 minutes, three spectral components are measured [9]: the very low

frequency (VLF, 0.04 Hz), low frequency (LF, 0.04–0.15 Hz) and high frequency (HF, 0.15–0.4 Hz). The HF reflects the activity of the parasympathetic nervous system, while in the other hand, it is commonly accepted that LF reflects sympathetic activity [45]. Several studies support this, but many others suggest that this component may result from both sympathetic activity and parasympathetic activity. Additionally, it is proved that the RMSSD parameter is correlated with the HF power, and thus, can give an insight of parasympathetic activity when shorter-term recordings of HRV are considered (< 5min) [45]. On the other hand, SDNN values reflect sympathetic and parasympathetic activity. However, this measure does not discriminate between changes in HRV that are caused by an increase in sympathetic tone or vagal withdrawal [46].

HRV analysis in the frequency domain is commonly performed using FFT, as previously mentioned. Time-frequency transforms are important in the analysis of cardiac activity, especially regarding HRV, because they allow the decomposition of complex signals into their frequency components, which is useful for quantifying parasympathetic and sympathetic activity. Furthermore, short-time Fourier transform (STFT) is a signal processing technique that has been used to give additional insights about HRV [47], [48]. This time-frequency transform allows a more detailed analysis of the HRV signal, as it decomposes the signal into a series of frequency components over time. This allows to assess how the balance between sympathetic and parasympathetic control of the autonomic nervous system changes over time, allowing to identify possible changes in ANS balance that may be related to external stressors.

Finally, non-linear methods are also used to analyze HRV. The most common measures are the Poincaré plot, approximate entropy (ApEn), sample entropy (SampEn), detrended fluctuation (DFA), correlation dimension and recurrence plots [10]. SampEn is a method that quantifies the complexity and unpredictability of a time series signal, while ApEn is an improved variation of SampEn more robust to small perturbations present in the time series signal. The analysis of such measures can give more information about the degree of irregularity in the HRV and quantify pattern repetition in the time-series signal. The sensitiveness to these changes in HRV makes the use of such measures a possible way of detecting different physiological and pathological conditions, such as heart disease, and stress [49].

The time-domain, frequency-domain, and nonlinear methods for HRV analysis are summarized in Table 2.2.

TABLE 2.2. Heart rate variability parameters

Parameters	Units	Definitions
Time-domain analysis		
Mean HR	bpm	Mean of heart rate values
Mean RR	ms	Mean of RR interval time series
SDNN	ms	Standard deviation of successive NN intervals
RMSSD	ms	Root mean square of successive NN interval differences
SDSD	ms	Standard deviation of differences between adjacent NN intervals
NN50	ms	Number of successive intervals differing more than 50 ms
Frequency-domain analysis		
VLF, LF, HF	ms^2	Power in Very-Low, Low, and High frequency range, respectively
LF/HF	-	Ratio between LF [ms^2] and HF [ms^2]
Non-linear methods		
ApEn	-	Quantifies the regularity and complexity of the time series. It measures the unpredictability of the variation of successive RR intervals.
SampEn	-	Improved evaluation of time series regularities (Modification of ApEn).
DFA	-	Quantifies the presence or absence of fractal correlation properties of time series data. It permits the estimation of long-range correlation in non-stationary time series [50].

2.1.2. Exploring the effects of external Stimuli on the Autonomous Nervous System and Stress Levels

A. Music Stimulation

The positive effects that music sound stimulation presents on a subject's health, HRV and cognitive performance have been addressed in the literature for the last decades. Investigations in this area started more than twenty years ago, one example being the experiments conducted by Honda et al. [51], in which they intended to study the effects of music and noise on heart rate variability.

Exploring the effects of music on arousal and relaxation will depend on the characteristics of the music pieces themselves. Relaxing music genres typically feature a slow tempo of approximately 60 bpm, minor dynamic changes, simple rhythms and sounds of nature, as suggested by therapists [52]. In contrast, exuberant, happy, and exciting emotions are generally associated with music pieces that feature fast *tempo*, loud dynamic levels, and higher pitches. Besides these characteristics, the instrumentation part can also bring different emotive responses to music.

Preference for heavy metal and rock-and-roll music was found to have a substantial positive correlation with anxiety states in most participants [53]. This may be explained by the instrumental timbres of electric guitars and distortion sounds, heavy bass and dense drum sounds present in the heavy metal music genre.

As initially observed by Honda [51], noise and rock music were more likely to induce stress than classic music and tended to cause discomfort among participants, as seen by the apparent stimulation of the sympathetic nerve. Regarding this musical genre, classical music has shown to bring benefits on the cardiovascular system. Bernardi et al. [54] examined the effects of music with vocals, orchestra, and progressive crescendos on heart rate, respiratory rate, blood pressure, middle cerebral artery flow and skin vasomotion. Specific musical auditory stimulation, according to the authors, may synchronize autonomic responses, hence regulating cardiovascular physiology. Independently of individual choices, cardiorespiratory variables increased with faster tempo.

More recently, Kirk et al. [55] also investigated whether music can be an alternate way to improve cognitive performance as well as providing positive physiological effects. Piano, Jazz and lo-fi beats music were considered for these experiments. HRV assessment was made using an ECG, and elevated parasympathetic activity, denoted by higher RMSSD, was present in all the three music groups, when compared with a no-music testing group. Moreover, music that was familiar to the subjects induced an immediate improvement of cognitive performance and increase of HRV levels.

Similarly, Trappe et al. [56] monitored cardiovascular activity during classical and pop music stimulation. The measured variables comprised diastolic blood pressure, heart rate and serum cortisol concentrations. It was observed that classical music significantly lowered systolic and diastolic blood pressure and heart rate levels, unlike pop music genre. Characteristics of a compositional form such as tempo, harmonic sequences and dynamics have a major influence on nervous system activity and, in turn, on the cardiovascular system. The authors also did not find an association between musical genres and the subject's listening preferences on blood pressure changes and heart rate.

Introducing a faster-paced musical genre, Amaral et al. [57] investigated the effects of baroque and heavy metal music with different intensities, i.e. different sound levels, in HRV of female volunteers. When compared to a control group (resting period before auditory stimulation), heavy metal music stimulation at higher intensity lowered the SDNN index. The investigation showed that at lower intensities, auditory stimulation with baroque and heavy-metal music reduced global HR modulation. However only heavy metal at higher sound levels lowered the HRV. When making the same experiments with men volunteers, musical auditory stimulation of various intensities presented no effects on cardiac autonomic regulation [58].

The beneficial effects of music sound stimulation on human physiology have also been studied among participants with particular medical conditions [59]–[61]. Mir et al. [62] conducted an experiment with 15 pre-hypertensive young adults that received music therapy based on relaxing piano and flute soundtracks for 4 weeks, along with a dietary plan for treating hypertension. A control group of pre-hypertensive only following the dietary plan was considered. Authors observed that music therapy significantly lowered systolic blood pressure and HR, indicating that there might be a potential intervention for preventing the development of pre-hypertension towards hypertension in young adults.

Additionally, stress levels, which may lead to the occurrence of several physiological events, not only are monitored through the analysis of HRV parameters [63], can also be measured through the perception of changes in skin conductance, through galvanic skin response (GSR), as well as through the monitoring of bioelectrical activity of the brain, using EEG. GSR, for instance, is often used to assess the user's emotional states, other than stress, and it is an additional method that has increasingly been considered by researchers for improving music recommendation systems [64]. Alternatively, Paszkiel et al. [65] evaluated the impacts of different sounds - rap, relaxing music and autonomous sensory meridian response (ASMR) triggering music - in stress levels, based on the analysis of EEG signals. That study indicated that rap music negatively affects stress levels reduction when compared to a control group with no sound, denoted by a decrease in brain alpha-wave frequencies and an increase of blood pressure. On the other hand, relaxing music and ASMR induced calmness and relaxation much quicker than silence.

When exploring the applicability of musical stimuli for older age groups, particularly for elderly with dementia, it was reported in literature that this type of stimulus brings positive outcomes. Maseda et al. [66] reported positive effects on mood and behaviour of older adults with severe dementia, as well as a decrease in heart rate and increase of blood oxygen saturation after individualized music interventions. A systematic review performed by Lam et al. [67] also validates the positive impact of music therapy on older people living with dementia, where several studies report significant improvements in language fluency and reduction of anxiety and depression feelings.

Based on the observations made in these studies, our current research aims to analyse the effects of musical stimuli involving ambient, classical, and metal music genres. In addition to music with more relaxing characteristics, the heavy metal music genre was considered since it is a music genre that is connoted as a possible cause of stress and anxiety, in contrast to classical and ambient music. Thus, we intend to verify such hypotheses and whether in fact this music genre may induce levels of anxiety and stress, using HRV analysis.

B. Stress Noise Stimulation

Other auditory stimuli also present in the environment in which we live every day include background noise. These sound stimuli, which may include several types of sounds differing in frequency and intensity, may have several effects on our health, namely on the nervous system. Several studies in the literature have analyzed how these stimuli and these potential stressors affect HRV. For example, Sim et al. [68] analysed the impact that different types of noise below 50 dBA may have on the ANS of men volunteers, unlike other studies that consider sounds above 50 dBA. Significant alterations of several HRV parameters were observed after noise exposure. Higher noise levels ranging from 50 dBA to 80 dBA also showed to affect the ANS balance, especially in the LF/HF parameter from HRV, as reported by Lee et al. [69]. Focusing more on the noise frequencies, Walker et al. [70] reported several changes on the stress responses of men to short-term exposures to low-frequency noise (31.5 Hz – 125 Hz) and high-frequency noise (500 Hz – 2000 Hz). Although no significant changes were found in blood pressure and salivary cortisol, the noise exposure seemed to have a negative impact on HRV, specially the low-frequency noises. Similarly, Nakajima et al. [71] changed the frequency components of a music piece by amplifying the high and low-frequency domains. The authors found that enhancing the high frequency components of the music have a positive impact on stress levels, since stress recovery was more pronounced after listening to the high-frequency version of the music when compared to the low-frequency or even the original music piece.

Most studies are only considering young volunteers, in their 20s, and most of them are males. Although it has been proven that HRV varies with gender and age, it is necessary to include a greater diversity of ages and genders, therefore increasing its validation, so the system to be proposed is suitable for elements of any age and gender. By addressing the limitations presented in previous studies, no restriction was applied to the age and gender of participants in these experimental studies.

2.2. Body Motion and Daily Activities Monitoring

In addition to the monitoring of physiological signs, there is another equally important concept in AAL, which is the monitoring of gait parameters that characterize a person's locomotion, and the monitoring of activities of daily living (ADL).

2.2.1. Body Motion Monitoring and Fall Detection

Monitoring an individual's walking patterns can provide important data about their health conditions. Gait disorders, for example, may be caused by neurological conditions, orthopedic problems, and medical conditions [72]. Moreover, the need for detecting fall events has become increasingly important, since older adults require great care, especially in this matter. Falls are one of the most common problems among the elderly and can lead to serious health problems if not detected in time. They are the leading cause of accidental death globally in people over 60 years old [73]. However, for all age groups, it is the second leading cause of unintentional injury death, preceded by road traffic accidents. Injuries following a fall tend to become more severe with advancing age, with more than half of all falls resulting in at least a mild injury, such as a bruise or muscle strain. There are several factors that may trigger a fall, resulting from a combination of balance and mobility problems, the presence of obstacles that hinder walking, loss of mass and muscle strength, neurological or cardiovascular problems, vision problems, among many others [74]. Frequently, there are no symptoms felt by the person before the fall. However, in some cases a sensation of dizziness or an irregular heartbeat may appear. The urgency in treating these injuries is a factor that exponentially helps the person's survival rate. The speed of response to this problem will depend entirely on whether the individual is alone in the environment where the fall occurred or not. In cases where the individual lives alone at home, or even in a nursing home, remote monitoring is indispensable so that relatives and health entities can respond and act as quickly as possible.

For monitoring such events, several solutions are available in the literature. Vision-based systems and cameras are very useful to monitor gait activities and fall events. However, despite the high accuracy achieved, there are some constraints that limit their use. Some limitations include privacy issues, and the fact that the user must always remain in line of sight and within a specific range from the camera, which somehow prevents continuous monitoring of gait activity. Alternatively, wearable motion sensors based on accelerometers and gyroscopes are a great solution to assess gait dynamics and body posture. Several key features can be extracted from the sensors based on the linear and angular motion measurements obtained from body kinematics [6].

Most fall detection systems follow a common methodology, which starts by data collection, data pre-processing, feature extraction and finally the classification and evaluation of such activities [75], [76]. Wearable sensors are often used for data acquisition, as they enable the collection of a variety of

data, such as kinematics and physiological signals. Kinematic information expresses measurements related to the motion or movement of an object. These features can be collected by a variety of wearable sensors, such as accelerometers, gyroscopes, and magnetometers, and can be used to detect fall events. However, many researchers solely rely on the use of one sensor for fall detection, such as the accelerometer [77]–[80]. The performance of a Machine Learning (ML) model may be lower in this case compared to the cases where multi-sensor data fusion is considered. The introduction of other data such as the rotational speed of the body in the X, Y and Z axes, measured by a gyroscope, will improve the ML's ability to distinguish between different activities. Other researchers have also used barometric pressure sensors in conjunction with an IMU [81], as well as instrumented insoles that measure the pressure and forces applied during movement [82].

In AAL systems, the use of wearable sensors based only on inertial measurement units (IMU) has been a usual approach in the detection of the most common activities of daily living, like standing, walking, sitting, laying down and going upstairs and downstairs. Hiram Ponce et al. [83] analyzed single IMU sensors placed at different locations in the body to determine the minimal number of sensors needed to develop an accurate fall detection system. The best position was found to be at the waist. A minimal sensor-based fall detection system was then implemented using a smartphone, which achieved an overall accuracy of 87.56%. Good performances are achieved by ML algorithms in distinguishing these activities. However relevant information regarding the person's location when performing those activities is not collected. Technologies for indoor localization are integrated in AAL systems to address this limitation.

Other fall detection systems will be further addressed in Section 2.4.

2.2.2. Indoor Localization for Daily Activities Monitoring

Monitoring systems for assisted homes may include the capability of recognizing behaviors and certain patterns of human daily activities, to mediate and detect possible symptoms of a certain disease, whether mental or physical. ADL addresses the daily life activities of people in their own home environments, without requiring any assistance to execute them. The ability to perform such elementary routines while aging determines the person's physical and psychological health status and their ability to live independently. Such monitoring helps to track possible developments of mental illnesses associated with aging, namely Alzheimer's, Parkinson, and other levels of dementia. ADLs mainly comprise activities that are based on hygiene, mobility levels, dressing, eating and continence (Figure 2.6). In short, ADL addresses any task associated with physical self-maintenance that is essential to ensure the health and well-being of an individual.

FIGURE 2.6. Activities of daily living. Source: [84]

There are many factors to consider when monitoring such activities, namely the choice of technology to be used for activity recognition, as well as its ability to be deployed in households, its usability and privacy levels. Several studies regarding the monitoring of the user's behavior and daily routine are expressed by systems based on wearable sensors, video surveillance, appliance monitoring and distributed sensors throughout the house. However, the implementation of such sensing technologies may raise several privacy concerns, due to their ability to assess relevant information about people's lives. In fact, the most accurate mechanisms for activities recognition and monitoring include video-based strategies, such as video-cameras or thermal-cameras. The implementation of such technology is not always accepted by the users, and most rooms cannot be accessed due to heavy privacy violations. As an alternative, the use of low-informative sensors, such as magnetic switches, infrared motion sensors, pressure sensors, ultrasonic sensors, among others, poses as a better strategy that preserves the desired privacy levels. Despite being less informative about human activities, the installation of multiple instances of these sensors throughout the house and the implementation of sensor data fusion can overcome that limitation.

The most used technologies for indoor localization are included in Table 2.3, and are expressed by mechanical, magnetic, acoustic, radio frequency and light-based methods.

TABLE 2.3. Classification of indoor tracking and localization technologies.

Mechanical	Magnetic	Acoustic	Radio Frequency	Light
Pressure sensor	Magnetic field sensor [85]–[88]	Ultrasonic sensor [89]–[92]	Wi-Fi	Infrared sensor
Proximity sensor			Bluetooth	Photelectric sensor
Vibration sensor		Microphone [93], [94]	ZigBee [95]	Camera/Video recording [96]
Accelerometer [1]			RFID	
Gyroscope [1]			UWB	LIDAR

[1] Wearable Sensors

Some mechanical-based systems are considered obtrusive, such as accelerometers and gyroscopes, since they need to be attached to the surface of a target, in this case, the human body. Nonwearable sensors are less intrusive and can be placed in stationary locations of a house or a room. They can provide significant information about performed activities whether by monitoring the operational status of objects, detecting movement in a room, measure room temperature, monitor the opening/closing of doors, and so on. As an example, Fleury et al. [93] developed a system for detecting ADL based on different sensing technologies: Infrared presence sensors were used for location purposes (e.g. detection of movement) and placed at strategic locations; door contacts were fixed on relevant home appliances (e.g. fridge, cupboard and dresser) to monitor its usage; microphones were used to process and identify different sounds of daily living activities (e.g. speech, door shutting, phone ringing, walking sound, among others); and wide-angle web cameras were deployed to timestamp ADLs for supervised machine learning algorithms. The authors also placed temperature and hygrometry sensors in the bathroom to detect activities related to hygiene. Additionally, a wearable kinematic sensor with accelerometers and magnetometers was also implemented to detect and classify transitions in posture and walking periods.

The authors in [97] recorded data relative to ADL in two different households for one week. The user's localization was based on multiple low-informative sensors fitted in the house, such as magnetic contact and motion sensors, microphones, and power meters. These sensing technologies were considered enough to get an insight into the user's activities and were strategically placed over different rooms of the house.

More projects for ADL monitoring include the Washington State University's project named CASAS (Centre of Advanced Studies in Adaptive Systems) [98], that was meant to develop a smart home and detect broad activities such as eating, sleeping or wandering. The smart apartment was populated with various types of sensors to detect movements (mainly by infrared/light sensors), the usage of certain home appliances and items, energy consumption and environmental temperature, and to perceive the

state of doors and lights. An example of the sensor's distribution for such monitoring systems is presented in Figure 2.7. The CASAS project also implemented machine learning techniques for human activity recognition, based on generated events from the sensors.

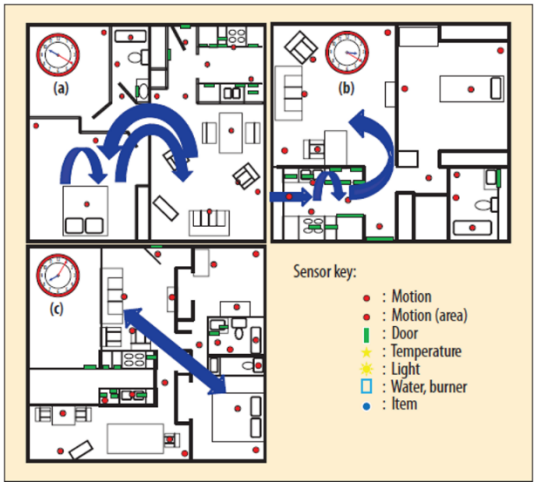

FIGURE 2.7. Distribution of low-informative sensors in a house for ADL recognition. Source: *[98]*

Considering the implementation of sensor networks for detection of behavioral patterns, the use of light dependent technologies, such as infrared and photoelectric sensors, can lead to some issues. These sensors may produce wrong outputs (e.g., false positive or false negative triggers). Failure in these sensors can lead to a misinterpretation of the subject's health status and bring negative consequences to their health. Regarding this limitation, Nancy ElHady et al. [99] made a systematic literature review on sensor fault detection and fault tolerance in AAL environments. A sensor failure in a AAL environment can be considered as a fault if the sensor has stopped responding (fail-stop failure) or if the sensors are still responding but the reported values are not representative of the measured variable, nor the type of event that is supposed to be detected (non-fail-stop failure) [100]. The last type of failure can be caused by external factors that trigger these false events, such as changing the location of the furniture where the sensors are installed to a different area, or slightly changing the position of sensors, or due to the covering of sensors whether by unwillingly placing objects in front of them [100]. The authors concluded that this research area still needs an intensive investigation in order to ensure the implementation of robust sensor fault detection systems in AAL environments in the future.

2.2.3. Radio-Frequency solutions for Indoor Localization

Regarding radio communication protocols, several have been used to provide indoor localization services, such as Bluetooth (IEEE 802.15.1), Radio Frequency Identification Devices (RFID), Ultra-Wideband (UWB) (IEEE 802.15.4a/z), Wi-Fi (IEEE 802.11) and ZigBee (IEEE 802.15.4).

A. Bluetooth

Bluetooth, or IEEE 802.15.1, is a strong candidate for indoor localization systems and it is used in many studies [101]–[106]. Bluetooth is a standard based on a wireless radio system and it is designed for short-range wireless communications. It is mainly oriented to establish wireless connections between closely connected devices and is widely used in IoT systems due to its high energy efficiency. Bluetooth Low Energy (BLE) provides improved speed, greater coverage range and versatility when compared with its older version, Bluetooth Classic. This protocol is best used for localization purposes when beacon communication is used. Devices and sensors that use BLE interface can be placed in different areas and programmed to send broadcast messages, to be received by listener devices (e.g. a mobile device or sensor node used by the patient)[107]. It is then possible to know the approximate location of the user based on the received signal strength indicator (RSSI), which is used to estimate the distance between the transmitter and receiver device. This technology has been widely used in the marketing industry for costumer engagement and proximity marketing at stores, museums and events. Commercially available BLE based protocols include iBeacons (by Apple Inc.) and Eddystone (by Google Inc.), which are specially designed for proximity detection.

Solutions based on Bluetooth beacon technology for indoor positioning estimation were addressed by Xin-Yu Lin et al. [108], which implemented a mobile-based indoor positioning system based on the iBeacon solution. The goal of this research was to help medical staff track the locations of their patients inside a hospital. To evaluate this approach, the beacons, with transmitting signals ranging about 30 meters, were placed at the ceiling of four hallways and two rooms of an experimental test-bed environment. A mobile application was used by the patient to collect the signals from the beacons, based on RSSI values. The authors claim to achieve an accuracy of 97.22% on classifying the location of the patient.

The study presented in [101] also used Bluetooth beacon technology for ADL recognition. The beacons were placed in each room (e.g., bedroom, kitchen, and bathroom) of an inhabited home and served mainly as an indicator of the user's presence in a room. The receiver device consisted of a smartphone using a RSSI-based algorithm for estimating location context, based on the closest proximity of the patient's smartphone to a Bluetooth's beacon.

This technology does not provide an accurate and precise location of the user and it is mostly used for context aware proximity services, which is satisfactory for AAL environments.

B. Radio Frequency Identification Devices (RFID)

The use of RFID is also an alternate and great solution to monitor in-house daily activities that require proximity to certain appliances and furniture, as presented in the literature [109]–[112]. This protocol is based on electronic tags (RFID tags) that exchange data through radio waves to RFID readers. These tags are made up of an antenna and an integrated circuit. The first component allows the transmission and reception of radio frequency (RF) waves, while the second one is used for processing and storing data, as well as for modulating and demodulating radio waves. Considering the detection range and power source, there are three types of RFID systems: Active, Passive and Semi-Passive [85]. Active RFID tags need an internal battery source and can operate at a range of hundreds of meters from the RFID reader. They work in the Ultra High Frequency (UHF) and Microwave frequency range and are mostly used for localization and tracking of objects [113]. Passive RFID tags have no internal energy source (current is induced on the antenna by the RFID reader) and have a limited range between 10 cm to a couple of meters. They can operate in the Low, High, UHF and Microwave frequency range and, despite not being good for indoor localization systems, due to its limited range, they can be used to monitor the usage of certain appliances at home. Semi-passive RFID tags are like active tags because they have their own energy source, which is not used when communicating with the reader, like with semi-passive tags. The battery is only used to power up the microchip, which helps to increase the amount of energy reflected from the RFID reader to the RFID tag, thus allowing a higher read range than normal passive RFID tags.

There are two ways in which RFID systems can be used for indoor location [111]: the RFID tag acting as a target and carried by the patient is sensed by RFID readers distributed in specific areas of the house, or, the RFID reader is attached to the patient and senses different RFID tags that are placed in specific places of the house. A more practical case regarding the use of RFID technology applied to AAL environments is the project HABITAT (Home Assistance Based on the Internet of Things for the Autonomy of Everybody) [114], whose main objective was to monitor and assist elderly in their daily life activities. The developed system was based on an RFID system for indoor localization. Multiple active tags were worn by the patient and two or more RFID readers were strategically placed on the walls. The system showed a good estimation of the user's location, presenting an average error of about 18 cm.

C. Ultra-Wideband (*UWB)*

Ultra-Wideband (UWB) is a radio technology that offers the highest accuracy and precision for indoor localization systems [13], [14], and has been widely used in the literature [115]–[117]. It is based on the transmission of short pulses across the wide spectrum frequency with a period of less than 1 nanosecond (ns) and over a high bandwidth (500MHz) [113]. It can track the location of individuals with up to 10 cm of accuracy and it is a low power solution. A UWB system is composed of UWB anchors

placed at fixed locations in the environment, and an UWB tag, which will be used by the person or object we want to track. Its different signal type and radio spectrum makes UWB immune to interference from other signals, which helps this technology achieve its precision and accuracy in indoor localization systems. The UWB measures its position using Time of Flight (ToF), which is the measurement of the time that a radio wave takes to travel between the tag and the anchor. At least three UWB anchors are needed to calculate the position of the tag using the trilateration method.

Being a technology with strong growth in the market, it has increasingly become a low-cost solution, achieving better ratings than the common Wi-Fi, BLE and RFID technologies, in terms of price and accuracy ratio.

Compared to BLE technology, which has an accuracy of 2-5 meters, UWB can reach a much more accurate positioning of 10-30 cm, which is ideal for classifying specific tasks being performed in a room when considering ADL recognition. This major difference is related with the way these protocols work: UWB measures the position through ToF, and not through signal strength, as BLE does.

Wi-Fi positioning systems do not surpass the accuracy and effectiveness of UWB, and they are not as accurate as they offer an accuracy of around 5-15 meters.

When considering real-time positioning with active RFID, this technology can only reach 3 meters of accuracy and has a failure rate around 5% that can go up to 20%, making UWB a more advantageous solution with better performance.

The only technologies that surpass UWB in terms of accuracy are the light-based, such as LIDAR (1 cm accuracy) and camera (1 mm accuracy). However, these solutions can pose relatively higher costs. Camera-based positioning based on visual light positioning (VLP), and LIDAR are not scalable as the UWB [118]. Table 2.4 summarizes the different indoor localizations in terms of accuracy, scalability, real-time capability, and their suitability to be used in indoor environments.

TABLE 2.4. Comparison of the different indoor localization technologies

	BLE	**Wi-Fi**	**RFID**	**GPS**	**LIDAR**	**UWB**	**Camera**
Accuracy	5 m	5 – 15 m	3 m	30 cm – 5 m	1 cm	10 – 30 cm	1 mm
Scalability	✓	✓	✓	✓	✗	✓	✗
Real-time	✓	✓	✓	✓	✓	✓	✓
Indoor Environment	✓	✓	✓	✗	✓	✓	✓

2.3. Indoor Environmental Quality Monitoring

Monitoring human physiological status is the most important factor to consider when creating an AAL system, as it helps diagnosing human health conditions and prevent possible at-risk situations. However, environmental conditions also play a vital role on the population's health and well-being and can be remotely monitored in real-time to prevent dangerous and adverse situations, namely associated with poor air quality. Indoor Environmental Quality (IEQ) is an indicator of the general quality conditions of indoor environments that may have an impact on human health. The IEQ indicator is composed of multiple sub-domains [119], including air quality, lighting quality, noise levels, thermal comfort, among others. This section aims to address the most important IEQ factors and how their monitoring and control can be achieved.

2.3.1. Indoor Air Quality

Air pollution is one of the greatest risks for human health. It can potentially cause numerous respiratory problems such as asthma, chronic obstructive pulmonary disease (COPD), allergies, and in a more extreme case, lung cancer. While most people are aware that outdoor air pollution has a major impact on their health, few have the idea that indoor pollution can be far more harmful. According to the United States Environmental Protection Agency (EPA) [120], indoor pollution levels can be 2 to 5 times higher than at outdoor environments. IAQ monitoring systems are essential in every smart home and AAL environment since the population usually spends approximately 90% of their time inside buildings.

Particulate matter (PM), ozone (O3), sulphur dioxide (SO2), nitrogen oxides (NOx) and carbon monoxide (CO) are the most common air pollutants present in urban areas and can either be formed by both outdoor and indoor sources of pollution [121]. According to [122], the air contaminants that are most linked to asthma-related hospital emergencies comprise PM10, NO2 and O3. Additionally, outdoor air pollutants greatly affect indoor environments, since the air exchange between these two environments is constantly done through mechanical ventilation and natural ventilation [123]. However, most pollutants created by indoor sources have a greater impact on indoor air conditions. These pollutants usually come from combustion sources, cleaning products, air conditioners without proper maintenance, smoke, cooking oils, building materials and many other indoor sources. The acceptable limits of concentration for some of these IAQ contaminants are presented in Table 2.5.

TABLE 2.5. Maximum recommended concentrations for specific IAQ contaminants [124], [125]

Parameter	Averaging Time	Limit for acceptable IAQ	Unit
Particulate Matter [1]	24 hours	50	µg/m3
Volatile Organic Compound	-	0.5	mg/m3
Carbon Dioxide	-	1000	ppm
Ozone [1]	8 hours	120	µg/m3
Nitrogen Dioxide [1]	1 hour	200	µg/m3
Carbon Monoxide	15 minutes	100	mg/m3
	1 hour	35	
	8 hours	10	

[1] Associated with the triggering of respiratory distress [122].

Apart from air pollutants, other factors, such as indoor temperature and relative humidity, need to be considered regarding asthma distress prevention and well-being. A temperature between 18-24°C and a relative humidity between 40%-60% is considered the ideal for indoor environments [126], as it minimizes most adverse health effects. Values of relative humidity above 60% will turn the air harder to breathe – besides narrowing and tighten the airways, humidity also makes the air stagnant and traps pollutants and allergens, which can help trigger asthma attacks [127].

Different IAQ monitoring systems have been proposed in the literature, along with different distributed sensing solutions. Considering the adoption of primary-prevention strategies to help avoiding the triggering of potential asthma attacks and COPD, the authors in [128] developed a distributed smart sensing network for IAQ assessment. Gas sensing units based on semiconductor heated sensors and electrochemical cells were used to measure gas concentration, and an additional channel was implemented to measure temperature and relative humidity. The system could estimate the air quality index of the indoor environment based on the measured gas concentration. A smartphone application was developed to notify the user of possible asthma and COPD attacks, based on previously stored threshold values. However, strategies to improve indoor air conditions rely on user actions (e.g., manually opening the window to allow air flow and displacement of indoor pollutants), which can be a limitation for patients with low mobility.

Automatic adjustment of IAQ based on the use of actuators (e.g., air conditioner and mechanical ventilation units) is one of the great benefits of home automation systems. Following this strategy, Salamone et al. [129] implemented a smart object that helped improve the overall air quality by automatically controlling the air exchange system. However, the air quality evaluation was solely based on the measurement of concentrations of CO2.

Considering the monitoring of a wider range of air pollutants, the authors in [130] developed an embedded monitoring system to measure air quality parameters such as temperature, humidity, as well as CO and ozone. The authors monitored each node's current consumption in real-time and made a notification alert mechanism for when measured values of IAQ were considered unsafe. Based on a WSN, the study in [131] proposes an air quality assessment system that could simultaneously obtain CO2, CO, Ozone and volatile organic compounds (VOC), as well as temperature and relative humidity, from different locations. The calibration of the gas sensing units was done by comparing the data from the sensors with a professional air quality measurement system. Similarly, Jung Kim et al. [132] developed a gas concentration monitoring system for detecting a wider range of air pollutants - Ozone, CO, NO2, SO2, VOC and CO2, and particulate matter (PM). Several aspects were considered, such as the optimal number of required sensor nodes and their correct placement in the environment according to the type of pollution sources.

2.3.2. Indoor Lighting Quality and the Impact of Noise in Health

Poor air condition does not only affect individuals with respiratory illnesses. Common symptoms that are often linked to poor air quality for most people include headaches, fatigue, shortness of breath, coughing and dizziness [120]. However, these are not necessarily caused by poor air quality. Indoor lighting quality (ILQ) and indoor noise levels also have a great impact on human health, and thus, may be the cause of the manifestation of such symptoms.

ILQ plays an important role in an individual's visual ability and has several positive biological effects. The benefits of adapting both light levels and color temperature throughout the day in indoor environments are numerous. The recommended light levels [133] for each area of the building and for each type of working activity must be considered. Adequate lighting levels during the day and night can regulate circadian sleep-wake rhythms and vastly improve an individual's health, productivity, and comfort. Circadian lighting is a concept that is becoming often present in various sectors, from healthcare to corporate [134]. It follows the circadian rhythm, a 24-hour internal clock that cycles between sleepiness and alertness at regular intervals. Lightness and darkness have a direct impact on this sleep-wake rhythm. The eyes send signals to an area of the brain called hypothalamus, that will report if it is night-time or daytime. The hypothalamus, in turn, controls the amount of melatonin that needs to be released, associating sleepiness with darkness and alertness with lightness [135]. Given

that most of the population does not have access to natural light in their working environments and at home, they are often exposed to non-natural electric light. Electric light is usually kept mostly within certain wavelengths of blue light, which can lead to negative impacts on melatonin production. Smart lighting systems have been recently helping to address these problems [136] and can be provided by some commercial products such as Yeelight LED Smart Bulb [137] and Philips Hue [138]. Capable of changing its light temperature color and intensity, these systems can be used to support human health and regulate sleep-wake rhythms.

Another important factor that has a remarkable impact on human health is the daily exposure to high levels of noise. With population growth, increased vehicular traffic and industrial activities, noise is increasingly present in the daily lives of millions of people. Although the notion of noise may vary from individual to individual, depending on their subjectivity or auditory sensitivity, prolonged exposure to sounds above 80 dBA may cause permanent damage to the auditory system. Guideline values of noise for specific environments, such as the recommended by the World Health Organization [139], must be followed in order to minimize the underlying critical effects on human health. Problems such as sleep disturbances, stress, difficulty in communication between people and loss of concentration are among the most frequent effects caused by this physical agent [140], [141]. Therefore, monitoring noise levels and notifying the individual for when values exceed an acceptable threshold for a certain period is an equally important factor in preventing hearing damage and helps to ensure productivity, well-being, and human health.

2.4. The role of Artificial Intelligence on Smart Tailored Environments

Activity recognition, especially ADL, and fall detection is at the core of every AAL system since it provides information about cognitive health progression or degradation. Such health assessment is critical for the doctors or family to decide whether the patient should move to an assisted living environment with constant supervision or to other care facilities. As previously mentioned, monitoring of the user activity and behavior is obtained through indoor localization technologies that can be expressed by several sensors distributed through the house, or by other wireless systems based on radio frequency communication. Moreover, the monitoring of other human activities and fall occurrences can be achieved by collecting acceleration and rotation data of the human body. Information from sensors, which is often considered high-level, cannot be obtained by a direct observation of their raw data. It must be processed by suitable algorithms usually based on machine learning, signal processing and data analysis [142].

The application of such algorithms depends on the chosen activity recognition approach. Visual based indoor localization, such as camera/video recording, requires computer vision techniques to recognize activities from several visual observations on the user's actions, gait patterns, as well as

environmental changes [143]. With the usage of sensor network technologies, for instance, data must be analyzed through datamining and machine learning algorithms applied to build activity models that later will be used as the basis of ADL recognition.

This section addresses studies reported in the literature that support the system presented in this thesis for the creation of a smart tailored environment, namely ADL classification, human behavior monitoring and fall detection, stress level monitoring and estimation of human thermal comfort levels.

2.4.1. Machine Learning for ADL Recognition and Behavior Monitoring

There are two categories in machine learning algorithms used for activity recognition, where the differentiation between the two lies on how the user's activities and their ADL profile are represented and modeled. The first category refers to the generative approach, which consists of creating a statistical model of the joint probability distribution of samples and activity labels. The most typical generative models include the Hidden Markov Models (HMM) and Bayesian networks. The second approach is a more heuristic approach and is based on creating a model of the conditional probability of the activity labels, given the samples [144], [145].

Discriminative models include Support Vector Machines (SVM), which present high accuracy and good performance when a limited dataset is considered, conditional random fields (CRF), k-nearest neighbor algorithms and artificial neural networks (ANN), with the most prominent ones being recurrent neural networks (RNNs). Several datasets of smart home projects are publicly available and can be used for testing the most suitable machine learning algorithms for ADL. In most of these datasets, human activities are perceived by a sequence of state-changes expressed by the activation of several sensors (e.g., infrared motion sensors, pressure sensors and so on) installed on every day's used objects. Some datasets include CASAS dataset [146], MavHome [147], ARAS [148], MIT Activity Dataset (Tapia) [149] and Kasteren [150], among others.

The CASAS project [98] created an activity recognition software that provides real-time activity labeling of sensor events (e.g. cooking, eat, enter home, sleep, work, etc.), based on a support vector machine (SVM). The analyzed data was based on the sequence of sensor events (e.g., "ON" and "OFF") of several motion sensors distributed throughout the house. Other machine learning algorithms, including hidden Markov models and naïve Bayes classifiers, were tested - however, the SVM achieved the best performance. Similarly, Fleury et al. [93] made ADL classification based on SVM as well. Bayesian classification and neural network methods were not suitable given the small number of collected samples. The authors in [43] used HMM to recognize a behavioral patterns expressed by state sequences. Activity recognition was based on the user's location, which was obtained by an impulse radio UWB positioning system. Yegang Du et al. [151] developed a three-stage framework for recognition of human activities, able to predict the next probable activity. This recognition was based

on the manipulation of daily used objects (e.g., chair, bed, sofa, toothbrush, knife, etc.). The detection of its usage was done by attaching passive RFID tags on the objects. For human activity prediction, time sequences were considered, as certain activities tend to happen right next to a previous activity (e.g., watching TV after having dinner). Long short-term memory (LSTM), a sub-set of Recurrent neural networks, was used for activity prediction, as well as for object-usage. The authors achieved a recognition precision of 85.0% and prediction accuracy of 78.3%. Their solution showed a stronger performance and accuracy than the classical Naïve Bayes method [151].

The authors in [97] evaluated different methods of classifying ADL. The classified activities included going to toilet, taking a shower, going to bed, eating, drinking, etc. SVM, random forest, HMM and fisher kernel learning (FKL) classifiers were tested on three data sets with different types of sensors at each different location. The first dataset was from Kasteren [150]. It described the daily activities performed by a single person in his apartment. All the used sensors (including motion, pressure and reed switches) gave binary outputs. The hybrid generative and discriminative method, FKL, presented a better performance for the three datasets, when compared with HMM, SVM and random forest algorithms.

Considering ADL recognition systems based on motion, with data extracted by accelerometers and other mechanical-based sensors, Chernbumroong et al. [152] were able to detect nine different ADL of an elderly person based on the information provided by wrist-worn multi-sensors from a sports watch, such as a temperature sensor, accelerometer and altimeter. When compared with neural networks, SVM proved to be the best algorithm for the classification of activities, with an overall accuracy of 90.23%. Future work [153] included the addition of four more sensors – heart rate monitor, light sensor, gyroscope and barometer – to improve the activity classification accuracy. By using the SVM classification model, which was still considered the best classification algorithm for their dataset, the authors achieved approximately 97.20% of accuracy when classifying activities.

Davis et al. [154] evaluated three machine learning algorithms – SVM, HMM and ANN – on a dataset based on information collected with an accelerometer and gyroscope of a smartphone. SVM and ANN classifiers achieved a good performance (97.6% and 91.4%, respectively), but the combination of both SVM and HMM methods vastly improved detection accuracies to 99.7%. Other classifiers, such as Decision Tree algorithms and its variants, have also been used for human activity recognition systems [155]–[157].

These algorithms present good performance results when detecting human activities based on acceleration patterns, as previously seen. Yet, it is necessary to pre-process the data involving the feature extraction of accelerometer and gyroscope raw information, which is typically the acceleration in m/s^2 and rotation in degrees for the X, Y and Z-axis. This can be time-consuming and adds more complexity to the ML algorithm.

2.4.2. Machine Learning for Fall Detection

The use of Deep Learning models, such as LSTM, to classify both ADL and fall events, has been addressed over these past years. LSTMs have been trained with tri-axial accelerometer data to detect falls, having achieved good results [158]. Multi-sensor data based on accelerometer and gyroscope for LSTM training was also proposed in [159] and [160]. The LSTM algorithm is good at automatically learning the features from raw data [161]. This makes it unnecessary to perform feature extraction of accelerometer and gyroscope raw values, which helps to reduce the complexity and processing power required by the implemented algorithm. Moreover, LSTMs can process entire sequences of data, learn long-term dependencies, and extract and learn time-series patterns in a more effective way than Convolutional Neural Networks (CNN) and other conventional Deep Learning algorithms.

Other neural network architectures such as temporal convolutional networks (TCN) and gate recurrent units (GRU) produce similar results to LSTM. However, LSTM can still have fewer computational complexity than these other two models [162].

Sarabia-Jácome et al. [163] presented an innovative intelligent system to detect falls based on a 3-layer fog-cloud computing architecture and deep learning models. The proposed system employed a wearable 3-axis accelerometer and a smart IoT gateway as a fog node to remotely collect the patient's monitoring data. The authors deployed two deep learning models based on Recurrent Neural Networks (RNN) (LSTM/GRU), having achieved highly efficient results of 98.75% accuracy. The use of a smart gateway as a fog device showed significant advantages over a smartphone choice and was appropriate for seamlessly covering indoor environments, where undetected falls mostly occur. Liang Ma et al. [164] proposed a solution to the problem of detecting falls in private locations for the elderly by using impulse-radio UWB monostatic radar. The proposed method combined CNN and LSTM to extract spatiotemporal features for fall detection. The proposed method was tested on six different activities and achieved a sensitivity of 95% and a specificity of 92.6% at a range of 8 meters.

2.4.3. Machine Learning for the Estimation of Human Thermal Comfort based on Heart Rate Variability Parameters

Besides having a strong presence in ADL recognition, machine learning techniques are also applied to extract relevant information about physiological conditions provided by wearable biomedical sensors. Considering the impact of different indoor thermal and air humidity conditions on a subject's well-being, several studies have been conducted in order to investigate the influence of different environmental conditions on human health, namely in terms of thermal comfort, through the analysis of cardiac activity and HRV [165]–[168].

A small number of recent studies have been focusing on using machine learning (ML) approaches for estimating a person's comfort based on physiological and environmental parameters.

The authors in [167] tested the performance of ten ML classification algorithms for predicting human thermal comfort based on HRV and a rating scale of self-reported thermal sensation. Some of the used algorithms included Logistic Regression (LR), k-Nearest Neighbors (KNN), Decision Trees (DT), Multilayer Perceptron (MLP) neural networks and Support Vector Machines (SVM) - the latter one being the classifier that provided higher accuracy. Similarly, Morresi et al. [168] relied on the use of SVM, Random Forest (RF) and Extra Tree Classifiers (ETC) to classify between warm-induced and cold-induced discomfort based on HRV and self-reported thermal sensation, having reached successful results.

2.4.4. Machine Learning for Stress Detection

In addition to HRV analysis, mental or emotional strain can be estimated by applying machine learning methods to physiological data. Many of the data used in these algorithms are based on features obtained from an ECG signal, EEG, GSR or even HRV parameters, depending on the final application of the problem. For emotion classification, for instance, physiological parameters extracted from an ECG or PPG, GSR or EEG signal are typically used [169]–[171]. The utilization of machine learning for the development of real-time mental stress detection systems has become widespread in recent years. A comparison of the best machine learning techniques to detect psychophysiological stress was studied by Smets et al. [172], based on physiological responses obtained from ECG, GSR, RR and skin temperature in a controlled environment. In [173], support vector machines (SVM) and k-nearest neighbours (kNN) algorithms were used to make a binary classification of stressed and relaxed states based on ECG, RR, GSR and BP features. The individualized model created by the authors achieved an accuracy of 95.8%. Other studies have considered the use of Fuzzy Logic to make the same binary classification based on GSR, HR and respiratory data [174]. With the addition of a wider range of physiological features, such as EMG, ECG, GSR and RR, the authors in [175] used MLP, Naïve Bayes, RF, kStar and DT to classify three different levels of stress – low, medium and high. The highest accuracy score was achieved for the k-star algorithm, with the authors claiming having reached very good classification results (>95%) using the ECG signal alone. In [176] the quantification of three different levels of mental stress were made using EEG. An SVM algorithm combined with Error Correction Code was used for the classification problem, in which an accuracy of 94.8% was achieved. Mental stress can be monitored using the patterns of ECG signals with the help of deep learning methods, as proposed by Hwang et al. [177]. Using HRV parameters has a standard for stress evaluation, the authors achieved an accuracy as high as 87,4% in recognizing stress conditions. Since HRV is used to measure the activity of the autonomous nervous system, the HRV analysis allows the identification of mental stress. In this way, machine learning and deep learning methods have used HRV data for stress recognition and prediction. One example is the study by Giannakakis et al. [178], who used machine learning techniques to identify a sense of stress using HRV features. The study involved exposure to different stressors and a collection of subjective feedback from each participant upon induced stress scenarios. The authors achieved a good correlation between the sense of stress and the HRV parameters considered. Their stress recognition system achieved an accuracy above 70% for the RF and SVM algorithms when using only HRV parameters. Considering an unsupervised approach, Oskooei et al. [179] used deep learning algorithms for an unsupervised detection of mental stress using short-term HRV data. Convolutional autoencoders [180] seemed to have a consistent and successful stratification of stressed versus not stressed samples, which were verified by HRV parameters, such as RMSSD, mean HR and the ratio between LF and HF components.

Table 2.6 summarizes machine learning classifiers that have been used in the literature for ADL recognition.

TABLE 2.6. List of machine learning classifiers used in the literature

Machine Learning Classifiers	Research Topic	Reviewed Works
Support Vector Machine (SVM)	ADL and Fall Detection	[93], [97], [98], [152]–[154]
	Thermal Comfort	[166], [167]
	Stress Detection	[172], [175], [177]
Decision Tree / Random Forest	ADL and Fall Detection	[97], [154]-[156]
	Thermal Comfort	[166],[167]
	Stress Detection	[174], [177], [179]
Neural Networks (LSTM, MLP, etc.)	ADL and Fall Detection	[150], [153], [157]-[159], [162], [163]
	Thermal Comfort	[166]
	Stress Detection	[174], [176], [178]
Hidden Markov Models (HMM)	ADL and Fall Detection	[43], [97], [98], [154]
Naïve Bayes	ADL	[98], [151]
	Stress Detection	[174]

2.5. The Importance of Exergames and Immersive Environments for Physical and Cognitive Stimulation

With the increase of life expectancy and retirement age over these recent years, the risk of mental illnesses, particularly dementia and strokes, has been a raising risk for most of the elderly population. Not only do the risks of mental illness arise at this age, but there is also an emergence of negative events, such as the loss of a loved one, lack of close family ties, loneliness, social isolation and decline of mobility and physical exercise. These issues lead to an urgent need to provide healthcare systems that can contribute to medical rehabilitation and enhance social well-being among the elderly. The exergames, which combine physical exercise with digital gaming, have proved to bring great benefits to the participants' physical, cognitive and psychological well-being [181], [182]. Most importantly, elderly can use these systems in their own home, where they feel emotionally more comfortable and where the rehabilitation process can be more efficient. Many studies have proved the great benefits of using exergames in improving participants' physical and psychological health.

Besides revealing their importance in ambient assisted living deployments and under free-living conditions, wearable biomedical sensors have allowed to study the contributions of physiotherapy sessions and evaluate physical and cognitive outcomes during the rehabilitation process. Moreover, it allows the study of VR serious games direct contributions on the rehabilitation process and health conditions of the patient. In this context, exergaming has been showing promising results regarding player performance and engagement when practicing physical activity. Kafri et al. [183] showed that energy expenditure (EE) and exercise intensity from post-stroke participants after playing upper-limb and mobility Kinect and Wii-based exergames was considered of moderate intensity, regarding inherent clinical implications, according to the three levels of exercise intensity considered: low, moderate and vigorous. Besides EE, the percentage of predicted maximal HR rate of perceived exertion (RPE) and respiratory exchange ratio (RER) were used to characterize different games.

Jinhui Li et al. [181] conducted a literature research on exergame studies and concluded that the interaction of elderly population with these type of video games have promising results regarding the enhancement of social well-being, including the increase of positive attitudes and social connection, and also reduction of loneliness.

Munoz et al. [184] focused on finding how physiological parameters were regulated in elderly users during exergaming sessions of different difficulties and audio-visual stimuli. This study is based on the analysis of physiological data obtained through wearable sensors that acquired electrocardiograms and electrodermal activity signals. HR and HRV parameters were extracted, as well as maximum oxygen uptake (VO2max), Energy Expenditure (EE), Metabolic Equivalents (METs) and Galvanic Skin Response (GSR). The exergame, which was an adaptation of the famous two-dimensional Pong game, mostly relied on lower limbs movements, as the player needed to move horizontally to control a virtual paddle projected on the floor. The experimental procedure was based in a control and exergaming group, and the obtained results suggest that parasympathetic activity based on HRV analysis is significantly different between the control and exergaming group rather than between different difficulty levels (easy, medium, and hard).

Chan et al. [185] studied the influence of virtual reality (VR) technologies in cognitive functions of older adults and concluded that VR based training programs significantly improved repetition and memory retention compared to usual programs.

VR training has shown significant improvements in strength and balance in elderly adults [186]–[191], which has been evidenced by objective measurements of postural components [192]. A recent study also showed the ability of immersive VR environments to improve postural stability of the elderly as well as increasing their levels of engagement during motor rehabilitation exercising [193]. The effectiveness of applying an exercise routine based on VR exergaming in the elderly population has been proven by several studies, with similar or even superior effects of exergames on cognitive functions, when compared to traditional types of exercises [194]. Common physiological measures used in these studies for monitoring physical performance and exercise intensity include the monitoring of heart rate, assessment of the rating of perceived exertion (RPE), heart rate reserve (%HRR) and average percentage of maximum heart rate (%HRmax).

With the aim of exploring how the HRV indices and the ANS response are modelled and improved through exergaming, Eggenberger et al. [195] conducted a 6-month training session composed of traditional cognitive-motor exercises and exergames for healthy older adults. The authors not only discovered a substantial correlation between HRV indices and cognitive executive functions, but also found great improvements in global and parasympathetic autonomic nervous system responses in the elderly when physical training was associated with exergaming.

With a special focus on providing a cost-effective way to support mental wellbeing and physical and mental rehabilitation for elderly at home, E. Vogiatzaki and A. Krukowski [196] proposed an automated home system that combines augmented reality and virtual reality gaming, multi-modal user interfaces and innovative embedded micro-sensor devices combined with a Personal Health Report System (PHR). This system was intended to support the delivery of individual and patient-centered electronic health services at home, hospitals and other types of environments, and its usability was confirmed by technical validation tests.

Not particularly focused on physical rehabilitation or training, the creation of immersive environments has also been addressed by several AAL projects, some of which have been supported by the European Active Assisted Living (AAL) program [197]. SENSE-GARDEN [198], [199] is a project based on the development of immersive environments which provides different stimuli for basic senses, such as balance, smell, touch, hearing and sight. These environments integrate music, films, pictures and scents, and are specifically tailored for the individual, as they automatically adapt to their personal memories and preferences. All this was achieved by the design of a virtual space, composed by: a reality wall with projection of landscape videos with familiar scenarios; an augmented reality game to improve balance and physical activity stimulation; an interactive touchscreen showing family photographs; a stationary bicycle placed in front of a film; sound speakers playing background soundscapes and familiar music and a dispensary system releasing familiar scents [198].

FIGURE 2.8. Example of immersive environments created by the SENSE-GARDEN project [198], [199].

CHAPTER 3

Smart Tailored Environment

The system follows a healthcare IoT framework and is composed of a wireless sensor network that enables physiological parameters assessment, environmental quality monitoring and indoor localization and human activity recognition. In this chapter, a description of the developed system' hardware and software components is made.

3.1. Physiological Parameters Sensor Nodes

3.1.1. Ballistocardiography Sensing Node

The first biomedical sensor node for cardiac and respiratory activity estimation is based on an unobtrusive sensing unit expressed by a BCG sensor. The selected BCG system requires mechanical connection between the subject's body and the sensor. Thus, to facilitate its use, without causing any discomfort to the user, the sensor is embedded on the seat of an office chair. The BCG sensing unit is expressed by a lightweight and flexible electromechanical film (EMFi) sensor – EMFIT L-3030 with 29 x 30 cm dimensions (Figure 3.1). It is a flexible and thin polypropylene film with electrically conductive layers that converts mechanical energy to an electrical signal. These layers are separated by air voids that are 10-100 µm wide and 3 µm high [37]. When pressure is applied on the sensor, the thickness of the air voids changes, and electrical charge movements occur in the void interface, therefore generating a voltage. This sensor presents a capacitance of 45 pF/cm2 at 1kHz, that was measured with a B&K precision bench LCR meter, model 891. Aside from the external noise that might be caused by movements in the chair, the mechanical activity is generated by the repetitive micro vibrations of

FIGURE 3.1. Ballistocardiography sensor, EMFIT L-3030 (left image) and its placement on a chair, together with the signal conditioning circuit (right image)

the user's whole-body associated with cardiac contraction and ejection of blood in the vessels, as well as with the respiratory activity.

The BCG sensor is connected to a signal conditioning circuit and its output is acquired by an ESP32 microcontroller. The conditioning circuit includes a filtering block with a 2nd order Butterworth low-pass filter (cut-off frequency fc= 28Hz) that uses a TLV2764 quad rail-to-rail operational amplifier. In order to have a higher precision ADC, an ADS1115 device with 16-bit ADC resolution and an internal programmable gain amplifier (PGA) was connected to the ESP32 over I2C, as depicted in Figure. 3.2. The signal is acquired at 1kHz sampling rate by the ESP32 and is sent through the Bluetooth communication protocol in real-time to the gateway node for data processing and analysis.

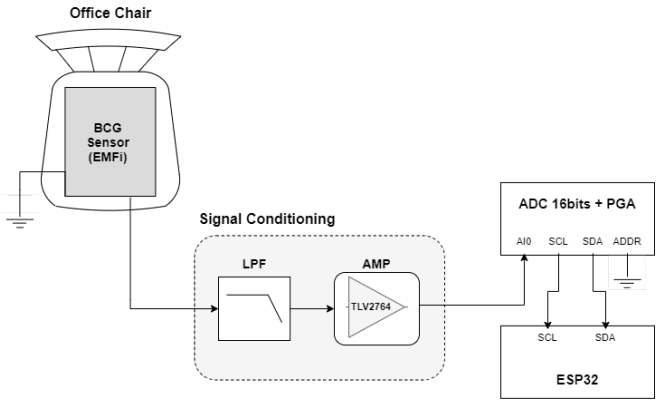

FIGURE 3.2. BCG acquisition using an EMFi sensor, a 2nd order low pass filter with a TLV2764 operational amplifier and a data acquisition board expressed by an ESP32.

A. BCG Signal Processing

Although BCG poses as more convenient and comfortable method for monitoring vital signals, its signal analysis is a challenging process. The signals collected from the BCG sensor have low signal-to-noise ratio (SNR), especially due to the respiration activity, some muscle activities or even due to electrical interference. To improve the SNR of the ballistographic signal, a low pass active filter (LPF) was employed, as previously mentioned. The signal, that is wirelessly acquired by the gateway node, is observed in Figure 3.3, with blue color. These signals were obtained from a young and healthy adult while seated on the chair, performing regular office work while executing light hand movements (e.g., working on the PC or writing). This information is processed by a computational unit with more processing power, that in this case is represented by the smart gateway. For heart rate and respiratory rate estimations, additional digital filtering techniques were implemented using SciPy signal processing library for Python programming language. A high pass filter with cut-off frequency of 30 Hz was applied to remove the baseline wander of the signal, induced by respiratory activity (Figure 3.3). To obtain the heart rate estimation and to extract the time interval between each consecutive heartbeat (J-J intervals), a peak detection algorithm was implemented. The number of peaks and their location in the time axis was obtained. Time differences between peak occurrences were also calculated for HRV

analysis in the time-domain and frequency domain. In Figure 3.3, an example of the acquired BCG signal for a 60s-window (top) and a 15s-time window (bottom) is presented, where the IJK wave complex is depicted.

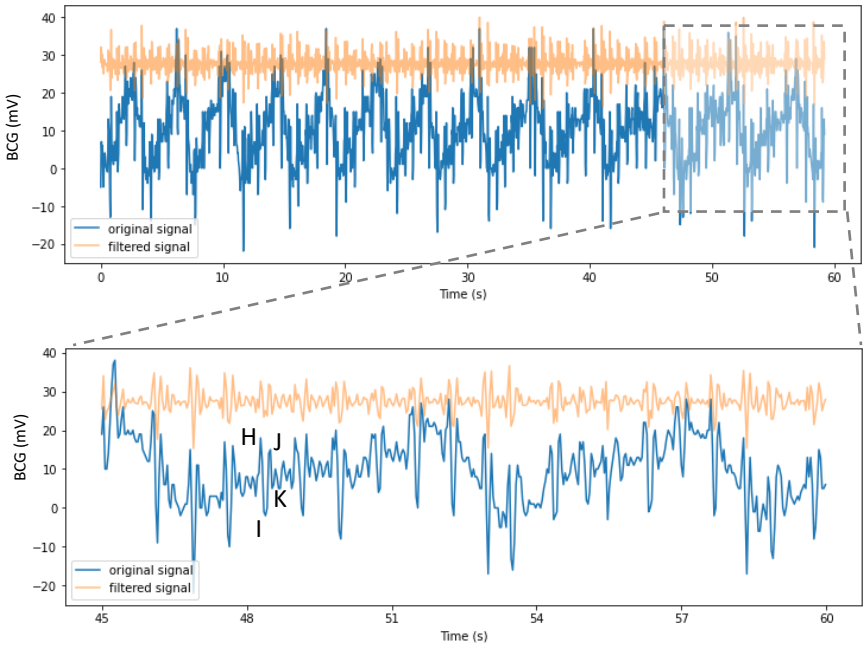

FIGURE 3.3. Ballistocardiography signal associated with the seat of a chair before (blue) and after (orange) removal of the respiratory signal component.

This type of signal, with lower interference and higher SNR, is regularly obtained in the whole experiment since the subjects are seated in a relaxed position while working on a PC, which induces reduced movement artifacts. For estimating the respiration signal (Resp), a method based on Discrete Wavelet Transform (DWT) was used. This method consists on the implementation of a digital filter bank of pairs of digital high-pass (HPF) and LPF filters that follow a tree structure [200]. The BCG signal is decomposed at each scale (e.g., j scale) into detail coefficients (d_j) at the HPF output, and into approximation coefficients (a_j) at the LPF output. The values of these coefficients can be expressed by the following inner products [201]:

$$d_j(k) = \langle x(l), \psi_{j,k}(l) \rangle \tag{1}$$

$$a_j(k) = \langle x(l), \phi_{j,k}(l) \rangle \tag{2}$$

where $\psi_{j,k}(l)$ and $\phi_{j,k}(k)$ represent the scaled and translated versions of the basis functions associated with the HPF and LPF impulse responses:

$$\psi_{j,k}(l) = 2^{-\frac{j}{2}} \psi\left(2^{-j}\, l - k\right) \tag{3}$$

$$\phi_{j,k}(l) = 2^{-\frac{j}{2}}\,\phi\left(2^{-j}\,l - k\right) \tag{4}$$

A study regarding the optimal mother wavelet type and decomposition levels (j=1 to 4) for DWT that allowed an accurate estimation of the respiratory activity was conducted. A comparison of different orders of Daubechies mother wavelets (e.g., Daubechies db1, db2, db3, db4) revealed that accurate estimation of respiratory signal was obtained with orders higher than 2, where optimal results were achieved with wavelet decomposition based on a 4th order Daubechies mother wavelet (db4). Regarding different DWT decomposition levels, graphical representations of the BCG signal and respiratory signal using 2, 3 and 4 levels of decomposition (cA2, cA3, cA4) in a 60s-time window are presented in Figure 3.4, respectively.

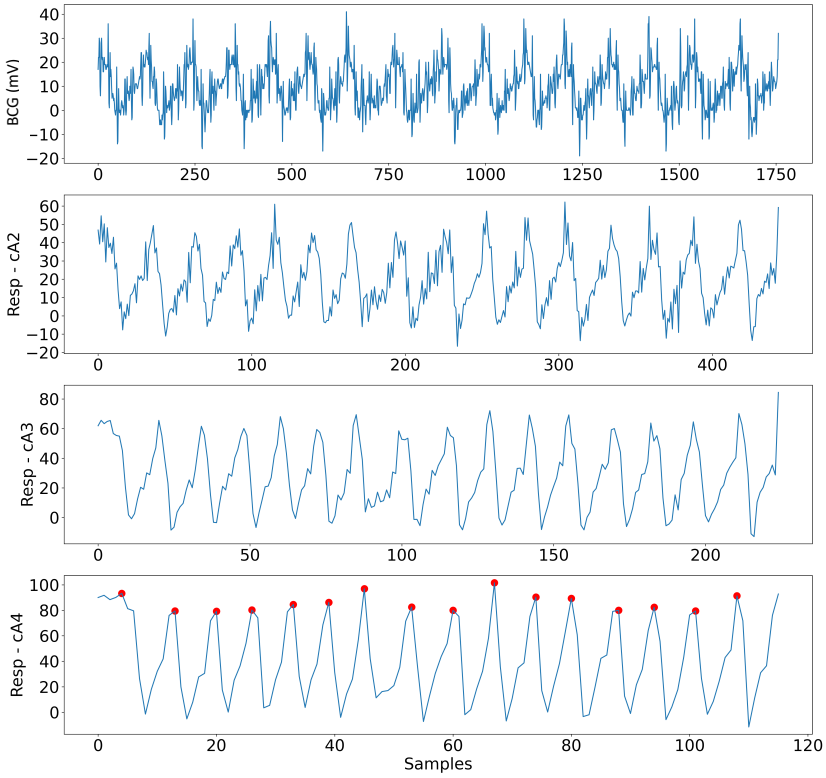

FIGURE 3.4. BCG signal and reconstruction of the respiratory signal based on discrete wavelet transform (DWT) with db4 mother wavelet, and comparison of 2nd, 3rd and 4th levels of approximation. Signal peak detection marked in red, on the 4th scale approximation.

For respiratory rate estimation using a signal peak detection procedure, the best results were achieved for a 4th wavelet approximation (*j*=4), as presented in Figure 3.4. The respiratory signals, Resp(n), are obtained by combining the products between the decomposition coefficients and the basis functions, which are given by the following equation [201]:

$$Resp(n) = a_4(n) = \sum_{k \in Z} a_j(k)\,\phi_{j,k}(n) \tag{5}$$

The respiratory rate estimation obtained with such methods was validated by counting how many times the chest raised for five minutes straight. A percentage error of approximately 4% was obtained when comparing the number of peaks of the extracted respiratory signal with calculated peaks using the peak detection function. Signal processing based on DWT was implemented offline by using the wavelet transform software PyWavelets for Python programming language.

3.1.2. Photoplethysmography Sensing Node

A. First Prototype

The wearable sensor node was designed to enable vital sign's monitoring and Pulse Rate Variability (PRV) analysis, commonly referred to as HRV, based on the PPG technique. The sensor being used follows a reflective photoplethysmography architecture, which is based on the measurement of the reflected light from the skin induced by volumetric variations of blood volume in the microvascular bed. The sensor is connected to an ESP32's ADC and transmits data at a sample rate of 160 Hz. Its internal circuit already includes amplification and analog filters; thus, no extra signal conditioning was needed. The ESP32 microcontroller presents both Wi-Fi and Bluetooth (IEEE 802.15.1) wireless connectivity capabilities, a 32 bits dual core CPU with a clock frequency up to 240 MHz, 520 kB of RAM and 12-bit resolution ADCs. Other than these remarkable features that make this board a strong opponent to other common microcontrollers, its power saving strategies is what makes it an ideal option to be used in the designed wearable sensor node. Low-power strategies such as the deep-sleep mode, as it is going to be addressed, is being considered to improve the node's autonomy. Figure 3.5 and 3.6 shows the developed prototype.

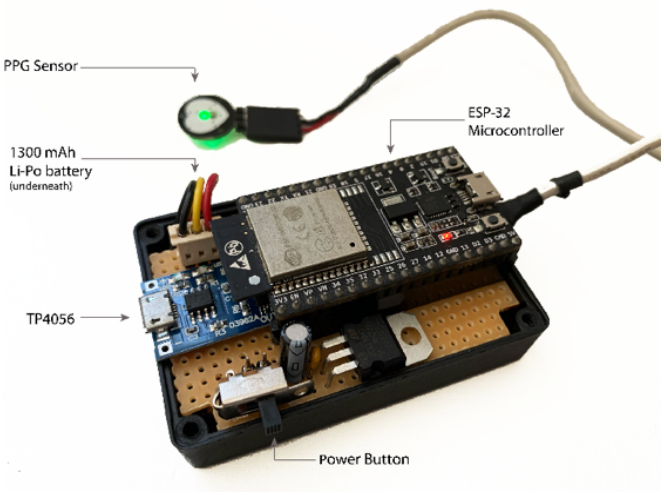

FIGURE 3.5. Design of the PPG wearable sensor for HRV measurement

Other than the PPG sensing part and the wireless microcontroller module, the node includes a 4.2V Li-Po battery with 1300 mAh capacity, a battery charger (TP4056), with a 3.3V low-dropout (LDO) regulator, since the ESP32 operates at 3.3V, and a switch. This first prototype was designed to be comfortably attached in the arm using an adjustable strap and the PPG sensor can either be placed in the earlobe or used in a finger. In the future, a ESP32 printed circuit board module will be dispensed and the chip itself will be embedded in the board together with other components, so it becomes less than half the size of this first version.

FIGURE 3.6. Example of the PPG wearable sensor usage

The sensor node has three stages of functioning: (A) PPG signal acquisition and calculation of PRV parameters, (B) data transmission and (C) deep sleep mode.

The PPG signal is collected for 5 minutes. During this time, real-time measurements of the time interval between two consecutive beats (inter-beat intervals), which are observed through an amplitude peak in the ADC that exceeds a pre-defined threshold, are stored. After the timer reaches 5 minutes, the microcontroller is configured to calculate the HRV parameters in the time-domain. These parameters include the average RR interval, average HR, maximum HR, SDNN, RMSSD and NN50.

After these calculations, the HRV information is transmitted to the gateway node using Wi-Fi with the MQTT protocol. Once data is sent, the microcontroller enters in the deep sleep mode.

Figure 3.7 presents the current consumption of the designed sensor node measured with the Keithley 2000 digital multimeter with the amperemeter function selected, for the three stages.

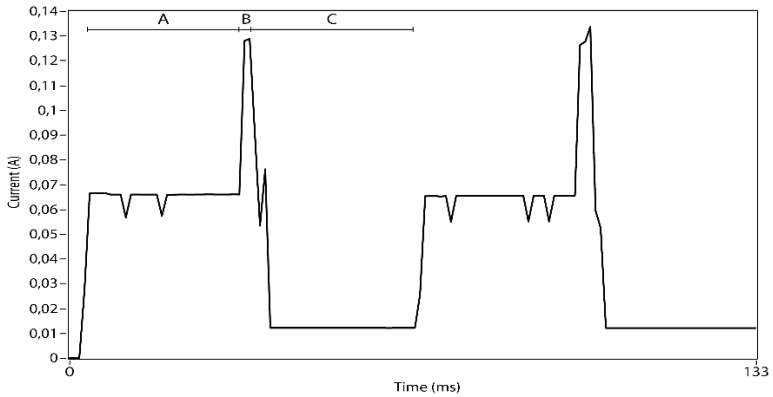

FIGURE 3.7. Current consumption during: A) Acquisition of PPG signal, B) Data transmission, C) Deep sleep mode

For demonstration purposes and calculation of current consumption, both wake up and deep sleep periods were configured for a duration of 30 seconds. During stage (A) the node's current consumption was around 67 mA, in (B) it reached 130 mA and on deep sleep node (C) it reached the minimum consumption of 10 mA. Considering that the sleep mode will last 30 minutes, if the sensor node is to be deployed in an AAL scenario, for instance, the node will have an autonomy of approximately 122 hours (5 days).

B. Second Prototype

Another wearable prototype for PPG signal acquisition was also developed. This wearable device, a much smaller version when compared to the previous one, is expressed by a Seeed Xiao BLE sense with 12-bit resolution ADCs, a 32-bit ARM® Cortex™-M4 CPU at 64Mhz, which is suitable for small machine learning applications. It also has two onboard sensors, such as a digital microphone and a 6-axis IMU, which can be applied for movement/activities recognition. This computer platform, which also integrates deep sleep mode for power saving strategies, reveals to be a great alternative to the commonly used ESP32 and it will be considered in future implementations of sensor nodes. The prototype runs the same algorithm for calculating the HRV mentioned in the previous sub-section.

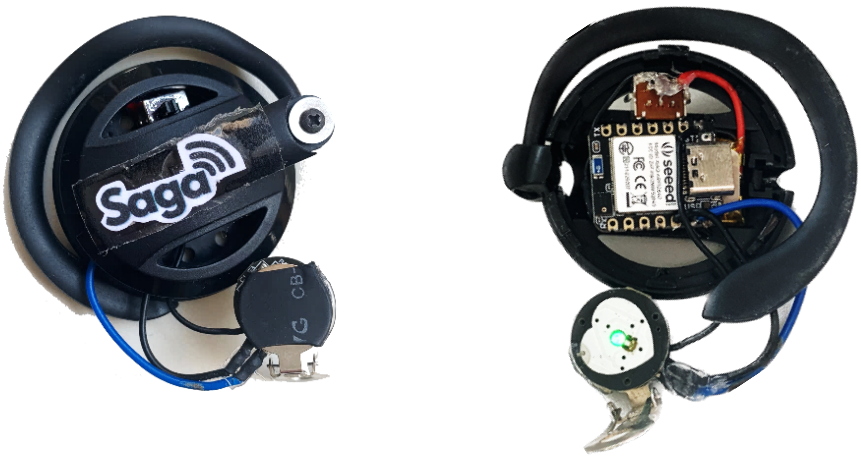

FIGURE 3.8. 2nd Prototype design for the PPG ear-worn sensor node

3.1.3. Electrocardiography Sensing Node

For the validation of the developed PPG wearable sensor node (1ST prototype), that will be addressed in Chapter 4. Section 4.2.4 and for the study presented in Section 4.3, a commercial wearable biomedical device characterized by the Shimmer3 ECG unit, was used for ECG signal acquisition. It is a compact and small wearable module frequently used in academic and biomedical research [202]. Its baseboard is composed by a MSP420 ultra-low power microcontroller, from Texas Instruments^{TM}, and its communication module relies on a Chipcon CC2420 radio transceiver, compliant with IEEE 802.15.4, and a RN42Class 2 Bluetooth module. This platform has proven its effectiveness on collecting physiological signals, and is a CE-certified wearable medical device, suitable for ECG Holter monitoring [203], [204]. A five-lead ECG monitoring with AgCl electrodes is used and all electrodes are placed on the chest, in the positions mapped in Figure 3.9. b). The bipolar limb leads are placed away from the heart towards the joint of a specific limb (RA -Right Arm, LA-Left Arm, RL-Right Leg, LL-Left Leg), and the unipolar lead is placed in the right side of the sternum (V1), a position that prevents the appearance of motion artifacts generally induced by limb movements. The signal is recorded at a sampling frequency of 512 samples/s, and it is transmitted to a personal computer in real-time through the Bluetooth communication protocol. LabVIEW software is used to configure the Shimmer module and collect the ECG data, which is then saved in a local file for later processing.

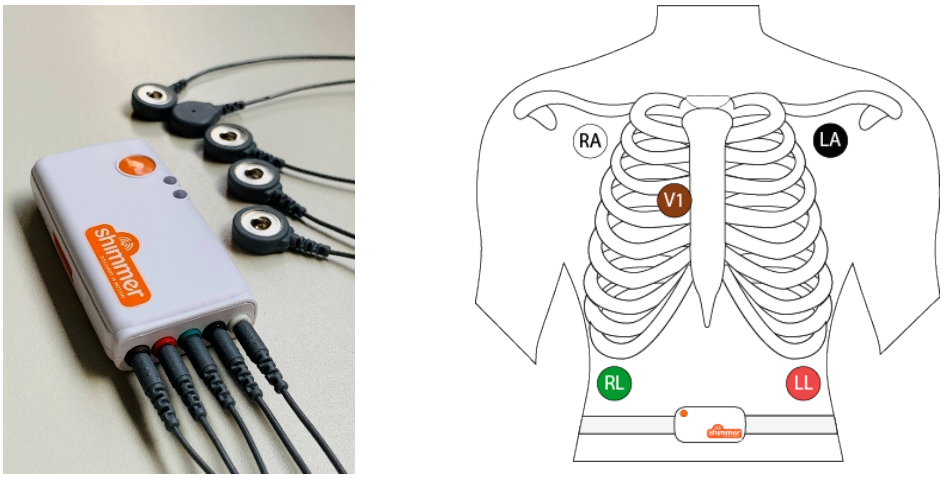

FIGURE 3.9. a) Shimmer3 ECG unit and b) RA, LA, RL, LL and V1 electrodes placement on the chest

The ECG signals rely on the use of various digital filters to clean the signal before applying the methods for analyzing the HRV. Digital filtering methods consisting of a HPF with cut-off frequency of 0.5 Hz were applied to remove baseline wander of the ECG signal (Figure 3.10). A peak detection algorithm based on the SciPy signal processing tools was implemented to extract temporal position of R peaks and thus calculate the R-R interval time series, which are to be used in HRV analysis (Figure 3.11).

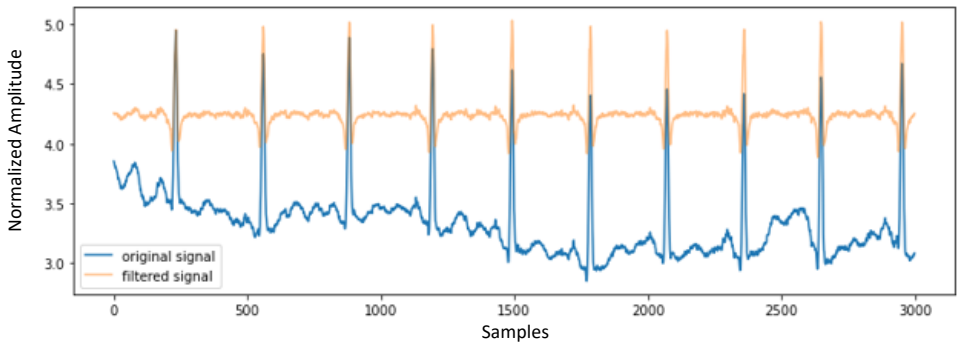

FIGURE 3.10. ECG original and filtered signal (HPF with cut-off frequency of 0.5 Hz)

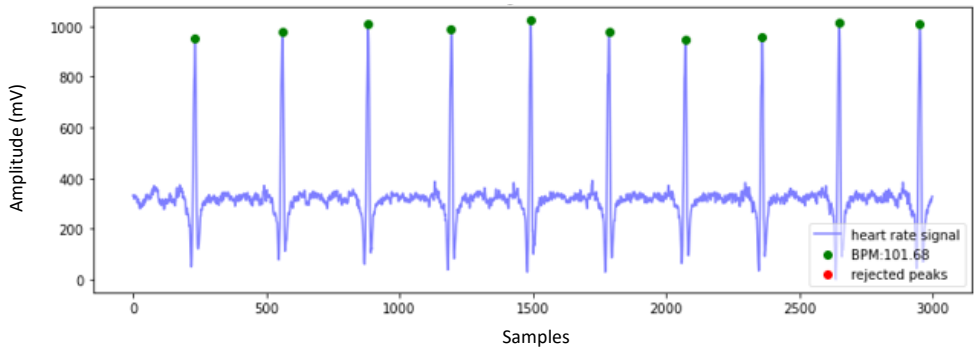

FIGURE 3.11. Peak detection of the ECG filtered signal

The HRV analysis is performed in both time-domain and frequency-domain, using the Python package HRV-analysis [59]. Additionally, the respiratory rate can also be analysed, since the Shimmer3 unit includes real-time respiration demodulation from the ECG signal. To extract the respiratory rate (breaths per minute), a peak detection algorithm is applied to the signal.

3.1.4. Galvanic Skin Response Sensing Node

To measure electrodermal activity (EDA), a biomedical sensor Shimmer3 GSR+, was considered [202], [204]. It uses an MSP430 ultra-low power 16-bit microcontroller, from Texas Instruments™, and integrates Bluetooth radio for wireless connectivity. The small and compact unit is powered up by a 450mAh Li-ion battery and it supports a variety of software development tools for data analysis and interface development. This unit has two electrodes that can be attached to two fingers from one hand, as depicted in Figure 3.12. The GSR signals are acquired at a sampling frequency of 1024 samples/s and transmitted to a computer through Bluetooth, for later analysis.

FIGURE 3.12. Shimmer3 GSR+ unit and the electrodes placement on the hand. Source: [205]

The acquisition of the EDA signal, also known as GSR, was done for measuring the changes in the emotional state of the participants throughout the experimental sessions that will be addressed in Chapter 4. Section 4.2 and correlate it with the modulation of sympathetic activity. All GSR signals are represented as resistance (kOhms), measured between the two electrodes placed in two fingers. The obtained signal represents the electrical conductivity of the skin measured over the entire length of a stimulation session. A GSR signal is composed of two components: phasic component and tonic component.

The phasic component represents the rapid changes of the GSR signal and its peaks, known as skin conductance response (SCR). It measures the sudden changes of emotional arousal and reflects sympathetic nervous system activity. In this way, it is possible to relate these changes with a specific stimulus. It can be obtained using a HPF with a cutoff frequency of 0.05Hz.

The other component is the tonic component. It reflects the slow variations in the GSR, and it is more linked to thermoregulation and general arousal. The analysis of such signals was performed in Python, using the NeuroKit2 package [206]. An example of the acquired signals is presented in Figure 3.13.

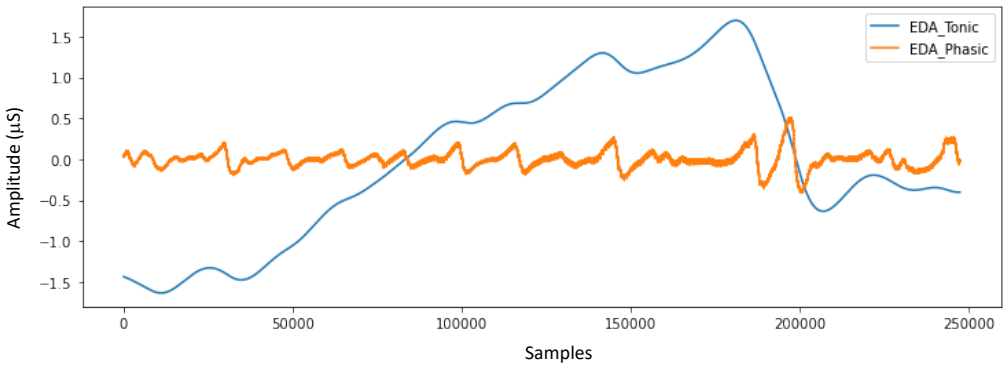

FIGURE 3.13. Tonic and Phasic component of an EDA signal

3.2. Indoor Environmental Parameters

3.2.1. First Prototype

Indoor environmental quality (IEQ) is composed of multiple sub-components, in which thermal comfort quality and air quality are present [207]. Considering the implementation of an IAQ monitoring layer, different air quality sensors have been selected. As presented in the literature, ozone (O_3), sulphur dioxide (SO_2), nitrogen oxides (NOx) and carbon monoxide (CO), smoke and particulate matter (PM) are the most common air pollutants in urban areas [208]. The system includes a highly selective PM sensor that can provide precise measurements of concentration of particles with different diameters. The Particulate Matter Sensor SPS30, from Sensirion, was used in this study [209], and the particle detection size range includes $PM_{1.0}$, $PM_{2.5}$, PM_4 and PM_{10}. Its mass concentration resolution is 1 µg/m^3 and it ranges from 1 to 1000 µg/m^3. The sensor provides a fully calibrated digital output for PM number and mass concentration values and includes UART and I2C interfaces. It has an MCERTS specification, which confirms that this sensor can be integrated into applications that comply with the European Air Quality Standard DIN EN 15267 [210].

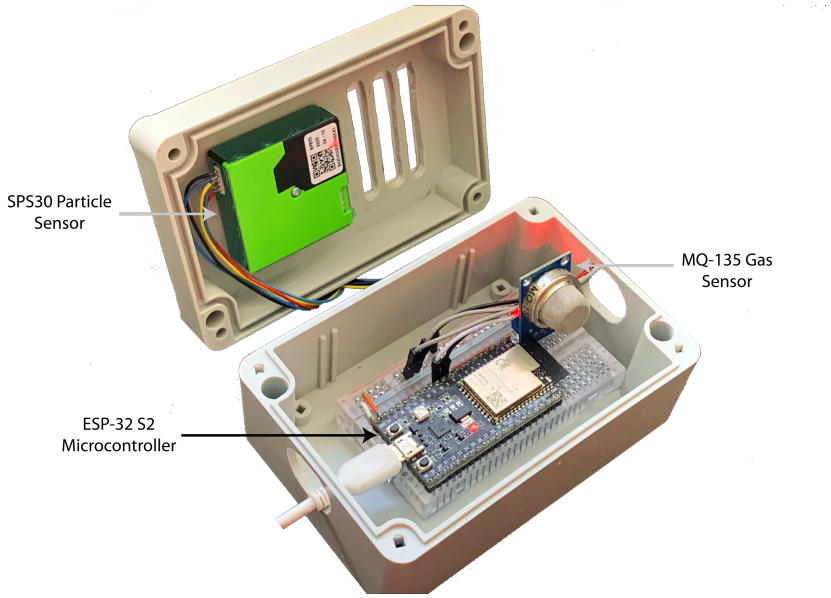

FIGURE 3.14. 1st Prototype of the air quality assessment node composed by an ESP32-S2 microcontroller, a SPS30 particle sensor and a MQ-135 gas sensor.

To measure indoor gas concentrations, including those considered relevant to the triggering of asthma crisis and COPD exacerbation, the MQ-135 is used in this 1st IAQ prototype. The MQ-X family sensors include a heating element and an electrochemical sensing unit expressed by a SnO2 metal-oxide (MOX) semiconductor. The heater is required because the sensor's sensitive surface is only reactive at certain temperatures. This surface has a low electrical conductivity when exposed to clean air. Whenever the sensing element detects gases and particles in the air, its electrical conductivity increases. The MQ-135 is an air quality sensor with low selectivity, sensitive to Ammonia (NH3), Nitrogen Oxides (NOx), Alcohol, Benzene, Smoke and Carbon Dioxide (CO2). Its calibration was done accordingly, and it is documented in [211].

The node is characterized by an ESP-32 S2 microcontroller. This model only has a Wi-Fi communication module, and it is quite similar to its predecessor in most specifications. A remarkable feature is its ultra-low power (ULP) co-processor based on the RISC-V architecture, which enables a very low power consumption and more processing power when compared to the ESP32.

3.2.2. Second Prototype

A more sophisticated sensor node was developed, providing additional features when compared to the previous prototype. The 2nd prototype includes temperature and relative humidity measurements, particulate matter concentration monitoring, CO, VOC, and CO measurements, as well as sound levels measurements.

Air temperature and relative humidity readings are performed by a Si7021 solid state sensor from Silicon Labs. This chip already performs signal processing and data calibration, and it has low power consumption. Relative humidity measurements have ±3% accuracy and a measurement range of 0-80% RH. Temperature measurements have an accuracy of ±0.4°C for a 10°C to 85°C measurement range [212].

As for the VOC and CO_2 measurements, the Adafruit CCS811 air quality sensor breakout is used. It is an I^2C gas sensor that provides readings of the total volatile organic compounds (TVOC) and equivalent carbon dioxide (eCO_2) in the environment. The breakout features a MOX gas sensor, and a tiny microcontroller that controls the power of the MOX's sensor hot-plate and reads the analog voltage. The eCO2 concentration is measured within a range of 400 to 8192 parts per million (ppm), and the TVOC concentration is measured within 0 to 1187 parts per billion (ppb) [213]. Relatively to CO measurements, these are made by an MQ-7 gas sensor.

The noise level measurements are performed by an electret microphone based on the Adafruit MAX9814 amplifier. This model is a high-quality microphone amplifier with automatic gain control (AGC) and low-noise microphone bias, which helps avoiding distortion when sound levels change randomly. Its operating frequency goes between 20 and 20 kHz, which is the frequency range of human hearing, and has an automatic gain from 40dB to 60dB [214].

The air quality portable sensor node also features an OLED screen that displays real-time readings of temperature, relative humidity, PM_{10} and $PM_{2.5}$, CO_2, tVOC and CO levels.

A light indicator expressed by a LED ring placed at the front of the sensor node displays 3 different states (Figure 3.15):

- Purple LED: It's the initial phase of the node's functioning and it starts whenever it is powered on. It is when the PM sensor activates the fan and performs its calibration process, which lasts for 10 seconds.
- Blue and Green LED: When the sensors read air quality parameters that are equal or below the recommended concentration levels presented in Table 2.5.
- Red LED: When the sensors read air quality parameters that are above the recommended concentration levels presented in Table 2.5.

FIGURE 3.15. 2nd Prototype of the air quality assessment node, and 2 feedback states: a) Calibration phase; b) Good air quality levels.

The portable sensor node is characterized by the ESP-32 S2 microcontroller and is powered up by a 3.7V Li-Po battery with 1800 mAh capacity.

3.3. Indoor Localization and Activity Recognition

The wearable node is part of an indoor positioning system based on a UWB tag and an IMU for activity classification (Fig.2). In this study, the activities being classified using both technologies comprise sitting, standing, and falling. The controlling platform of the wearable node relies on an ESP32-S2 microcontroller, that presents Wi-Fi (IEEE 802.11) wireless connectivity and a 32 bits dual core CPU with up to 240 MHz clock frequency. The microcontrollers' ADCs provide 12-bits of resolution. Also, the board's ultra-low power (ULP) co-processor enables lower energy consumption when compared to other available boards from the ESP family. The ESP32-S2 board was programmed in C++, using Arduino IDE.

The wearable also integrates an UWB tag from Pozyx®, which sends positioning data, such as the horizontal plane coordinates X and Y, and the elevation coordinate, Z. The positioning data is calculated by having as reference five UWB anchors placed in the room at fixed locations, as presented in Figure 3.16. The anchors transmit at 850 kbps bit rate with 64 MHz pulse frequency. The Pozyx® system uses the multilateration method to calculate the tag's position [215].

The positioning data is transmitted to the ESP32-S2 via I^2C at 24Hz sample frequency and using Pozyx® official Arduino library to interact with the UWB device. To enable 3D positioning, four of the UWB anchors were positioned 2.46 meters above the floor, and the remaining one was placed at a different height, in this case, located 7 cm from the floor. The environment where the UWB system was deployed was heavily furnished.

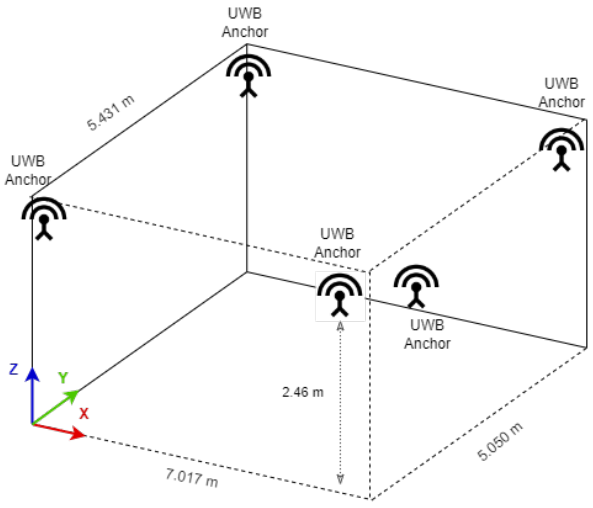

FIGURE 3.16. Positioning of the UWB anchors in the experimental room

The UWB anchors were calibrated automatically with the autocalibration method offered by the Pozyx® system. Table 3.1. presents the X, Y and Z coordinates of the four UWB anchors. The positioning coordinates measured by the UWB tag are collected by the ESP32 and are transmitted to the gateway node.

TABLE 3.1. UWB anchors coordinates

UWB Anchor ID	Coordinate X (mm)	Coordinate Y (mm)	Coordinate Z (mm)
0x7611	7890	6840	2460
0x7621	650	6837	2460
0x7653	6475	2013	2460
0x7674	-477	2456	2460
0x7649	3537	6650	70

As for the IMU, it is responsible to acquire acceleration and gyroscope data from the performed activities for a given position provided by the UWB indoor localization system. In this case, an MPU9250 based device was included in the wearable node. It is a 9-axis micro-electromechanical system (MEMS) sensor with an integrated Digital Motion Processor (DMP). In this study, only the 3-axis accelerometer and 3-axis gyroscope data are being considered. The device provides an accelerometer sensitivity up to 4800 LSB/g, the accelerometer range goes between 2 – 16 g, the gyroscope range is between 250 – 2000 °/s and gyroscope rate noise is 0.01 (°/s) rtHz. The sensor is connected to the ESP32-S2 via I2C and transmits data at 24Hz sample frequency. It is programmed to send raw accelerometer and gyroscope data up to 6 decimal places, along with the X, Y and Z coordinates from the UWB system through Wi-Fi and using the MQTT protocol.

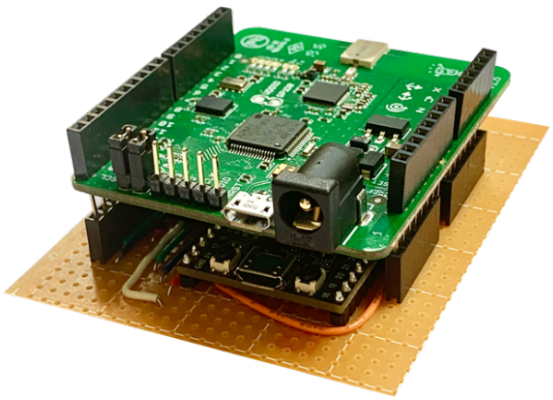

FIGURE 3.17. The wearable sensor node composed by an UWB tag (on top), ESP32-S2 and an IMU (beneath the tag)

The accelerometer and gyroscope tend to introduce a small offset, or bias, in the signal output. This could induce a misalignment of the features used in the ML classification tasks and affect the results. The sensor bias was compensated by performing a calibration when initializing the sensor node. This was done programmatically, by measuring the bias values of the sensor in a resting state (i.e., placing the wearable node on top of a surface) and subtracting those values from the raw sensor data during normal operation. The average accelerometer biases during the sensor's calibration step were 0.01, 0.02 and 0.15 m/s^2 for the X, Y and Z-axis, accordingly. The average gyroscope bias was -0.71, -0.39 and 0.17 °/s for the X, Y and Z-axis, respectively. The calibration process and the conducted experiments were made at a room temperature of 24°C. Beyond sensor bias calibration, digital low pass filters with cut-off frequency of 20Hz were applied for both accelerometer and gyroscope measurements.

The microcontroller's program uses 5.36 Mbits of storage space, corresponding to 51% of its memory capacity. The sensor node's autonomy is assured by a 2500 mAh Li-Po battery. The node's current consumption is on average 0.279 A providing a total autonomy of 8.96 hours. The wearable node can be placed at the torso or waist, using an elastic strap, as demonstrated in Figure 3.18.

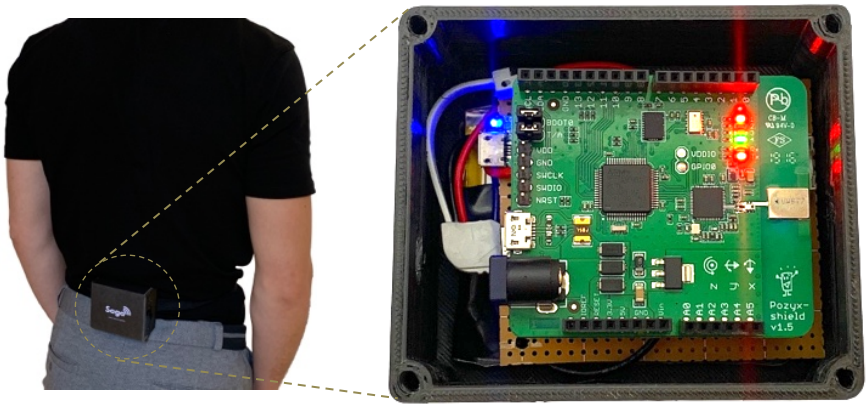

FIGURE 3.18. UWB wearable sensor node usage on the waist.

3.4. Edge Computing Layer

Regarding the edge computing layer, the Raspberry Pi 4 Model B, 8GB RAM, was selected to serve as the gateway/aggregator node. This new Raspberry model features much better performance levels when compared to its predecessor, with a much faster CPU speed and better performance levels thanks to its Quad core Cortex-A72 (ARM v8) 64-bit SoC with 1.5GHz clock frequency. These specifications are an advantage as additional processing power is going to be required for the future integration of the generated ML models in this system.

This computing platform functions as a Message Queuing Telemetry Transport (MQTT) server, and it is responsible for collecting and processing the data that comes from the wireless sensor nodes. MQTT is an efficient and extremely lightweight messaging protocol based on a publish/subscribe model. It runs over TCP/IP and it is mainly used in IoT deployments, as it is ideal to collect data from multiple connected sensors. Eclipse Mosquitto is configured on the gateway node as the MQTT message broker [216]. The Node-RED programming environment is used to configure the MQTT connections and process the collected data using JavaScript functions and the Python programming language. The gateway is configured to collect and process the data from the wireless sensor nodes and transmit it to cloud services expressed by a MySQL database when a Wi-Fi (IEEE 802.11) connection is available. When such condition is not met, the information is stored locally on a microSD card.

FIGURE 3.19. Gateway/aggregator node expressed by a Raspberry Pi 4 B

A security layer was implemented in the communication between nodes (MQTT clients) and the MQTT server, with username and password-based client authentication. Figure 3.20 shows an example of the interactions between the computing platform of a sensor node with the gateway node.

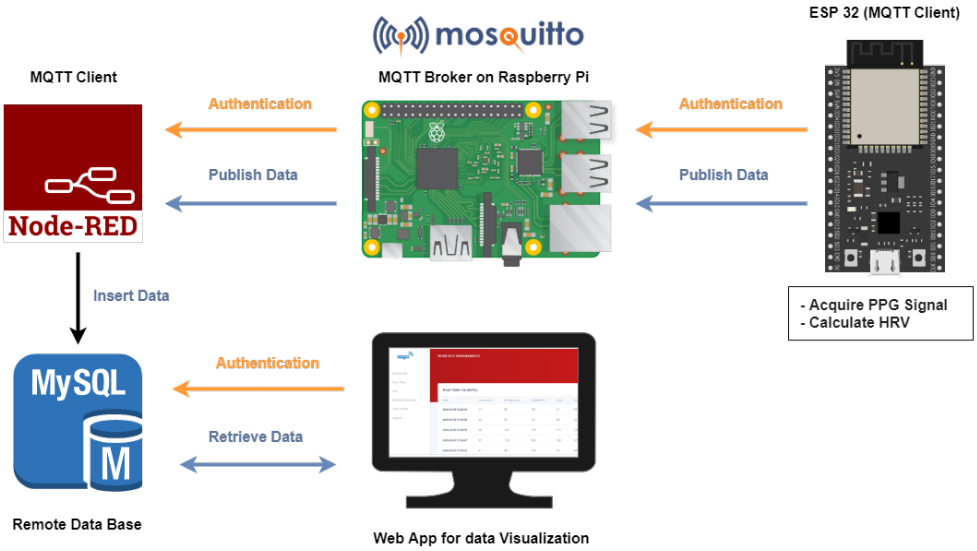

FIGURE 3.20. Sequence of interactions between a sensor node from the device layer with the gateway node and its further actions

CHAPTER 4

Measuring the Effects of External Stimuli on Human Physiological Parameters

This chapter addresses the utilization of the developed sensor nodes on three different experimental studies that aimed to estimate the effects of external environmental factors and *stimuli* on human physiological status and well-being. It begins with the analysis on how various indoor air conditions characterized by different temperature and relative humidity levels affect the autonomic nervous system and human thermal comfort. Then, the addition of an external stimulus based on music sound and stress noise, and its impact on human well-being is evaluated, as well as a prediction of stress levels in the presence of such stimuli. Moreover, this chapter explores the positive influence of virtual reality exergames on physiological and cognitive status. Lastly, a conclusions section closes this chapter.

4.1. How different Indoor Environmental Conditions affect the Autonomic Nervous System

4.1.1. Overview

Thermal comfort has been considered a reference for human well-being and work productivity. It is a term referred to the assessment of one's perceived feeling regarding the thermal conditions of an environment. High and low levels of temperature and relative humidity (RH) may cause discomfort and even lead to serious health problems related with cardiac diseases and respiratory distress, particularly among young children and the elderly population [217]. The monitoring of thermal comfort levels along with indoor air quality needs to be considered specially in ambient assisted living environments, where smart healthcare systems and assistive services are deployed in living environments, to support more susceptible populations, e.g., elderly population and people with chronical diseases. A lot of attention has been given to ambient temperature and its effects on health in various studies from recent years, especially at a time when the effects of climate change are having a huge impact on society and on environmental health - the rise in temperature not only induces heat stress, but it also elevates outdoor concentrations of fine particulate matter, therefore affecting air quality levels [218]–[223]. Respecting to indoor temperature, levels higher than 26°C can lead to adverse health effects [224], including emergency hospitalization, higher cardiovascular mortality, and heatstroke, which is more frequent in elderly people than in patients from other age groups. People leaving with dementia may not have a correct perception of the ambient temperature and may not even recognize that they

are in a colder or warmer environment. Since people spend most of their time indoors, air conditioning systems and increased air motion (e.g., fans) to cool down the environment can help prevent heat-related illnesses.

Current directions of the research area of human thermal comfort have been considering the acquisition of physiological parameters to measure the comfort level of an individual in an environment characterized by different thermal conditions. The use of artificial intelligence algorithms to improve the environmental quality of an indoor space and thus make the environment more intelligent has brought innovation to this research area. In this context, future directions include the creation of an intelligent system that based on user comfort feedback - either subjectively or by collecting physiological parameters - will regulate room temperature based on the use of smart actuators. In this way, it is possible to improve the user's comfort levels and tailor the environment based on their own preferences, as well as helping the prevention of health problems associated with temperature and humidity, and other indoor environmental quality parameters.

The World Health Organization (WHO) establishes safe and recommended temperature levels for indoor environments that range between 18°C and 24°C, although optimal temperatures can slightly vary in different climate regions [220].

Besides bringing significant impacts on human physiological processes, relative humidity also facilitates the spread of allergenic organisms. It is an important parameter to consider specially in an office environment, where sensory irritation in eye and upper airways are two of the most common symptoms reported in such environments when lower relative humidity levels are measured (<30% RH), which can directly affect work performance and overall well-being [225]. In fact, higher relative humidity levels, e.g., 55% - 70% RH, can help improve IAQ as it suppresses resuspension of particles located in surfaces [226], [227]. However, there are some constraints regarding higher levels of air humidity (>60% RH), since it can also make breathing difficult in people with asthma, as it stimulates nerves in the lungs to narrow and tighten the airways [228]. Therefore, relative humidity levels that range between 40% and 60% reduce most adverse health effects and are considered ideal for indoor environments [229].

4.1.2. Study contributions

This study addresses the utilization of the components of the physiological parameter layer of the developed system addressed in Chapter 3 to analyse the impact of different indoor thermal and air humidity conditions on a subject's well-being.

The following steps are considered:

1. Validation of the developed physiological parameter monitoring system based on unobtrusive BCG signal acquisition and the indoor environmental quality sensor node, addressed in Chapter 3.
2. Study of human thermal comfort based on HRV analysis in a daily used office environment. Occupants of a daily used office were exposed to different air temperature and relative humidity levels that could be considered thermally discomfortable using smart actuator nodes. This part of the study was intended to analyse how adverse thermal conditions expressed by unusual temperature (30°C) and humidity levels (70%) can affect cardiorespiratory activity and the ANS response. Particulate matter concentration was measured throughout all experiments to perceive whether different humidity levels can indeed influence this air quality parameter in small office environments (9m^2) and to confirm that this parameter will not influence the cardiovascular activity of the volunteers.
3. Optimization of temperature and humidity sensor locations based on computational fluid dynamic (CFD) simulation. Since the considered workspace was a non-isothermal environment and not adapted for such kind of experiments, a simulation of the airflow produced by the rooms' HVAC system and temperature distribution was estimated using CFD. Such simulation provided relevant information regarding the number of temperature and humidity sensors that would be needed to effectively measure spatial distribution of air temperature, as well as the selection of the most effective locations for their deployment in the room.
4. Estimation of the subject's comfort and thermal discomfort using HRV parameters and ML classification techniques. A prediction of whether a subject is at a thermally comfortable environment or at a discomfortable environment characterized by high temperature or humidity levels was conducted. In this context, it is considered that discomfortable environments are characterized by indoor air temperature (>24°C) and relative humidity levels (>60% RH) that lie outside the recommended limits established by the WHO. The trained ML algorithms included SVM, DT, RF, KNN, LR and MLP neural networks. Data augmentation techniques were applied to the dataset to enhance the ML classifiers accuracy.

4.1.3. Methods

This study involved the participation of a total of 7 healthy young adults, 4 females and 3 males, aged 24 ± 0.8 years old with body mass indexes (BMI) 19.7 ± 1.2 kg/m^2. Some difficulties and challenges arising from the global COVID-19 pandemic limited the physical presence and the participation of a larger number of volunteers during the period in which the experiments took place. All participants enrolled after informed consent and they were advised to not consume caffeine nor alcohol approximately 8 hours before the experiment. Details regarding all procedures and the objectives of the study were given before each session.

The experiments were conducted in a small office room with the size of 2.65 m × 3.4 m × 2.80m, a total area of 9 m^2 and a volume of 25 m^3. This small office was considered more adequate to run experiments since it could generate the desired environmental conditions quickly. Volunteers were already familiar with this type of environment, namely the office where experiments took place, so there was no level of discomfort associated with that environment.

The volunteers were instructed to remain seated passively on a chair containing the BCG sensor node addressed in Chapter 3. Spontaneous breathing was allowed, and they performed their conventional office work on their laptops. A PPG sensor node was placed on the earlobe, where muscle activity and other motion artifacts tend to be minimal.

Air temperature and relative humidity were measured by six Si7021 sensors placed at different locations in the room. These sensors (S1, S2, S3, S4, S5, S6) were distributed and mounted on the walls, at 1.50m from the floor (Figure 4.1). The sensor's locations were based on a preliminary study of the temperature distribution in this specific environment through CFD simulation, as it is going to be addressed.

To change the room's humidity, a smart humidifier (A1) was placed 1.30m away from the subject. The Original SmartMi Air Humidifier from Xiaomi was used. It is an evaporative humidifier and can be remotely controlled by an API, as it enables Wi-Fi 802.11 b/g/n connectivity. Thus, it is integrated in this system as a smart device. The humidification amount is greater than 240 mL/h, and it is recommended for spaces between 10-15 m^2.

The IAQ sensor node addressed in Chapter 3 was placed on top of the volunteer's desk throughout the experiment. Different locations were considered for the positioning of this sensor node regarding spatial distribution of particles and gaseous pollutants. Each sensor node collected environmental data every 3 minutes and sent it to the gateway node.

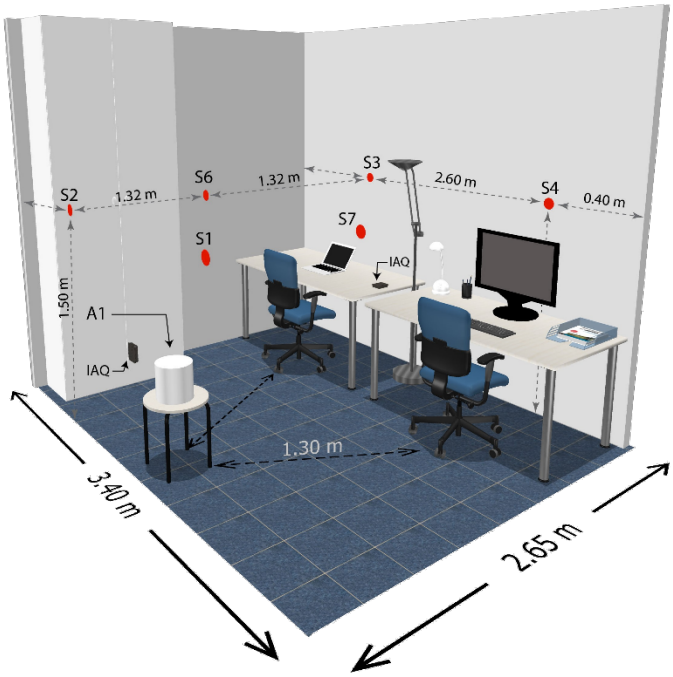

FIGURE 4.1. 3D Isometric plan of the room (S1, S2, S3, S4, S5, S6: temperature and relative humidity sensors; IAQ: Air quality sensor node positions; A1: Smart humidifier)

The system offers a graphical user interface for visualizing the data that the gateway node processes in real-time. The PM concentrations, temperature and relative humidity levels, as well as the BCG signal and the HRV analysis in the time-domain are displayed in the system's dashboard, as depicted in figure 4.2.

FIGURE 4.2. System's dashboard, displaying real-time values of the measured parameters

The experiments with volunteers took place between June and August 2021. Three different thermal conditions were considered for this experiment: (1) a neutral temperature of 24°C, with relative humidity near 50%; (2) neutral temperature of 24°C, with relative humidity near 70%; (3) hot

air temperature of 30°C, with relative humidity near 50%. The thermal conditions were changed by the built-in air conditioning system an using the smart humidifier. Such range of temperatures was selected according to common air temperatures that the human body can be exposed to throughout the year in mainland Portugal (range between 18°C – 30°C). During summer period, the lowest indoor ambient temperatures are around 24°C, thus being considered the neutral temperature for this experimental procedure.

Each participant started the experiment after being accustomated and thermally comfortable with the environment. Before each experiment, it was ensured that the initial temperature of the environment was 24°C, which was obtained by calculating an average of all temperature values read by the sensors distributed in the environment. As demonstrated in Figure 4.3, physiological data was collected for 10 minutes total during all three conditions, and HRV analysis was only preformed in the final 5 minutes, which is the standard duration of short-term recordings for HRV [230].

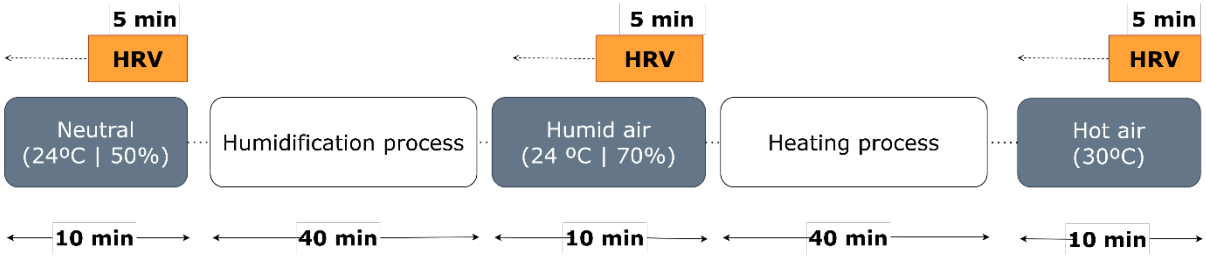

FIGURE 4.3. Experimental schedule for all different thermal conditions and the thermal climatization process.

After the initial condition (1) was met, the smart humidifier was remotely configured to achieve a target humidity of 70%, which took approximately 40 minutes to reach. Most participants stayed inside the room during the thermal condition changing process. Right after the end of the second condition experiment (2), the heating process took place, and the air conditioning system was set to achieve a room temperature of 30°C. After approximately 40 minutes, the third and final physiological measurements were taken.

4.1.4. Applied AI for Classification of Thermal Comfort and Discomfort

Supervised machine learning (ML) classification algorithms were implemented to create a model that could predict the comfort status of a person based on different thermal conditions environments. In this phase, the HRV metrics were extracted from a 90-seconds-long-time window. Then, the time window segment was shifted 50 seconds to compute new HRV values and thus prevent overlapping of samples. This procedure was carried out until the end of the entire recording with time length of approximately 10 minutes. It has been proven that ultra-short term recordings of 90 seconds provide reliable estimations of LF (ms^2 and n.u.) and LF/HF ratio [231], [232], as well as for all other HRV time-domain parameters [233].

This initial procedure allowed the generation of a greater amount of HRV samples for the dataset to be used in ML classification.

A. Data augmentation using generative adversarial networks

The ML model training based on the original dataset achieved poor model performance (accuracy between 61% and 73%). In this way, data augmentation based on the use of synthetic data techniques were applied to increase the size of the dataset and in turn help improve the performance of the traditional classification algorithms. Synthetic data examples were merged with original training data, obtaining an augmented and more balanced training dataset. Synthetic data is often used in healthcare industries to produce artificially generated datapoints with similar attributes to the real data, and therefore expand a limited dataset or allow the share of sensitive data more easily and without the associated privacy issues. Synthetic data generation was based on the implementation of a generative adversarial network (GAN). The GAN is an algorithmic architecture that consists of two neural networks that compete against one another [234]. One network is a generator, which tries to generate new data like real data, and the other is a discriminator, which has the goal of distinguishing between generated content and real content. In the GAN structure, the generator output is connected to a discriminator input, and the generator's weights are updated according to the discriminator's classification of fake/real data (Figure 4.4). Initially, the generator receives random noise as input, which will be transformed through a function, and then it is passed on to the discriminator, which will learn to decide whether the data has been produced by the generator or not. The loss function of the discriminator penalizes the discriminator whenever it misclassifies an instance, and the weights of the discriminator network are updated through backpropagation.

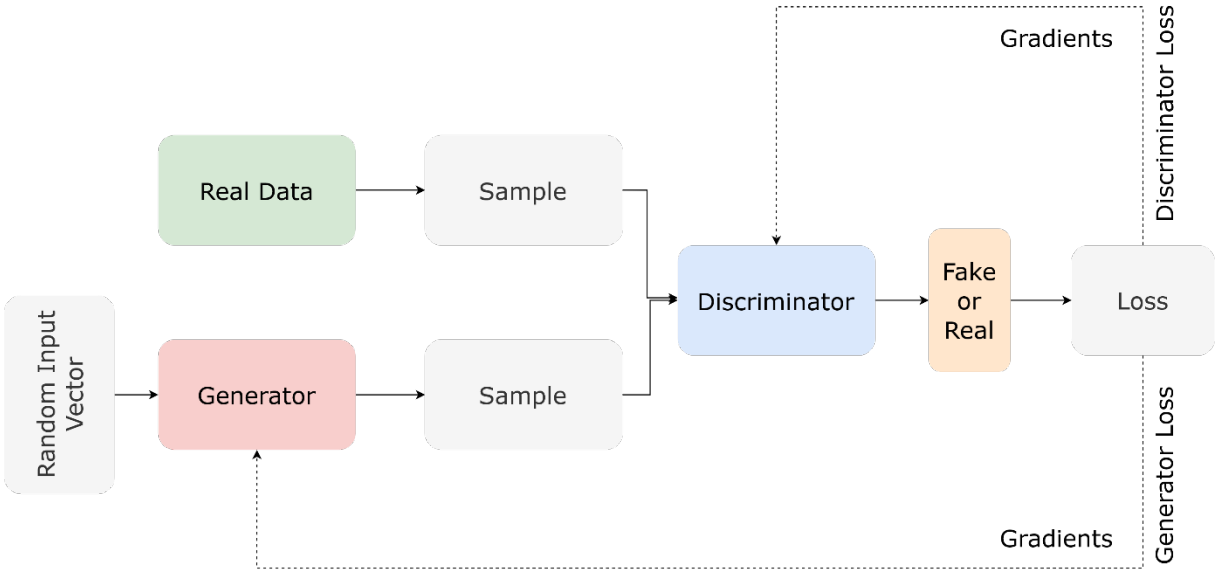

FIGURE 4.4. Generative Adversarial Network Architecture

In this study, the *ydata-synthetic Python* library was used for generating synthetic data based on GAN. A Wasserstein GAN with gradient penalty (WGAN-P) variant was considered, as it provided better results for the generation of synthetic samples when compared with simpler types of GAN, such as Vanilla GAN.

B. Machine learning classification

With the use of an expanded dataset, Support Vector Machine (SVM), Decision Trees (DT), Random Forest (RF), k-Nearest Neighbours (KNN), Logistic Regression (LR) and Multilayer Perceptron (MLP) neural network were used to predict if a subject is in a thermal comfortable environment (neutral) or discomfortable environment (hot/humid) based on HRV metrics.

The SVM is an algorithm that is based on the separation of data points by finding a hyperplane that maximizes the margin between the target classes. It is effective in high-dimensional spaces and robust to overfitting [235].

The DT is a non-parametric algorithm that builds a hierarchical tree structure of decision rules and their possible outcomes [236]. Each internal node represents a decision based on a feature, each branch denotes the result from that decision and each leaf node represents the class label. It is an algorithm that can handle nonlinear relationships. However, it may not perform well when the dataset presents imbalanced data.

RF algorithm combines the output of multiple DT to create a more robust and accurate model [237]. This algorithm tends to perform better when compared to single DT since it limits variance and overfitting by combining multiple trees. In this way, this algorithm is expected to produce more accurate predictions on new and unseen data.

KNN is a non-parametric classifier that uses the concept of proximity to classify and predict how an individual data point integrates a certain group. It assumes that similar data points can be found in close proximity. The algorithm's input is the K closest training example of the dataset. The algorithm identifies the nearest neighbors of a given query point by calculating the distance between this point and the others. Only then, the algorithm assigns a class label to that point.

The LR algorithm is a statistical method that models the probability of an event occurring based on a given dataset with independent variables. It applies a logistic function to a linear combination of features, giving a probability score between 0 and 1.

MLP is an artificial neural network (ANN) that is based on multiple layers of interconnected artificial neurons [238]. Each neuron is a computational unit that receives weighted inputs and produces an output by using an activation function on the weighted sum of its inputs. It is an algorithm that offers good performance on a variety of classification problems and can easily learn the non-linear relationships between features.

Since the volunteers performed the same activity during the different sessions and were not subjected to any external stimuli other than the room temperature variation, it is expected that the obtained results of the subject's comfort status are directly dependent of indoor air temperature variables.

Preprocessing operations included the normalization of HRV values, so that all variables are computed with the same scale, and label encoding of the prediction target. As a result, categorical variables that characterized the type of thermal environment were converted into the numerical values "0" (neutral) and "1" (hot). The dataset was based on eleven features (mean HR, maximum HR, minimum HR, mean RR, SDNN, RMSSD, LF, HF, LF/HF, VLF and Stress Index) and a target, which is the type of thermal environment (neutral/hot). All classifiers were implemented with Python programming language and Scikit-learn machine learning library.

Each ML classifier performance was estimated using cross-validation techniques based on K-fold cross validation with 10 folds, since the common train-test split method can cause an unbalanced distribution of the target classes and lead to bias in the training phase of the model.

The evaluation metrics for evaluating the performance of the ML models were based on classification accuracy, precision, recall and the F1-score. Precision refers to the ratio of correctly positive classified peaks to the total number of positive classified peaks. Recall measures the proportion of positive classified peaks that were classified correctly and F1 score is the weighted average of precision and recall.

4.1.5. Experimental Results and Discussion

Three different topics are going to be addressed in subsections: Firstly, a simulation of the air temperature distribution in the office environment where experiments were conducted. Secondly, the analysis of HRV parameters and respiration rate of the volunteers under different ambient temperature and relative humidity conditions is carried out. Finally, the third topic addresses the use of machine learning algorithms to estimate a user's comfort and discomfort based on the measured HRV indices.

A. Simulation of Indoor Air Temperature Distribution

A simulation based on computational fluid dynamics (CFD) was used to study the airflow patterns induced by the heating, ventilation, and air conditioning (HVAC) system (Figure 4.5), as well as the temperature distribution in the room. The ANSYS Fluent software [239] was used to perform the CFD analysis. Simulations were achieved in a transient state regime using the k-ε turbulence model and the energy equation. The transient solution was conducted for ~1200s of real-time. The boundary conditions included two outlet vents (in blue) and one inlet (in red), as depicted in Figure 4.6. Regarding the external walls, a convective heat transfer coefficient of 5 $W/m^2 \cdot K$ was considered, with free stream

temperature equivalent to the measured temperature outside the room during the days when experiments took place.

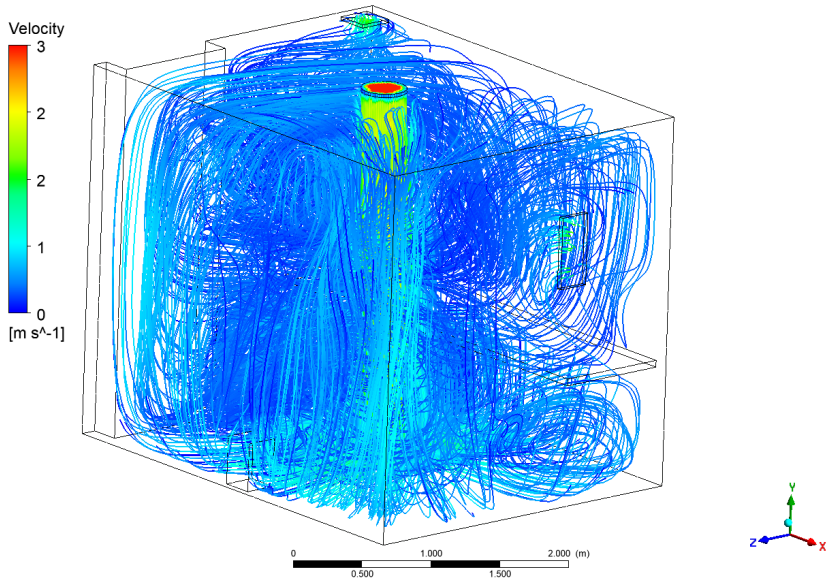

FIGURE 4.5. 3D Isometric plan with CFD simulation of the air flow distribution from the HVAC system in the experimental room environment, using ANSYS Fluent software

Results of the temperature spatial distribution in a XY plan after 90s of simulation are presented in Figure 4.6. An initial temperature of 22 °C was considered. The inlet vent, marked in red, was configured for 32°C air temperature and velocity magnitude of 3 m/s. According to the temperature scale indicated in figure (22°C - 32°C) and by observing the temperature distribution in both XY planes, it is possible to ascertain that the thermal stratification of the air in the indoor environment is not considerable near the walls. Moreover, temperature probes were used to measure the simulated temperature at specific locations near the walls, namely at three different heights – Y= 0.75m, 1.5m and 2.25m. The locations where probes were placed are marked in red in Figure 4.6.

Each height presented the same temperature level of 26.8±0.26°C, for both X-axis. The temperature variation between different heights is not significant, and thus the hypothesis of thermal stratification in this specific environment is discouraged by the obtained results. Therefore, the positioning and location of the sensors was quite optimised, thus eliminating the need to place several sensors at different heights. In this case, four sensors were chosen to be placed at the medium height of 1.5m, as marked in the figure by S1, S2, S3 and S4.

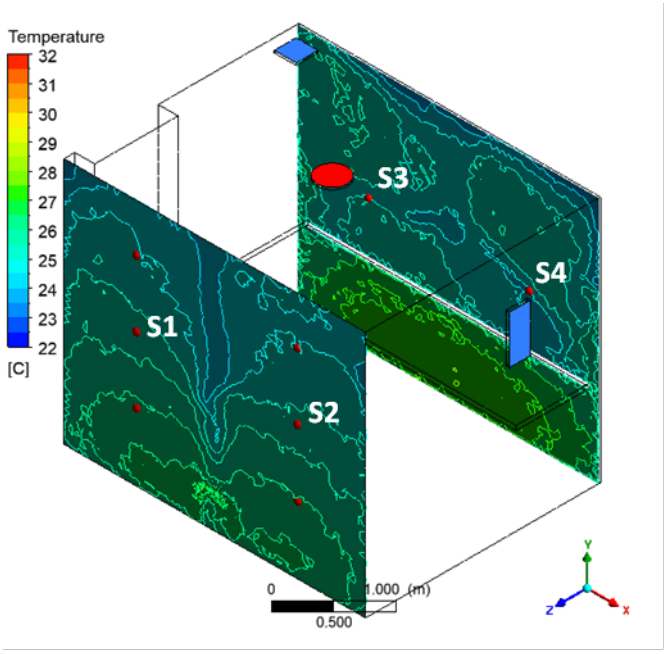

FIGURE 4.6. 3D Isometric plan with CFD simulation of thermal distribution in the room environment for two XY plans near the wall, for T= 90 seconds of simulation time. Outlet vents are presented in blue and the inlet vent in red color.

Considering the temperature distribution in the interior volume of the room, a YZ and YX plane has been considered for simulation purposes. Figure 4.7 depicts the temperature distribution after 20 minutes of running a simulated air conditioning system. One can see an incidence of hot air flow towards the inlet duct at the intersection of the two planes, which dissipates as soon as it comes in contact with the floor. Even so, the temperature reached 29°C uniformly along the planes and did not vary considerably along the Y axis, demonstrating once again that temperature stratification is not at all pronounced under these experimental conditions.

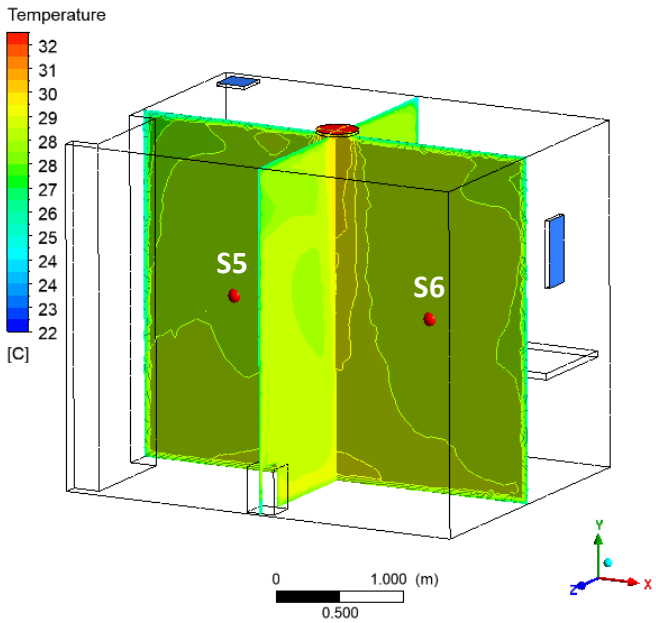

FIGURE 4.7. 3D Isometric plan with CFD simulation in the room environment for a YZ and YX plane, for T= 20 minutes of simulation time. Outlet vents are presented in blue and the inlet vent in red color.

The simulated results for temperature measurements and its time evolution in each selected sensor location (S1, S2, S3, S4, S5, S6) for a time sequence of 1200 seconds (T=20 minutes) are presented in Figure 4.8.

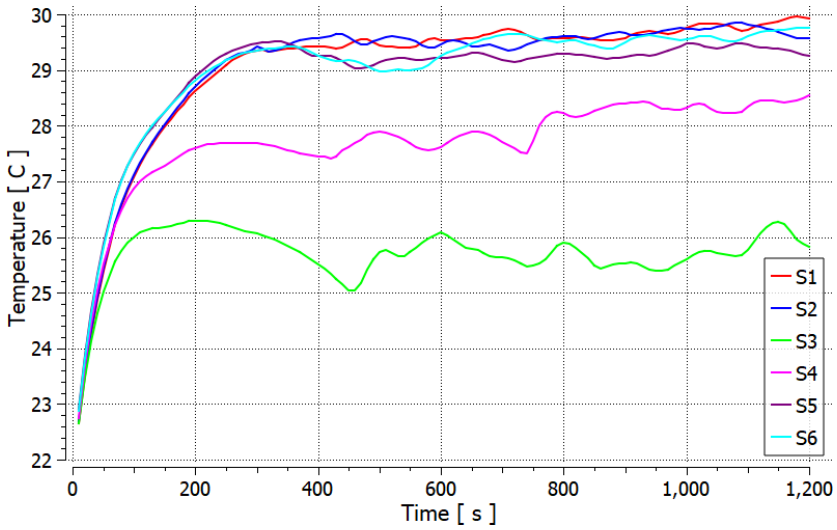

FIGURE 4.8. CFD simulation of temperature measurements and its evolution for each sensor location for a time sequence of 1200 seconds.

B. Measurements of indoor air temperature distribution and air quality in the experimental environment

Having chosen the positioning of these sensors based on the information provided by simulations, a final analysis with real data of the temperature distribution in the office environment was conducted using Si7021 sensors (Figure. 4.9). This allowed to detect any temperature deviation across all sensors' readings over time and helped to define the duration of each climatization process. This temperature and humidity distribution analysis was made during the winter season, where the average indoor ambient temperatures can range between 20°C and 22°C. The room remained unoccupied throughout this experiment.

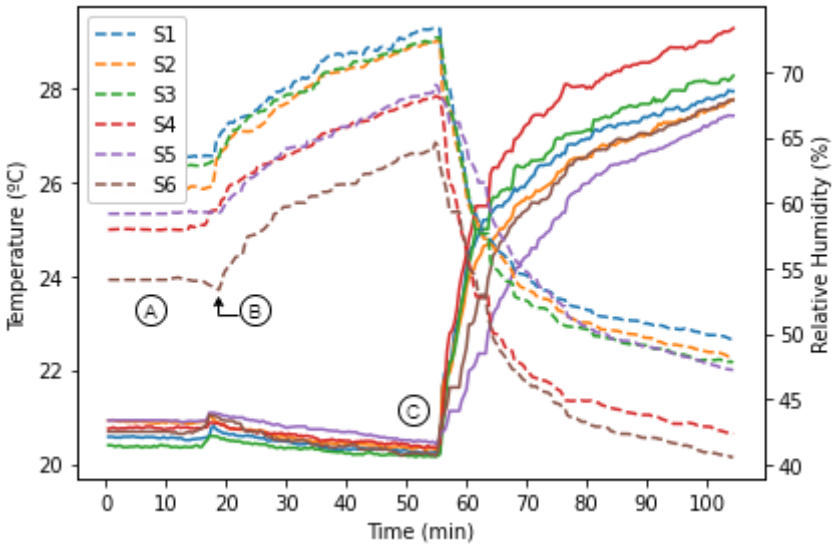

FIGURE 4.9. Air temperature and relative humidity distribution (dashed lines) measured by S1, S2, S3, S4, S5 and S6 in the experimental office environment. A: Neutral Environment (no actuators); B: Activation of humidification system; C: HVAC system turned on for heating process.

During the first 20 minutes, initial temperature and relative humidity measurements took place, without any influence from actuators, such as the HVAC system or the humidifier. An average initial temperature of 20.7°C and average relative humidity of 58% were recorded (A). This initial condition is equivalent to the first phase of acquisition of physiological signals. Next, following the protocol initially outlined, the humidification of the indoor space was initiated (B). The smart humidifier was remotely regulated for a target humidity of 70% RH, which took approximately 40 minutes to reach. For the next climatization process, the air conditioning was regulated to 30°C with its maximum air flow velocity (C). An average temperature of 28°C and relative humidity of approximately 46% RH was reached after 40 minutes. All Si7021 sensors showed a very similar response. However, dispersion of sensor characteristics regarding relative humidity readings is visible among different sensors (e.g., S6). Indoor air quality monitoring, which involved the analysis of particle concentration (PM_1, $PM_{2.5}$, PM_4 and PM_{10}), as well as of gas concentration levels, did not change significantly between the three thermal conditions. Figure 4.10 demonstrates PM concentration variation across three thermal

climatization conditions, which was measured during the analysis of temperature and relative humidity distribution presented in Figure 4.9. Overall, the air quality index was considered very good, since the indoor environment presented an average of 1.6 µg/m^3 of PM2.5 concentration during all experiments. The use of actuators for both humidifying and heating the air caused, however, slight changes in the concentration of particles. The following figure shows the three experimental periods: neutral climate, without actuators (A), humidification process (B), heating process through HVAC system (C). A 3rd order polynomial trendline was used to analyse PM Concentration measurements fluctuation across the different stages.

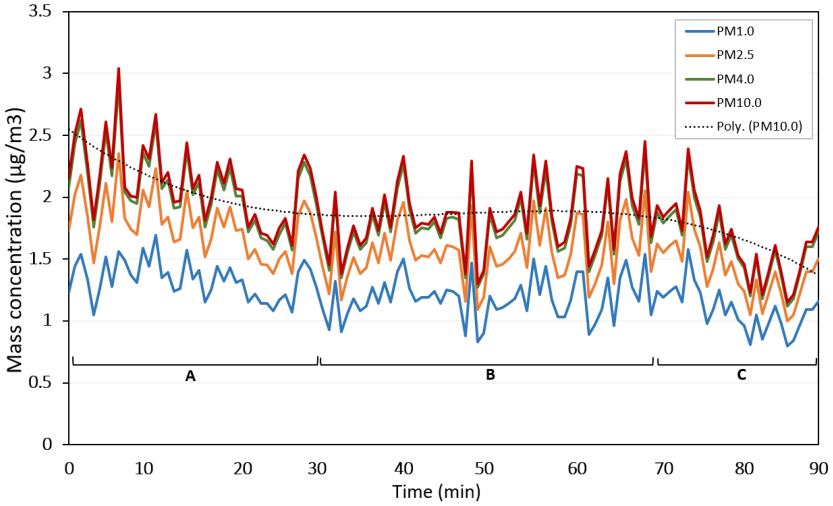

FIGURE 4.10. Particulate concentration measures (PM1.0, PM2.5, PM4.0, PM10.0) and associated trendline during three thermal climatization processes. A: Neutral Environment (no actuators); B: Activation of humidification system; C: HVAC system turned on for heating process.

A slight decrease was denoted in the period represented by (A), as there was no air movement induced by the occupation of the laboratory, a factor that contributes to an increase in the resuspension of particles located on surfaces. During the humidification process the concentration of particles remained stabilized (B). Although it is expected that higher relative humidity decreases PM concentration [227], a reduction of air movement in the room, since it remained unoccupied for 30 minutes, contributed to the reduction of particle resuspension.

During the final climatization process (C), which implies the use of mechanical ventilation with filtration, the PM concentration tended to decrease. The air extraction by the outlet vents as well as the efficient filtration of the HVAC system are factors that contributed to the reduction of PM concentration levels, as expected.

Regarding the MQ-135 gas sensor, the average gas concentration measured during ambient temperature, as well as during the humidification process, was around 3.18 ppm. Since the operating mode of this sensor that its heater coil remains at a constant temperature level to allow the proper functioning of its sensitive components, its standard detection conditions are set for a temperature of

20°C ± 2°C [240]. Thus, the measurements obtained for thermal conditions of 30°C were not considered.

The results obtained with both PM and gas sensors allowed us to infer that indoor air quality did not have an influence on physiological processes and HRV of the volunteers during all the experimental periods.

C. Human Thermal Comfort and HRV Analysis

BCG is always subjective to external noise and small artifacts that are generally caused by slight movements of the body, either by adjusting our sitting position or by performing hand or trunk movements. Since the objective of these experiments is to acquire data while performing regular office activities, the subject is free to perform any necessary movements. Taking this into consideration, the reliability of using the developed BCG sensor node for extracting HRV was studied. Firstly, a statistical analysis of peak detection classification in the BCG signal, using J-J peaks, was performed. A time window of the last 5 minutes recordings of both the PPG and BCG signals during neutral room temperature conditions for all volunteers was considered. The total number of peaks detected with the PPG, which is considered the reference node, was compared with the number of detected peaks from the BCG signal. In this classification, peaks were classified as true positive (TP), false positive (FP) and false negative (FN). TP classification refers to correctly classified peaks, FP to incorrect classifications and FN to J-J peaks not detected. To calculate the performance of the peak detection in the analysed BCG signals, in comparison with the PPG, four classification metrics were considered: accuracy (Acc), precision (Prec), recall and F1 score. Table 4.1 presents the results obtained for all 7 volunteers.

TABLE 4.1. Statistical analysis of peak detection for all seven volunteers using the BCG signal

Subject	TP	FP	FN	Acc (%)	Prec (%)	Recall (%)	F1
1	405	2	1	99.26	99.50	99.75	99.63
2	313	0	27	92.05	100	92.05	95.86
3	392	20	1	94.91	95.14	99.74	97.39
4	350	3	19	94.08	99.15	94.85	96.95
5	298	16	15	90.57	94.90	95.20	95.05
6	504	12	1	97.48	97.67	99.80	98.72
7	344	10	24	91.00	97.17	93.47	95.29
Total	2606	63	88	94.19	97.65	96.41	96.98

Generally, accurate results were obtained for most volunteers, where Subject 1 presented an accuracy value of 99.2% and F1 score of 99.63%, whereas worse BCG signal readings were obtained for Subject 5, with an accuracy of 90.57% and F1 score of 95.05%. In total, from 2606 detected peaks of all seven cases, 63 were classified as FP and 88 were missed (FN), which gives an accuracy of 94.19% and a F1 score of 96.98%. Ideally, the general accuracy of the peak detection classification using the BCG signal should exceed 95% in order to consider the analysis of HRV based on this method.
Moreover, a comparison between the HRV calculated with a 5-minutes sample of BCG and PPG was conducted. For this case, only 3 volunteers were analysed for both cardiac monitoring techniques, under neutral temperature conditions (Table 4.2).

TABLE 4.2. HRV parameters extracted from both BCG and PPG methods

Subject	**Mean HR**		**SDNN**		**RMSSD**		**LF/HF**	
	BCG	**PPG**	**BCG**	**PPG**	**BCG**	**PPG**	**BCG**	**PPG**
1	88	76	105	115	160	154	1.3	1.1
3	79	67	60	48	54	56	0.7	0.67
4	81	81	95	42	128	66	0.5	0.4
Average	82.6	74.6	86.6	68.3	114	92	0.83	0.72

A ±4 bpm standard deviation was obtained for mean HR, ±9 ms for SDNN, ±11ms for RMSSD and ± 0.05 for LF/HF.Since there are BCG samples with poor accuracy values (<95%), which were mainly caused by motion artifacts, this method will not be considered for HRV analysis in the present study and will only be used for respiratory activity assessment. Therefore, the following HRV analysis will be performed using PPG signals.

The average values and standard deviation of time-domain HRV parameters obtained for the three different thermal conditions for all 7 volunteers are presented in Table 4.3. The frequency-domain results are presented in Table 4.4. One-way analysis of variance (ANOVA) test was conducted to identify significant changes between the three conditions, where a p-value lower than 0.05 was considered statistically significant.

TABLE 4.3. Time-Domain Analysis (Average ± SD) of HRV under three different thermal conditions

Conditions (Temperature | Relative Humidity)	**Mean HR**	**Mean IBI**	**Max HR**	**SDNN**	**RMSSD**
24°C | 50%	76±11	804±100	92±13	64±27	84±44
24°C | 70%	76±13	809±117	90±14	65±30	81±45
30°C	82±16	758±115	96±16	50±21	54±27
***p*-value**	0.728	0.693	0.731	0.523	0.375

TABLE 4.4. Frequency-Domain Analysis (Average) of HRV under three different thermal conditions

Conditions (Temperature | Relative Humidity)	LF (ms^2)	HF (ms^2)	LF/HF	VLF	Stress Index
24°C | 50%	1329	2210	1.04	95	8.3
24°C | 70%	1074	1939	1.24	116	8.4
30°C	1316	1106	2.01	166	11
***p*-value**	0.847	0.517	0.341	0.557	0.382

This experiment did not show significant alterations of HRV parameters regarding the volunteer's exposure to different thermal conditions ($p > 0.05$). An average heart rate of 76 bpm was obtained for conditions (1) and (2), which considered a neutral air temperature and an increase of relative humidity levels (50%-70%). When considering short-term exposure to higher temperature levels of 30°C, average heart rate levels slightly increased to approximately 82 bpm. An estimation of the ANS behaviour and thermal comfort of the subjects under these different conditions was best analysed in the frequency-domain.

The LF component presented similar values when considering neutral temperature and hot temperature (~1300 ms^2), and slightly lower when a higher humidity environment was established (~1000 ms^2). Parasympathetic activity from all subjects decreased between the exposure from 50% to 70% relative humidity at a neutral temperature of 24°C, as assessed with the HF component.

A more pronounced decrease was observed between neutral (24°C) and hot air temperature (30°C) exposure (± 1104 ms^2), as also observed in the LF/HF ratio parameter (± 0.97) and VLF.

The RMSSD parameter is directly correlated with HF power [230] and gives information about the parasympathetic activity of the ANS using time-domain analysis. A decrease in RMSSD values, similar to that obtained with HF analysis, was also observed. This study demonstrated that hot air temperature at 30°C induced higher stress levels and contributed to reduce the human thermal comfort after a short period of exposure, as perceived by a decrease in parasympathetic activity given by higher LF/HF values. Such alteration of the ANS response maybe explained by the activation of thermal regulatory reflexes that include sweating and stimulation of reflex cutaneous vasodilation. Additionally, lower stress index values were obtained for an environment with neutral temperature (SI ≈ 8) when compared with a higher temperature exposure (SI = 11).

When considering a 20% increase of relative humidity at neutral temperatures, a slight change in the ANS response is obtained, especially a decrease in the parasympathetic tone (LF/HF = 1.04 for 50% RH; LF/HF=1.24 for 70%). Values above 60% are considered uncomfortable for indoor environments [241]. Although these experiments were carried out during short term exposures of 10-30 minutes, slight effects on HRV could still be observed when considering 70% RH. Consequently, a greater impact of RH would be observed with higher air temperature conditions, since higher levels of water molecules are also present in the air, which makes breathing more difficult.

The relation between the respiration rate and HRV has been evidenced mostly in the frequency-domain, when compared with the time-domain [242]. Parasympathetic branch activation is normally associated with a low respiration rate, where an increase of HF power and decrease of LF is obtained, which proves that slow-paced breathing shifts sympatho-vagal balance towards vagal activities [243]. This study also sought to analyse the relationship between the breathing rate in breaths per minute, performed with the BCG signal analysis and DWT, and HRV measurements were obtained for each environmental condition during the last 5 minutes. No significant differences were found between estimated respiration rates from these three different thermal environments ($p \leq 0.05$). Data regarding the respiration rate estimated with the system developed for each volunteer, as well as the ratio between LF/HF are shown in Figure 4.11.

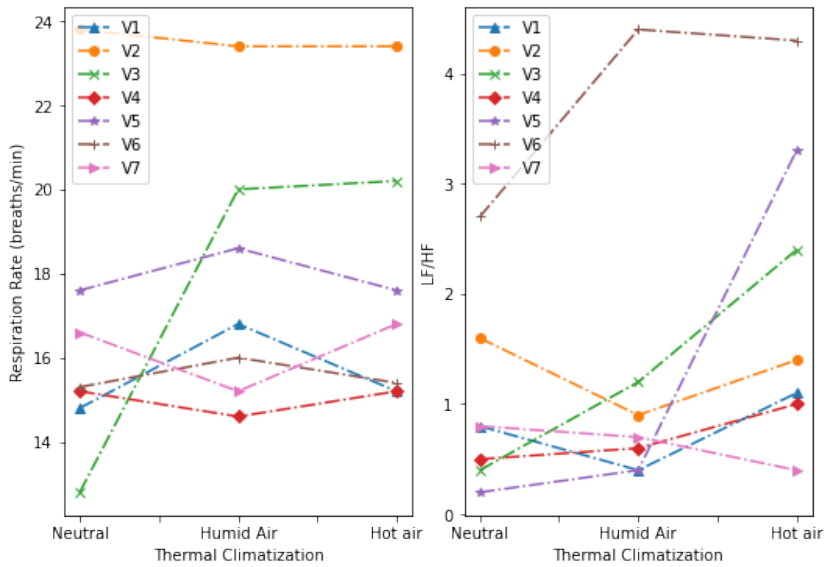

FIGURE 4.11. Respiration rate and LF/HF ratio for all volunteers under three different thermal climatizations.

It can be seen that for most of the volunteers, the average breathing rate rose slightly when comparing a neutral environment (24°C, 50% RH) with a more humid environment (70% RH). Still, three of those seven volunteers slightly lowered their breathing rate. Interestingly, all volunteers, not counting V3, maintained their breathing rate when compared with a neutral environment in a warmer

environment (30°C). When correlating the breathing rate with the ANS response, most of volunteers who presented a higher breathing rate, when comparing the first condition with the second one, also had a slight increase in the LF/HF ratio, which indicates greater sympathetic activity. In the same way, three of the seven volunteers who lowered their breathing rate also showed a lower LF/HF ratio, which proves the activation of the parasympathetic system in this scenario. Differences between results obtained for all different volunteers may be associated with different levels of well-being and climatic preferences, which differ from individual to individual. Regarding a warmer environment, although the respiratory rate was similar to that of a neutral one, the sympathetic system activation associated to the increase in LF/HF ratio was more pronounced in most cases, as previously analysed, and in this case, thermal stress induced by the heat, presented a greater impact on the well-being and thermal comfort of volunteers.

D. Comfort and Discomfort Classification based on Machine Learning

The degree of a person's discomfort can be derived from physiological responses expressed by changes in HRV indices, namely by a shift in sympathetic activity [244]. Therefore, a binary classification between comfort and warm-induced discomfort is considered in this part of the study.

In the data augmentation procedure using GAN, the number of generated samples was chosen to be the same number of real datapoints of each class (neutral, humid, hot). Figure 4.12 demonstrates the scatter plot of the original datapoints and the generated output using GAN at the initial training step and at the final training step. Mean HR and Mean RR features were selected for this comparison since both variables have a negative correlation.

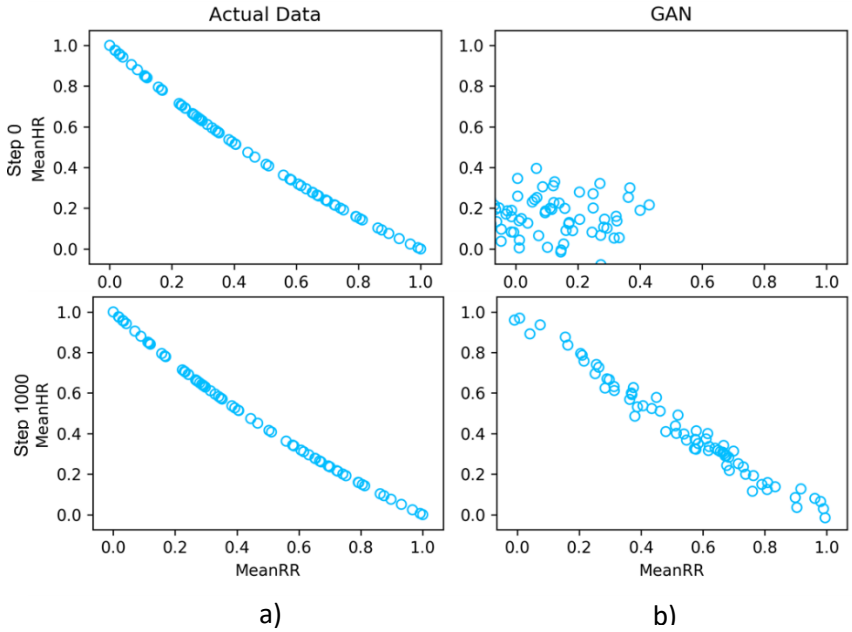

FIGURE 4.12. Comparison of a) original and b) GAN outputs at the initial training step and at 1000th training step

The GAN's ability to learn and replicate the pattern of both these features during training and predicting was quite efficient. The generated values at the 1000th epoch were quite similar to those of the original dataset for all features, as seen in Figure 4.12.

Synthetic data generation may not match entirely to the original data or may fail at capturing the different relationships between the dataset features. This is not completely undesired, since it is expected that generated data provides a certain percentage of dissimilarity in relation to the original data, especially when privacy is a fundamental right in health-related data and identity disclosure must be avoided [245]. However, the generated data must capture the inter-dependency between the characteristics of the features, as well as the distribution and statistical properties of the original dataset. Some metrics that can be used to assess the quality of a synthetic dataset are based on the use of heatmaps.

The heatmap presented in Figure 4.13 pictures the mutual dependencies between HRV features in the original dataset of humid environmental conditions and the generated dataset. A very close mutual dependency between the features of the real data and the synthetized one is achieved, as can be visualized by the similarity of colour distribution of the side-to-side heatmaps. This assured that the synthetized data could be used in the upcoming machine learning classification tasks. Good results were also achieved for the neutral environment conditions and hot air conditions datasets.

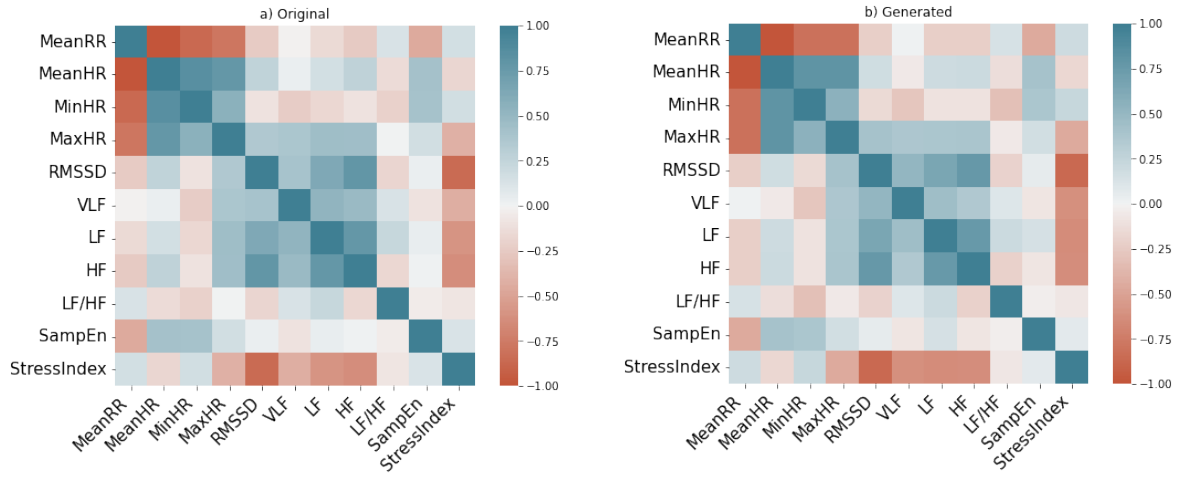

FIGURE 4.13. Comparison of mutual information between a) original and b) generated data features for the humid conditions' dataset

Figure 4.14 presents the average values of each analysed HRV parameter for both original and synthetized data in the neutral and humid conditions' datasets. The average values of the synthesized data for each parameter are very similar to the original values. This also confirms that the data utility of the generated dataset is expected to be high.

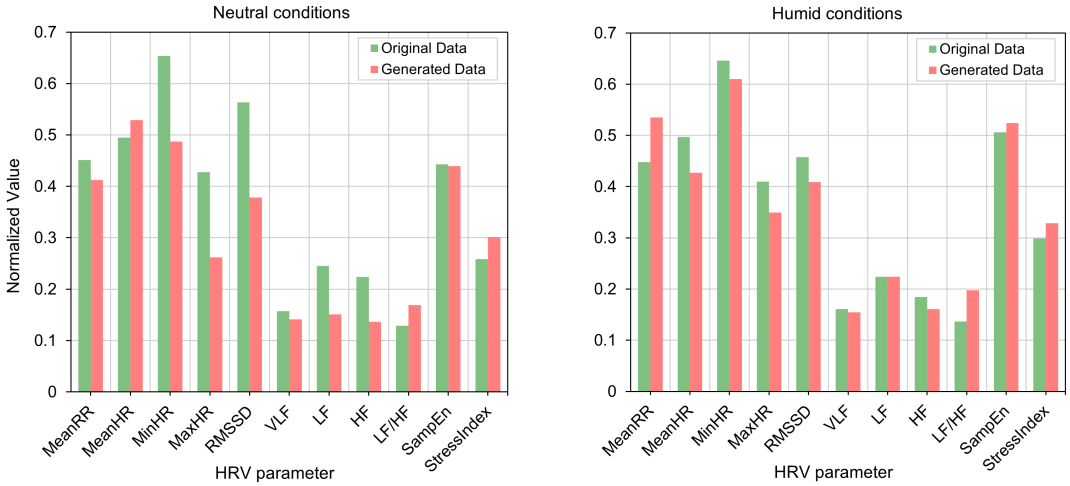

FIGURE 4.14. A comparison of original and synthetized data average values for each HRV parameter for a) neutral conditions and b) humid conditions

The ML models that were trained with original data only presented poor performance levels, having reached accuracy levels between 61%, for the case of LR, and 73%, for the RF.

Therefore, the synthetic data samples were combined with the original training data to create a more balanced and augmented training dataset for the ML classifiers. These models are going to be used to predict if the subject is on a thermally comfortable environment or in a discomfortable condition based on the HRV indices. The thermally comfortable environment is characterized by the neutral conditions (24°C) and relative humidity (50%), which are within the recommended levels of indoor temperature and humidity established by the WHO [220]. The discomfortable environments were characterized by indoor air temperature (>24°C) and relative humidity levels (>60% RH) that lie outside the recommended range [229]. Therefore, the binary classification was considered for two cases: to distinguish between comfort and warm-induced discomfort, and then between comfort and discomfort induced by high humidity levels.

The performance of SVM, DT, RF, KNN, LR and MLP algorithms for the first case are presented in Table 4.5. The algorithms were trained six times for the same dataset distribution, and a mean of the evaluation metric values for each classifier was calculated. Good model performances were achieved for all ML classifiers, except for the LR model, which presented lower performance (<70%). The KNN classifier provided the highest accuracy value of 86%, and the best F1-score of 0.867.

All ML models increased on average their accuracy by 17%, when compared to the original dataset without synthesised data.

TABLE 4.5. Performance of the ML algorithms for estimating comfort and discomfort under hot thermal conditions (24°C - 30°C)

Evaluation Metrics	SVM	DT	RF	KNN	LR	MLP
Accuracy	81%	75%	83%	86%	64%	80%
F1-Score	0.807	0.778	0.847	0.867	0.722	0.817
Precision	0.930	0.805	0.875	0.932	0.652	0.839
Recall	0.730	0.757	0.825	0.819	0.815	0.789

As for the binary classification between comfortable and discomfort induced by high humidity levels, presented in Table V, the algorithms were better at picking up the differences between both classes in general. The highest accuracy was again achieved by the KNN classifier, with a mean value of 88% of correctly classified instances and a mean F1-score of 0.892. Lower performances were achieved for both DT and LR algorithms. These results suggest that accurate predictions of whether the subject is on a thermally comfortable or discomfortable environment based on his HRV indices can be achieved with the use of ML classification algorithms.

TABLE 4.6. Performance of the ML algorithms for estimating comfort and discomfort under humid conditions (50% - 70%)

Evaluation Metrics	SVM	DT	RF	KNN	LR	MLP
Accuracy	77%	73%	84%	88%	73%	80%
F1-Score	0.809	0.731	0.853	0.892	0.759	0.817
Precision	0.733	0.801	0.846	0.899	0.712	0.812
Recall	0.927	0.682	0.867	0.891	0.836	0.857

4.1.6. Remarks

This study innovates when extending and improving on existing healthcare focused IoT systems using unobtrusive sensors for cardiac assessment to any indoor environment, while using the benefits of ML. We considered the analysis of temperature and humidity distribution in a real scenario, characterized by a non-isothermal office room. Simulations based on computational fluid dynamics were conducted to predict the air temperature distribution in this specific environment and to find the optimal location and number of temperature sensors to be distributed. Finally, physiological data was collected and analyzed under different conditions of temperature and humidity to ascertain possible changes in HRV associated with different levels of thermal comfort. For that purpose, the present study reports the development of a healthcare-IoT based system composed of an indoor environmental quality assessment, together with a cardiac and respiratory assessment layer based on PPG and BCG signal analysis.

Considering all three different thermal conditions, higher LF/HF was obtained under a short-term exposure to a hot environment at 30°C, which reflects thermal stress and activation of thermal regulatory activities by the autonomous nervous system. Although no significant changes in HRV were obtained for environments with different humidity levels (50%-70%), lower LF/HF were measured for a neutral environment of 50% RH when compared with more humid settings. This indicates that changes in ambient air temperature from a neutral to a hot environment led to the activation of thermal regulatory reflexes and thermal discomfort, perceived by an increase of LF/HF. Moreover, the respiratory rate extracted from the BCG signal was slightly higher in a more humid environment (70%) than on a neutral one (50%) for most volunteers. Evidence that respiratory rate is correlated with the ANS response was also verified in this study, when considering exposure to different thermal environments. Finally, supervised ML classification algorithms were used to create a model that can predict whether a person is at a thermally comfortable environment or discomfortable environments characterized by hot air or humid air conditions. The HRV parameters were used as inputs and the best results were achieved with the KNN classification algorithm, with 86% accuracy for the hot air thermal condition, and 88% for the humid air condition.

The study presented in this sub-chapter led to the publication of an article in a scientific journal: M. Jacob Rodrigues, O. Postolache, F. Cercas, (2022) "Unobtrusive Cardio-Respiratory Assessment for Different Indoor Environmental Conditions," in IEEE Sensors Journal, vol. 22, no. 23, pp. 23243-23257, 1 Dec.1, 2022 | https://doi.org/10.1109/JSEN.2022.3207522

4.2. How Stress Noise and Music Stimulation influences the Autonomic Nervous System

4.2.1. Overview

The adaptation of the surrounding environment to the physiological needs of its inhabitants has been one of the key objectives of smart environments. These environments are built around a sensor network that provides real-time data on environmental quality conditions, as well as the health status of an individual. The ability to process this data and act on it to improve the quality of life is what makes these solutions so indispensable, especially when considering their integration in ambient assisted living (AAL) environments [246]. These adaptations normally involve improving environmental quality conditions, such as air quality [247], thermal comfort, lighting comfort [248] and automation of some tasks. Additionally, the combination of auditory and olfactory stimuli has been proven to reduce anxiety levels, stress and even change emotional states [249], [250]. In fact, incorporating auditory stimuli into a smart environment, such as nature sounds and relaxing melodies, as well as other types of music, has been shown to be very beneficial for PRV and effective in lowering stress levels [251].

Stress is a physiological response resulting from the threat to body homeostasis upon exposure to extrinsic or intrinsic factors [252]. If this condition occurs only for a few minutes or hours, it is referred to as acute stress. A more serious condition where this stress state persists for days or even months is mentioned as chronic stress. The parts of the human body that are activated by stress and which will trigger all the necessary responses are the hypothalamic-pituitary-adrenal (HPA) axis and the autonomic nervous system [252]. The ANS is composed of two distinct divisions: the sympathetic nervous system and the parasympathetic nervous system [253]. Under a stressful condition, the sympathetic system is activated, generating an organism response that involves the release of hormones such as adrenaline and cortisol. In this way, the activation of this nervous system branch triggers a "fight or flight" response which increases the heart rate, lowers the PRV and inhibits the activity of certain organs, so that the organism can react effectively to dangerous and stressful events. On the other hand, activation of the parasympathetic system triggers a state of relaxation and unstress, presenting the opposite effects to those provoked by the sympathetic system - reduction of the heart rate, higher PRV, among others. The balance between these two branches is what maintains homeostasis in the human body.

One of the stress sources present in our daily lives is noise, and it is estimated to affect more than 95 million Europeans throughout the day [254]. It is a stimulus that can often be present without people realizing it, but which drastically affects our health, especially our nervous system balance. Continuous noise sounds triggers an acute stress response that will increase blood pressure and heart rate, which can then lead to serious health problems such as cardiovascular disease and cognitive impairment [255]. Other health-related symptoms that may be associated include loss of productivity at work, prevention of sleep (if these events happen during the night), and hearing loss. These emission sources are commonly present in urban areas, such as road vehicles, aircrafts, and even ventilation and air conditioning systems. Such sources emit low frequency noise (<500Hz), which propagates very efficiently. Similarly, higher frequency noises are equally present. Sounds as ordinary as flying mosquitos, whistles, glass breaking and even computer devices seem to pay a high price in our well-being and stress levels.

Therefore, the addition of music stimuli in an assisted living environment could bring valuable benefits to counteract all these effects induced by such common stress sources. Music therapy, for instance, is an approach known for helping enhance psychological and physiological relaxation [256]. These methods are not only suitable to stifle or silence external noises, but also for rehabilitation purposes.

A way of ascertaining the effects that these different auditory stimuli can have in our health is based on the analysis of the nervous system balance. This can be achieved with the collection of real-time physiological data by using biomedical sensors. This physiological data provides information about the nervous system balance, such as the sympathetic branch activity, associated with stress, anxiety or excitement, and parasympathetic activity, associated with relaxation and low heart rate levels [253]. The assessment of the ANS balance is generally done through heart rate variability (HRV) analysis, or pulse rate variability, which is based on the study of the time variation between two consecutive heartbeats. Such information is derived from cardiovascular signal analysis that can be achieved through many different techniques.

The biomedical devices used for such monitoring in an AAL scenario, for instance, are based on non-obtrusive and easy-to-use techniques. The photoplethysmography (PPG) technique has proven to be a great alternative to the standard electrocardiogram (ECG) when considering HRV analysis [257], [258]. For example, long-term monitoring of cardiac activity using ECG can be quite discomfortable, since wet electrodes, or Ag/AgCl electrodes, must be used, leading to possible skin irritation after several hours of use. Moreover, the multiple lead wires for connecting the 3 or more electrodes of the ECG can affect the daily activities of an individual, and affect stress levels [246].

4.2.2. Study contributions

This study addresses the utilization of the developed physiological monitoring system suitable for AAL systems, and mentioned in Chapter 3, as well as the exploration of short-term effects of music and noise sounds on HRV. More specifically, it intends to:

1. Validate the wearable sensor node based on the PPG acquisition technique for real-time monitoring of HRV parameters.
2. Perform a preliminary study of the influence of music sound stimulation on HRV of healthy subjects in order to verify if this stimulus can indeed be beneficial to the user's well-being.
3. Provide a comprehensive study of the effects of short duration noise as well as different music types on the balance of the nervous system to investigate the possible use of these methods to reduce stress levels. The addition of time-frequency analysis-based processing and electrodermal activity acquisition (EDA) to assess the impact of these different stimuli will be considered.
4. Estimate stress levels caused by auditory stimuli through the implementation of machine learning algorithms.

4.2.3. Methods

A total of 17 participants (6 females and 11 males) aged 23 to 55 years old (mean age: 34.8 ± 13 years) were enrolled in this study. A preliminary study was conducted in January of 2022, and a more comprehensive study was conducted between August and September 2022. Participants were enrolled after informed consent and were briefed about the study's objectives and methods. They had no health issues and did not ingest alcohol or caffeine all day long. They were seated in a relaxed upright position and under spontaneous breathing during all experimental sessions. In these studies, the developed wearable PPG sensor node (1st prototype) was used for HRV monitoring, alongside a Shimmer3 ECG sensor for validation purposes. Additionally, the Shimmer3 GSR+ unit was used for measuring electrodermal activity. The positioning of the ECG electrodes was mentioned in Chapter 3. The sensor from the PPG wearable sensor node was placed on one hand's index finger, and the GSR electrodes were placed on the index and middle finger of the other hand.

The study consisted of two distinct phases: a music selection phase and the experimental session. The first phase took place four months before the start of the experimental sessions. In this part, all participants were assigned a short duration listening experience of five song excerpts, approximately 60 seconds in length, from ambient, classical, and metal music genres.

The choice of songs involved a selection criterion that was based on music *tempo*, measured in beats per minute (bpm). This term is used to designate the rhythm and speed of music and was considered since it is one of the most important characteristics of a musical piece, and which may influence a person's emotional state.

For classical music, five music pieces with a medium tempo of 76-108 bpm (*Andante*) were selected. The fast-paced metal music pieces were aimed for having a faster *tempo* of >160 bpm (*Presto*). This selection criterion was not considered for ambient music. After each session, participants completed a questionnaire involving the following questions, rated from one to five: 1) How much did you like this music example; 2) How familiar was this music to you; 3) How calming was this music sample for you. At the end of each music genre demonstrations, participants chose the music they preferred, out of those five. The classification of the preference for each music piece can be seen in Figure 4.15.

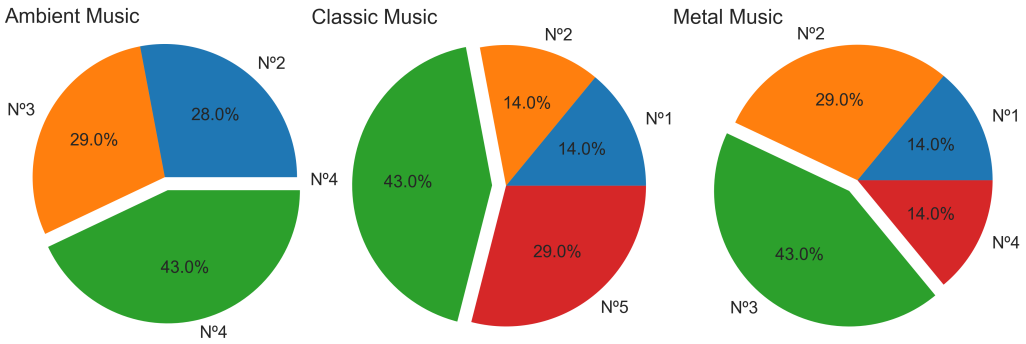

FIGURE 4.15. Classification in terms of preference of each music piece for the three musical genres. (Music pieces with 0% of preference are not depicted).

This listening experience and music selection was to ensure that the majority of the participants enjoy the music considered in the experiments. Listening to music that one dislikes can evoke negative emotions and create an aversive experience. This can result in feelings of discomfort, frustration, or annoyance. In this way, a consensus was reached between all parties involved and the songs selected for each musical genre were those that were most voted for by the participants.

Figure 4.16 shows the results of the above mentioned questionnaire for the selected musics, in order to obtain the participants' feedback regarding their reactions and emotions felt while listening to the music piece. At this preliminary stage, the subjective feedback demonstrates that ambient music induced a greater sense of relaxation for all participants compared to classical music. It is also possible to verify a greater preference for the ambient and classical music than for the metal music, which seems to be the less appreciated musical genre among the others involved. Moreover, this genre provided the lowest sense of relaxation, as expected. In the end, the preference for each music piece is due to the positive effects it induces. In the case of ambient and classical music, participants chose the music piece that induced more relaxation, while in metal music, the most important factor was the familiarity with the music.

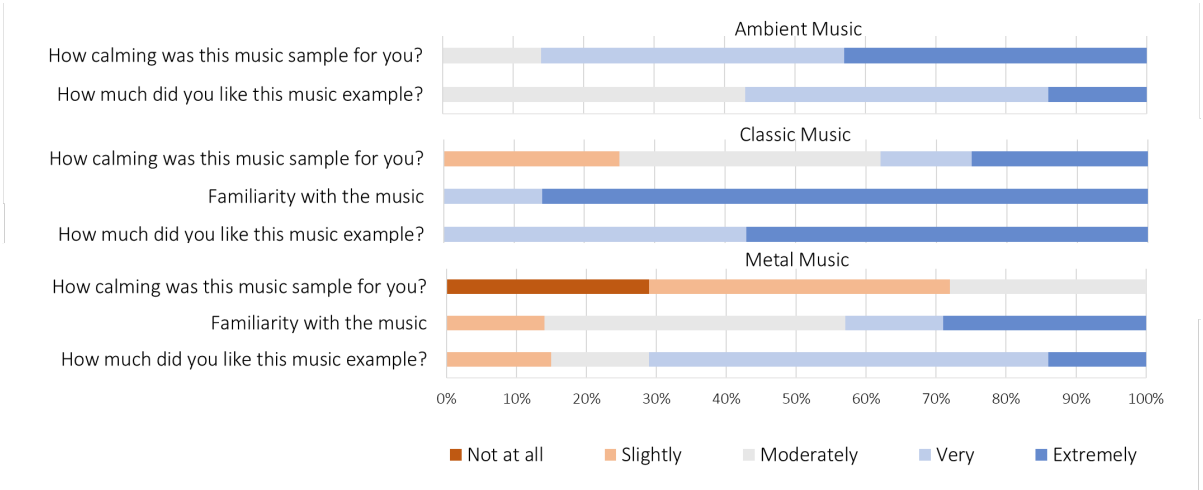

FIGURE 4.16. Results from the subjective feedback questionnaire for the preferred music pieces

Following the music selection phase, the experimental session involved a total of six exposures to auditory stimuli, as represented in the experimental schedule in Figure 4.17. The first session was a silent or “no-music” session without any auditory stimulus. This was done, not only to stabilize the heart rate, but also to obtain baseline HRV values.

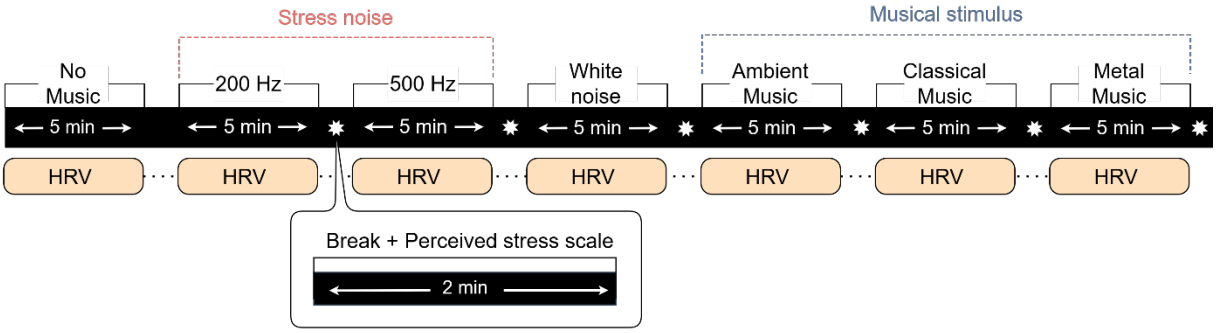

FIGURE 4.17. Experimental schedule for the comprehensive study on the influence of stress noise and three different music genres on HRV

During all sessions, participants watched a continuous calm video, simulating a space travel, transmitted by a television placed 1.40 m away from their seats (Figure 4.18). The surrounding environment was kept dark throughout the duration of the experiment, eliminating as much as possible any additional stimuli other than the auditory.

The sessions that followed the “no-music” session were the stress noise sessions. First, a sound was emitted at a frequency of 200Hz by two speakers positioned in front of the participant, at about 1.60m. The sound was emitted only for 3 min, to prevent possible hearing damage. The physiological data continued to be collected for the remaining 2 min, making in total 5 min of PRV measurements. The same happened with the higher frequency 500 Hz noise session, which took place 2 min after the end of the previous session. In the following session, white-noise was emitted for 5 min. The stimulus sessions following stress-noise were musical stimulus sessions.

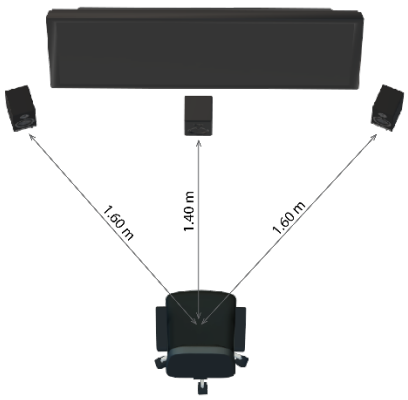

FIGURE 4.18. Setup of the experimental scenario: two speakers on each side, subwoofer and a TV in the center

Before starting the experimental sessions, an analysis of the intensity levels of the sound emitted by the speakers was made. A sound level meter, Tenma ST-95, was used for this purpose. This device has a measuring range from 35dBA to 130dBA, works with frequency ranges from 31.5Hz to 8 kHz, and features 3dBA accuracy, with 0.1dBA resolution, as well as Bluetooth communication capabilities. The device was placed at the position where the participants would sit. This was done to measure sound pressure levels approximately the same way as the human ear and determine the most correct sound level for the experiment. The maximum, minimum and average dBA measured during all sound stimuli are displayed in Table. 4.7.

TABLE 4.7. Maximum, minimum and average sound levels measured during each sound exposure sessions

Session	Max (dBA)	Min (dBA)	Avg (dBA)
200 Hz	65.2	46.7	59.8
500 Hz	72.5	46.7	69.4
Ambient Music	75.3	49.7	64.3
Classical Music	77.5	46.1	60.7
Metal Music	76.6	62.8	72.0

Figure 4.19 displays the real-time measurement of dBA during the five minutes of ambient, classical and metal music sessions.

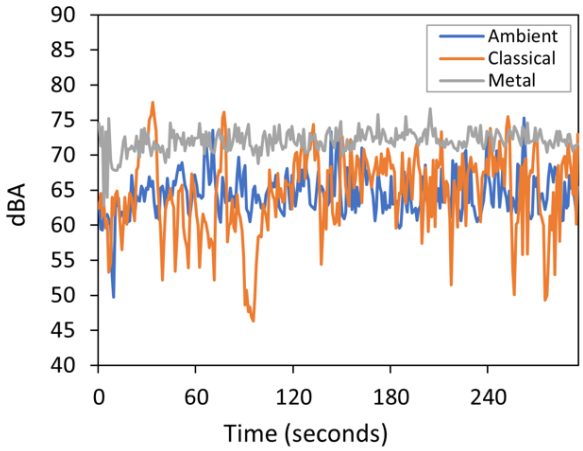

FIGURE 4.19. Measurement of sound levels (dBA) during ambient, classic and metal music session

As in the first study, the order in which the musical genres were emitted was: ambient music characterized by nature sounds and a harmonious background melody (Relaxing Music with Nature Sounds – Waterfall, from Youtube [259]), followed by classical music (The Blue Danube, Op. 314, by Johann Strauss II) and finishing with metal music (Creeping Death, Metallica).

A two-minute break was taken between all stimulus sessions. During these breaks, a perceived stress scale questionnaire was given to each participant as a mean of assessing their subjective evaluations of comfort feeling and stress levels. From a scale ranging from one to five, where one expresses no agreement with that statement, three is a neutral decision and five corresponds to total agreement, the following questions were made: 1) How happy were you during this period; 2) How stressed did you feel during this period; 3) How calm did you feel during this period; 4) How sad were you during this period. The results will be shown in sub-section 4.2.5.

4.2.4. Wearable PPG sensor node validation

The first goal of this study was to compare the time-domain PRV analysis computed by the developed wearable sensor node with the HRV obtained with a 5-lead ECG monitor. In this section, the PRV data collected in the three different music stimulation sessions is analysed. Each device signal acquisition technique recorded 21 samples in total. Mean values and standard deviation among the different PRV parameters for each device were calculated and are presented in Table 4.8. Pearson's correlation coefficient was employed to measure the degree of correlation between the values obtained with the developed node and the validation node during sessions.

TABLE 4.8. HRV during rest periods: Values obtained with the developed wearable PPG sensor node and the ECG validation node

HRV	**Time-Domain Analysis**		**Correlation (*r*)**
	Mean ± SD		
	Developed Node (PPG)	Validation Node (ECG)	
Mean HR (bpm)	82.9 ± 5.7	79 ± 4.2	0.936
Max HR (bpm)	100.1 ± 15.2	100.2 ± 7.9	0.386
Mean RR (ms)	721 ± 45.7	765 ± 39.9	0.931
SDNN (ms)	93.4 ± 52.7	66 ± 5	0.837
RMSSD (ms)	58.6 ± 31.8	43.1 ± 20	0.838
NN50	49.9 ± 37.6	53.8 ± 50	0.635

The Pearson's correlation plots of RMSSD and mean HR values are presented in Figure 4.20. During all sessions, the developed sensor node showed statistically significant correlations ($r > 0.7$, $p < 0.05$) for mean HR, mean RR, SDNN and RMSSD variables. However, maximum HR showed minimal correlation (r = 0.386), which could be motivated by incorrect readings from the PPG sensor, either due to light interference or caused by hand movements.

All the analysed time-domain PRV indices were correlated, apart from the maximum HR and NN50, which presented mean differences with the PRV indices from ECG. These results confirm that the use of the developed sensor node based on PPG is valid for HRV analysis during rest for most metrics.

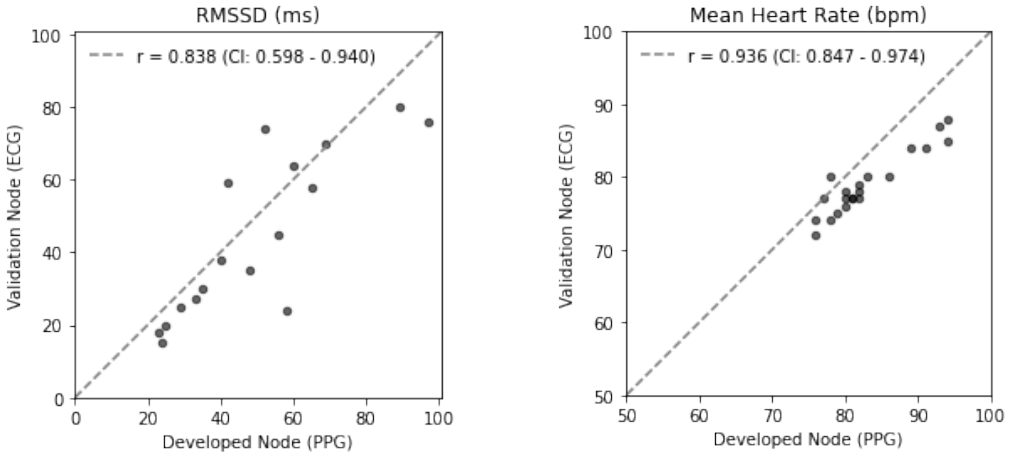

FIGURE 4.20. Pearson's correlation of RMSSD and mean Heart Rate obtained from the developed node (PPG) and the validation node (ECG).

4.2.5. Experimental Results and Discussion

This sub-section addresses the results of the comprehensive study on the effects of stress noise and musical stimulation on physiological functions of the human body, as well as an estimation of stress induced by auditory stimulus based on the implementation of ML algorithms.

A. Effects of Stress Noise and Musical Stimulation on HRV

The preliminary study, which took place in January 2022, allowed us to observe an influence of musical stimuli on the cardiac variability and, consequently, on the autonomic nervous system, as reported in [260]. This more comprehensive study, that involved the implementation of a new experimental protocol as depicted in Figure 4.16, took place between the months of August and September. The average temperature of the room where the experiments were carried out was 23 °C. All participants went through the same sequence of sessions. One of the participants presented a very noisy PPG signal at the 200 Hz session which did not allow a correct analysis of the HRV and therefore the corresponding measurements were not considered for this specific case.

In Table 4.9, the results of the perceived stress questionnaire associated with each participant after each stimuli session are presented. In this way, a subjective evaluation of the subject's comfort feeling, and stress levels was considered, which will later be correlated with the objective measurements collected by the biomedical sensors. In the stress noise sessions, most of them had a neutral evaluation. However, the high-frequency noise session (500Hz) was the one presenting the worst results in terms of stress felt by the participants, which on average felt quite stressed and unhappy during this session. In the opposite way, and as expected, the ambient music session was the one that most stimulated feelings of comfort and happiness.

Similarly, classical music appeared to cause no level of discomfort to most participants. Interestingly, metal music also had a very positive rating regarding the feeling of comfort, with most of them, except for volunteer 5 (V5) and 10 (V10), not experiencing stress levels associated with this session.

TABLE 4.9. Results of the perceived stress questionnaire for each session (Mean ± SD)

200 Hz	**500 Hz**	**White Noise**	**Ambient Music**	**Classic Music**	**Metal Music**
1 - How happy were you during this period?					
3 ± 0.7	2 ± 0.8	3 ± 0.7	4 ± 0.9	3 ± 1.8	3 ± 1.4
2 - How stressed did you feel during this period?					
3 ± 1.1	4 ± 0.6	3 ± 1	1 ± 0.6	2 ± 1.7	2 ± 1.2
3 - How calm did you feel during this period?					
3 ± 1.2	2 ± 1.2	3 ± 1.2	4 ± 0.7	3 ± 1.7	3 ± 1.3
4-How sad were you during this period?					
2 ± 0.9	2 ± 0.9	2 ± 1.2	2 ± 1.2	3 ± 1.9	2 ± 0.8

This explains in advance the good receptiveness of this participants group to various styles of music. Looking at the individual results of the questionnaire, only two of the participants were unhappy during the classical music session. Similarly, another two participants reported not enjoying the metal session, feeling somewhat stressed and unhappy (e.g., V7 and V10). These results demonstrate a diverse range of musical preferences in the group, consistent with the experimental design and its purpose.

A summary of the mean values of HRV parameters obtained for all the sound stimulus sessions is presented in Table 4.10. To evaluate the impact of noise sounds and different types of music on the ANS, the PRV analysis comprises time-domain, frequency-domain and non-linear parameters. A t-test method was applied to measure statistically significant differences on PRV results between the baseline session, also referred as “no-music”, with all the other sessions. A p-value of ≤ 0.05 was considered statistically significant.

TABLE 4.10. Mean of the PRV parameters for all sound stimulation sessions and t-test results

HRV	No Music	200 Hz	*p - value*	500 Hz	*p - value*	White Noise	*p - value*	Ambient Music	*p - value*	Classic Music	*p - value*	Metal Music	*p - value*
Time-domain analysis													
Mean PPi(ms)	776	780	(0.30)	778	(0.45)	753	(0.14)	772	(0.406)	758	(0.14)	767	(0.35)
SDNN (ms)	107	99	(0.32)	99	(0.10)	103	(0.268)	108	(0.477)	99	(0.23)	94	(0.18)
SDSD (ms)	162	139	(0.22)	138	**(0.01)**	143	**(0.049)**	136	(0.066)	140	(0.11)	123	**(0.05)**
NN50	240	221	(0.36)	234	(0.37)	237	(0.435)	232	(0.348)	227	(0.29)	212	(0.20)
PNN50	62	57	(0.40)	61	(0.38)	60	(0.392)	59	(0.315)	57	(0.18)	54	(0.18)

RMSSD (ms)	152	130	(0.20)	131	**(0.02)**	135	**(0.051)**	145	(0.391)	140	(0.25)	113	**(0.03)**
Mean HR (bpm)	80	79	(0.25)	79	(0.44)	82	(0.185)	80	(0.471)	81	(0.21)	80	(0.41)
Max HR (bpm)	128	131	(0.36)	120	(0.29)	126	(0.375)	119	(0.138)	119	(0.11)	122	(0.24)
Min HR (bpm)	53	50	(0.18)	52	(0.48)	53	(0.432)	54	(0.366)	53	(0.48)	52	(0.38)
Frequency-domain analysis													
LF (ms^2)	1738	1826	(0.38)	2581	(0.12)	2625	(0.212)	2862	(0.143)	2627	(0.18)	2254	(0.287)
HF (ms^2)	2432	2238	(0.41)	2149	(0.16)	2290	(0.327)	3881	(0.225)	3160	(0.27)	2009	(0.32)
LF/HF	0.91	1.23	(0.17)	1.20	**(0.03)**	1.19	(0.119)	1.02	(0.272)	1.06	(0.28)	1.41	(0.11)
Non-linear analysis													
ApEn	1.178	1.025	-	1.156	-	1.039	-	1.174	-	1.118	-	1.073	-
SampEn	1.725	1.540	-	1.670	-	1.531	-	1.681	-	1.503	-	1.441	-

The low-frequency noise exposure of 200 Hz did not appear to cause significant alterations on PRV, although, on average, an increase of LF/HF ratio was measured between this stress noise session and the "no music" session. The RMSSD decreased in both low and high-frequency noise exposure sessions, though the effect was not statistically significant.

As for the white noise exposure scenario, the average HR and LF components were the highest among all stress noise exposures, as seen in Figure 4.21. Significant differences were also found for SDSD and RMSSD. The highest value of ApEn was denoted for the "no-music" session, which means that the complexity of PRV was higher during a period where no external stimuli was induced.

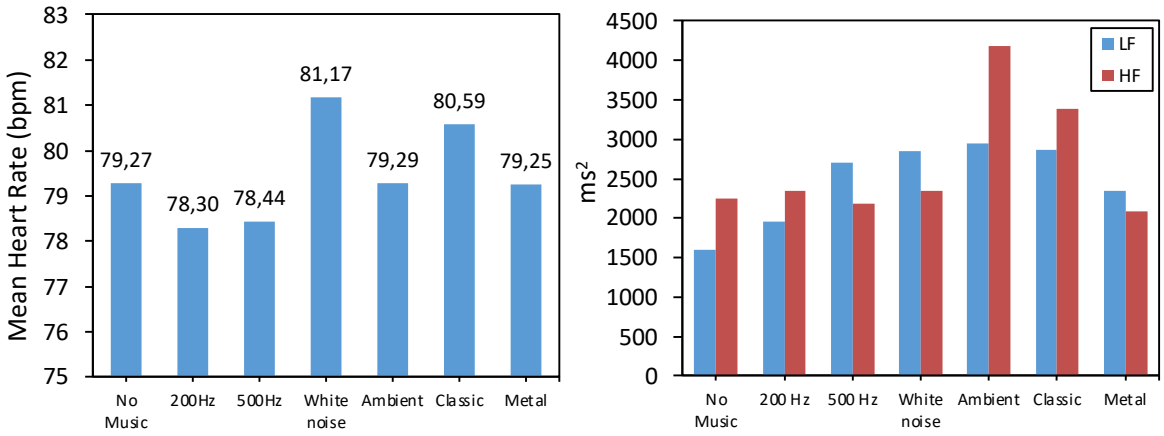

FIGURE 4.21. Mean heart rate and mean LF and HF component for all sound exposure sessions

Stress recovery seemed to happen during ambient music exposure, even though the session took place two minutes apart from the stress noise sessions. During the ambient music scenario, the LF/HF ratio values decreased. The HF power was the highest among all sessions. This indicates a parasympathetic recovery associated with a relaxing music scenario involving sounds of nature and harmonious melodies, and it comes in line with the sensations of calm and happiness that most participants felt during this period, as reported in the questionnaire.

During classic music exposure, the LF/HF preserved the lowest values following ambient music and "no-noise" sessions. Apparently, the values recorded with both ambient and classical music seem to indicate a feeling of comfort in general, when compared to the other auditory stimulus sessions. The PRV decreases to its extent during metal music exposure. The LF/HF reached the maximum values, and SDSD and RMSSD decreased significantly. Even though most volunteers did not feel stressed while listening to this type of music, the balance of the nervous system was evidently altered, and there was a higher prevalence of LF power over HF power when compared to all other sessions, including stress noise. The results observed here somehow resemble the results obtained by Nakajima et al. [71], who also observed an increase in LF/HF by stress-inducing noise, in this case, scratching board sounds.

Figure 4.22. shows the individual results for LF/HF ratio values for 10 volunteers. Most of the volunteers who said enjoying the metal type of music showed higher LF/HF values when compared to the other musical stimulus sessions. Only two of the ten volunteers reduced the ratio between the LF and HF component. The beforementioned volunteers were already well-acquainted with the music, so its melody, harmony and rhythm were quite familiar, which may explain the increase in the HF component. This comes in line with the observations made by Kirk et al. [55] regarding having familiarity with the music. It is possible that having a taste for that music genre activates the sympathetic nervous system since a certain excitement can be experienced when listening to a melody, namely a fast-paced music like this one. As expected, classical music would elicit a greater presence of the sympathetic system when compared to ambient music, for the same reasons stated above, since 70% of the people who said having felt happiness and calm during this music presented higher LF/HF values. This could help to prove the hypothesis that the LF component does not reflect sympathetic and vagal activity, which has been considered in several studies, but it can possibly represent both sympathetic and parasympathetic branches of the nervous system.

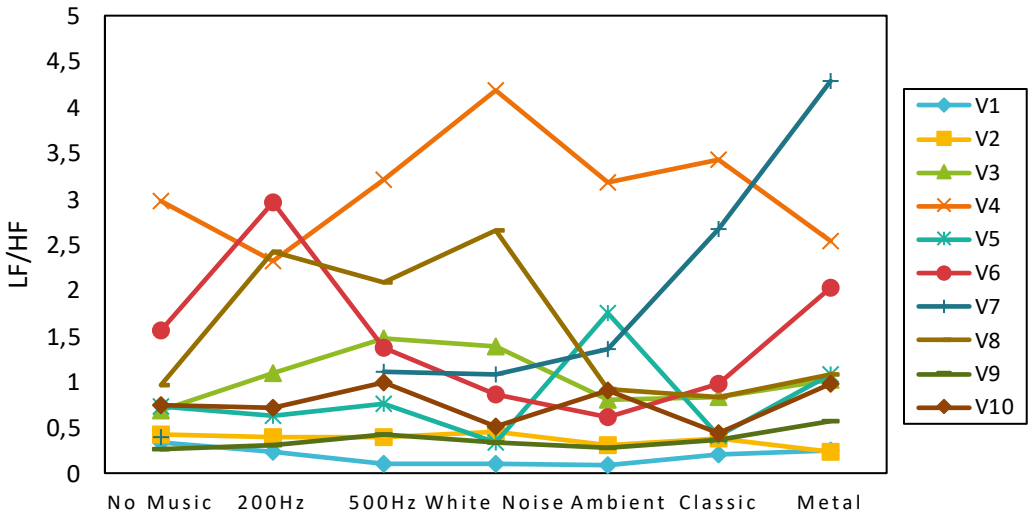

FIGURE 4.22. Individual LF/HF values for all sound exposure sessions

Regarding noise stress, all volunteers who confessed a very high feeling of stress and discomfort in the first 200 Hz session (e.g. V6, V8) showed an increase of the LF component in comparison to the previous silent session. Regarding the 500Hz session, only two participants showed lower values of LF compared to the initial session.

B. The Effects of Music Tempo in the Perception of Classic and Metal Music Genres

The characteristics of the music itself have a strong impact on its perception and the emotional effects it may bring to its listener. These characteristics can be based on the *tempo*, rhythm, pitch, timbre, and melody of the music piece. In addition to the study that was conducted, we wanted to find out whether the sympathetic activity of the ANS was stimulated by the different music tempos, or by the genre itself. Thus, an additional experiment which features exposure to classical and metal music genres with the same tempo, preceded by a 5-minutes "no-music" period, was conducted. The study had the participation of 6 of the 17 volunteers that were part of this experiment. Both classic and metal music pieces were selected to have a fast-paced tempo (160 bpm). The music pieces that follow these criteria were Creeping Death, by Metallica for the metal session, and Symphony No.45 in F-Sharp Minor, by Joseph Haydn for the classic music session. The HRV measurements obtained are present in Table VI.

TABLE 4.11. Mean of the PRV parameters for the three experimental sessions

HRV	No Music	Classic (160bpm)	Metal (160 bpm)
Time-domain analysis			
Mean PPi (ms)	835	808	823
SDNN (ms)	117	84	97
SDSD (ms)	126	87	105
NN50	167	151	136
PNN50	46	40	37
RMSSD (ms)	126	87	105
Mean HR (bpm)	74	76	75
Frequency-domain analysis			
LF (ms^2)	4297	1960	2151
HF (ms^2)	3208	1589	1773
LF/HF	1.2	1.3	1.5
Non-linear analysis			
ApEn	1.115	1.199	1.083
SampEn	1.461	1.665	1.486

The individual results of LF/HF ratio for the 6 volunteers are presented in Figure 4.23. There was a decrease in LF/HF following the classic music exposure. Moreover, when comparing both music sessions, the average LF/HF was higher for the metal music relative to classic music, even though the average tempo of both music genres are equal. Due to the variations in musical genres and their impact on the autonomic nervous system, exposure to metal music was likely to result in a larger LF/HF ratio than exposure to the classic music piece, as we verified in the previous study. The metal music piece is a fast-paced and intense heavy metal song that would stimulate the sympathetic nervous system most likely.

The classic music piece, on the other hand, is distinguished by its contrasting sections and variations in rhythm, dynamics, and tone. While it may still have an influence on the autonomic nervous system, it is likely to be less intense and stimulating than the metal music.

As mentioned earlier, the effect of music on the autonomic nervous system and PRV varies widely across individuals and is influenced by factors such as mood, stress levels, and personal preferences. With this experiment, we can conclude that the activation of the sympathetic branch and the possible appearance of some type of stress is mostly due to music genre itself, rather than the tempo.

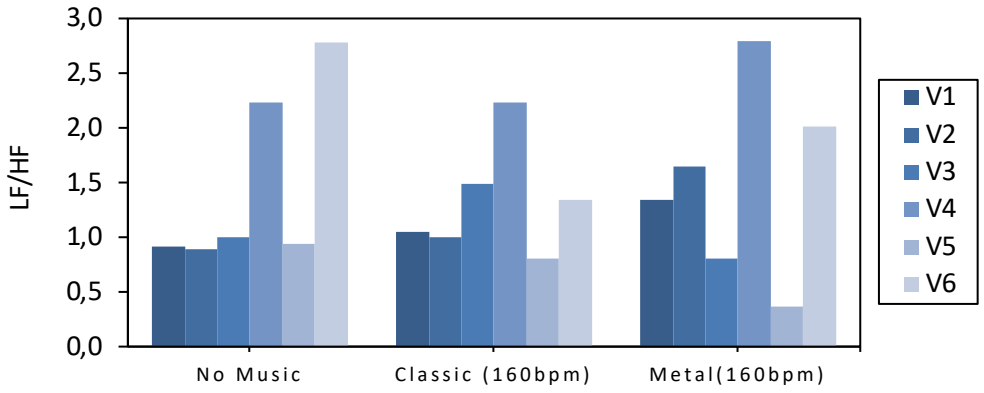

FIGURE 4.23. Individual LF/HF values for a music session of Classical and Metal music genres with 160bpm *tempo*

C. Implementation of Time-Frequency Analysis for HRV Assessment

An additional signal processing technique based on STFT was considered. We wanted to test an alternative way to obtain more valuable information about the ANS modulation over time, since the PSD computed by the FFT does not provide information about power distribution across a given period. The STFT technique allows to separate the signal into its constituent frequency-components and observe how they change over time.

Since PRV contains relevant information about the functioning of the nervous system through the analysis of both frequency and time domain information, STFT is used mostly to quantify the spectral properties of PRV, such as the power spectral density and the power distribution along the different frequency bands. In this way, the low frequency components of the PRV (0.04 to 0.15 Hz), associated with sympathetic activity, and the high frequency components (0.15 to 0.4 Hz), associated with parasympathetic activity, can be quantified by analyzing the power distribution along the different frequency bands of the STFT spectrogram. In this way, it is also possible to observe the activity of both branches of the ANS throughout a period.

We employed STFT to estimate the spectro-temporal variations of the VLF, LF and HF components of the PPi series for the different music stimulation sessions. LabVIEW 2022 Q3 was used for this purpose. The STFT was calculated for the whole range of the music session, which was 300 seconds long. Figure 4.24 shows the spectrograms obtained for V10 for the following sessions: No-music, Ambient, Classic and Metal music session, using a Hanning type window with a length of 64s. The FFT spectrum is also represented. This participant reported feeling a higher level of stress and discomfort during exposure to metal music, since it was an unappreciated music genre. On the other hand, the subjective feedback showed that the exposure to classical music brought a higher level of relaxation and happiness, for being a music genre quite appreciated by the participant.

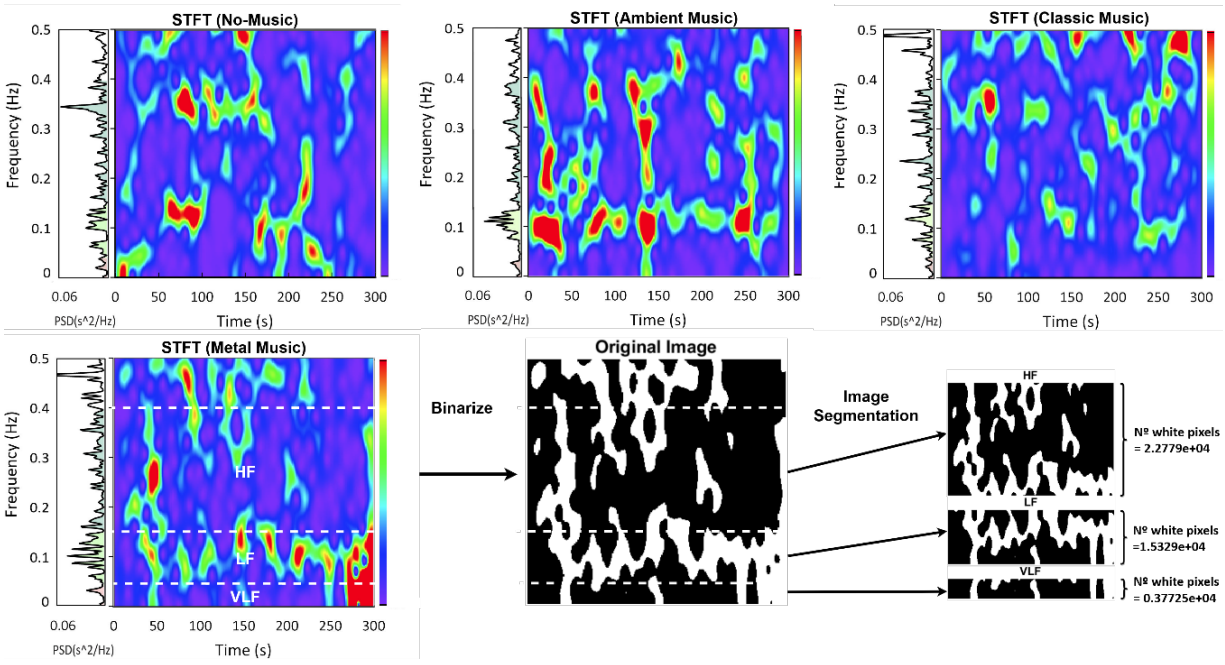

FIGURE 4.24. STFT spectogram analysis of the PPi time series for V10 during no-music, ambient, classic and metal music sessions (Hanning window, 64s window length). An image binarization of the spectrograms was applied to measure the number of white pixels related to higher spectral power density in each frequency band (VLF, LF and HF).

The spectrograms show a clear difference between Metal and Classic music exposure. Visually, it is possible to observe a great contrast in the low frequency band between these two spectrograms: the STFT referring to metal music has higher power density levels than in the classical music one.

To convert these observations into objective metrics, we considered the following procedure: first, the quantification of power distribution in each frequency band, which is used to reflect the level of activity of the parasympathetic and sympathetic branches of the ANS, was performed using an image processing technique with MATLAB R2022b. The technique consisted in converting the spectrogram to a binary image, exemplified in Figure 4.24. After this conversion, it is possible to visualize the more significant spectral power densities as white pixels ("1") and the less significant as black pixels ("0"). A global image threshold of 0.27 was used for the image conversion. The threshold value is proportional to the mean of the power scale of the spectrogram. In this way, we guarantee that the binarized spectrogram accurately reflected the presence or absence of valuable frequency components, regardless of the differences in their relative strength.

Then, a segmentation of the binary spectrogram image into the different frequency bands: VLF, LF and HF, was made. For each band, the number of white pixels present in that segment was calculated to obtain a numerical value of the power spectral differences between each frequency band. For this participant, the values obtained for each frequency band for the metal music session are shown in Figure 4.24.

A comparison between the power distribution in the binarized images and the LF and HF power values obtained using FFT are presented in Table 4.12.

TABLE 4.12. Mean of the PRV parameters for the four experimental sessions calculated using the STFT and FFT objective measures

PRV	**4. No Music**	**Ambient**	**Classic**	**Metal**
Power distribution in binarized STFT spectrogram				
LF (nº white pixels)	5.07e+03	6.68e+03	5.29e+03	5.35e+03
HF (nº white pixels)	1.20e+04	1.03e+04	6.77e+03	5.72e+03
LF/HF	0.42	0.65	0.78	0.94
Frequency-domain analysis based on FFT				
LF (ms^2)	1738.00	2862	2627	2254
HF (ms^2)	2432	3881	3160	2009
LF/HF	0.91	1.02	1.06	1.41

For instance, by analyzing the power distribution of the binarized STFT spectrogram, the LF/HF ratio was 0.42 for the no-music session, indicating a greater degree of parasympathetic activity. In the case of metal music, the ratio was 0.93, therefore indicating greater sympathetic dominance. Although the values obtained from the two methods differ, as different mathematical algorithms are being used by each method, the general pattern of LF and HF power distribution across the four conditions is relatively similar, indicating that the effects of different types of music on the ANS balance are consistent regardless of the method used for analysis.

D. Electrodermal activity acquisition for assessing the impact of different musical *stimuli*

GSR signals were collected to measure the intensity of emotions felt in response to the music listened to during each session. Such emotions are difficult to differentiate from being positive or negative, e.g., stress, thus, only the emotional stimulation caused by the music will be interpreted. Since the skin conductance is modulated by the sympathetic activity of the ANS, it will be possible to determine with more precision the instants in which it had more activity. Since the electrical conductivity of the skin increases with the emotional arousal, in a reciprocal way, the increase of the skin resistance will indicate the opposite.

The following figures show the GSR signals of one of the volunteers, V7. During the musical stimulus sessions, V7 presented greater LF/HF alterations according to the different types of music when comparing to the other volunteers. In this way, a comparison will be made between these variations, marked by an increase in the LF component, with the changes in the skin conductivity. In Figure 4.25 to Figure. 4.27 the GSR signal and its phasic component are represented. The phasic component allows to see the fast variations occurring in the GSR signal, referred as skin conductance responses (SCR). In these figures, we present the filtered GSR signal and the phasic component of V7 across the full extent of the ambient, classical and metal music sessions respectively. The melodic range spectrograms of ambient, classical and metal music, respectively, are also shown.

The melodic range spectrogram is designed to facilitate the identification of particular musically significant characteristics. In this way, we intend to correlate the changes of the SCR, and in turn of the activation of the sympathetic system, in response to the significant changes of rhythm and melody present in the music.

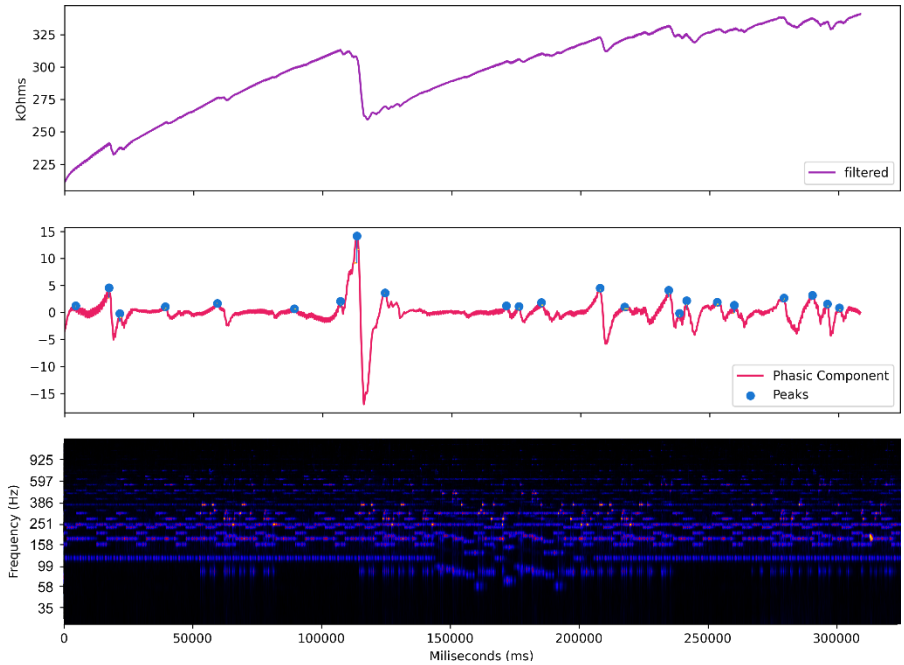

FIGURE 4.25. GSR signal and its phasic component for volunteer V7 during Ambient Music

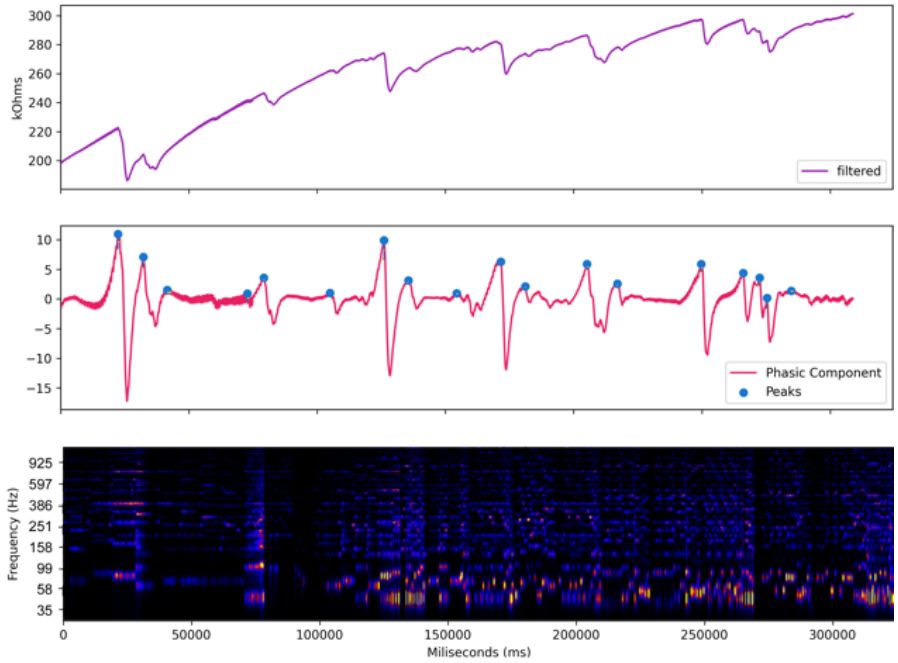

FIGURE 4.26. GSR signal and its phasic component for volunteer V7 during Classic Music

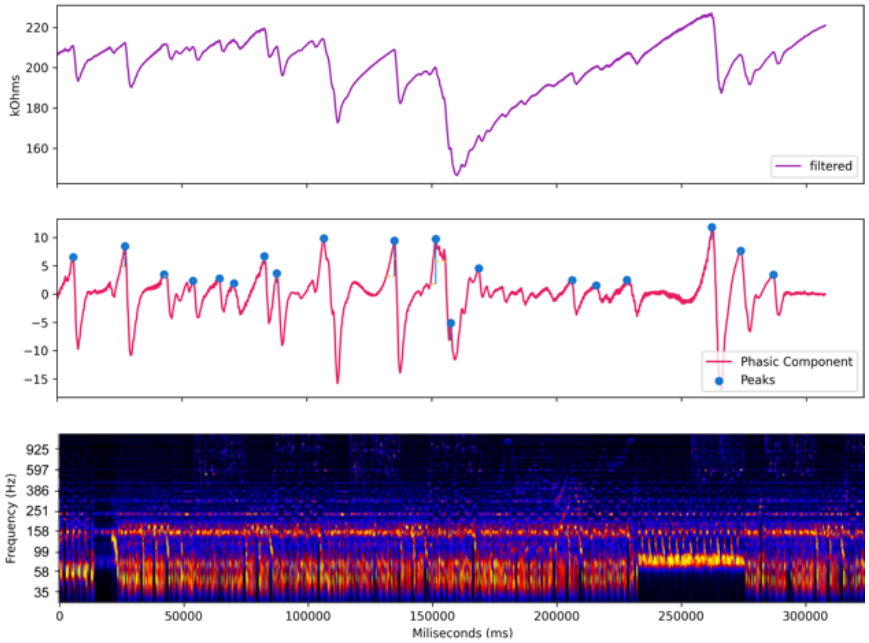

FIGURE 4.27. GSR signal and its phasic component for volunteer V7 during Metal Music

From ambient to classical music, an increase in the amount of rapid fluctuations of the skin conductivity was denoted in response to a greater amount of stimuli present in the Blue Danube classical music. It is possible to see the increase in skin conductivity according to the rhythm changes of the music as represented in Figure. 4.26. This indicates an activation of the sympathetic system upon the introduction of important musical events. If this is a music piece that the participant enjoys, as was the case, then these sympathetic system changes reveal positive emotions rather than emotions associated with stress. In an AAL scenario, this positive association can improve the person's well-being through the introduction of music sounds of their musical taste. When targeting patients with dementia, namely Alzheimer's, the introduction of these positive stimuli can bring many positive benefits - both emotional and behavioural. How these stimuli affect the patient may be analysed through the use of these methods.

In Figure 4.27 it was possible to verify a greater stimulation of the sympathetic nervous system by the fast-paced metal music. The melodic spectrogram presents a larger quantity of important events demarked by heavy instrumental parts and the phasic component of the signal presents many sudden alterations in the electric conductivity of the skin, which reveals more changes in autonomic arousal. Therefore, it was possible to associate the changes in the LF component with the variations in the electrical conductivity of the skin throughout the different types of music.

D. Estimation of Stress Induced by Auditory Stimulus based on Machine Learning Algorithms

There are still quite a few research works that are intended to perform automatic music selection based on the user's physiological response [64], [261]. Having assessed and evaluated the impact of different musical stimuli on HRV measured with the wearable sensor, future implementations of the proposed system are aimed to automatically introduce or change music genres in the surrounding environment by the means of a speaker or wearable audio devices, according to the user's physiological state and PRV at that moment. This aims to help change emotional states and reduce the feeling of stress of AAL inhabitants, thereby improving their well-being. For that purpose, some machine learning algorithms best suited to deal with small datasets were tested. A set of physiological data from 10 participants containing PRV measures for all auditory stimulus sessions was used. A total of 60 instances with 12 features (mean PPi, SDNN, SDSD, NN50, PNN50, RMSSD, mean HR, maximum and minimum HR, LF, HF and LF/HF) and a binary target was considered at first. The target consists of the subjective evaluations given by each participant in the questionnaire concerning their emotional state or stress felt during a given session. As preprocessing steps, data normalization and feature selection were applied, to discard irrelevant features. In this way, only five out of twelve features were used in the training process of the algorithms. As a binary classification problem that aimed to classify between "feeling stress" or "not feeling stressed" four different machine learning algorithms were considered: RF, DT, SVM and KNN. All classifiers were implemented in Python using the Scikit-learn machine learning library. A cross-validation technique was used to train the algorithm, with 4 folds in total. The 4-fold cross validation achieved better classification results when compared with other values of k. The performance metrics obtained for the models are presented in Table 4.13.

TABLE 4.13. Accuracy, precision, F1-score and recall values obtained for the four classification algorithms in a 4-fold cross validation

Evaluation Metrics	**RF**	**DT**	**SVM**	**KNN**
Accuracy	71.18%	69.24%	56.34%	69.95%
F1	0.516	0.571	0.108	0.514
Precision	0.571	0.551	0.186	0.632
Recall	0.487	0.635	0.087	0.426

The Random Forest was the one giving higher accuracy results, having achieved 71.18% accuracy when predicting the feelings of stress based on the PRV features. Decision trees and k-NN presented similar results, with 69.95% accuracy. The poorest results were obtained with SVM, which only achieved an accuracy of 56.34%. This was expected since it is an algorithm that does not perform well when the dataset contains overlapping targets, which was the case. Because most of the PRV parameters did not have significant differences between the subjective classification of having or not having feelings of stress, the algorithms will hardly achieve more desirable results. To improve the accuracy results and overcome the limitations encountered in this classification problem, a greater number of volunteers and an improvement of the hyper parameters of the machine learning algorithms will be considered in the future work.

The results presented in this study provide several advantages that make significant contributions to the field, such as the development of an innovative biomedical wearable system for cardiac assessment and the analysis of the autonomous nervous system balance based on HRV. This healthcare focused IoT system was designed to be perfectly suited for implementation in smart homes and ambient assisted living environments. The development of the hardware, software for HRV analysis and data visualization, as well as the implementation of ML algorithms for classification of the stress state derived from musical stimulation, make this system stand out from others reported in the literature. Moreover, an alternative technique was used for analysing the activity of the nervous system and quantifying the spectral power density of high and low frequencies over time, using STFT spectrograms and image processing techniques. This approach sets this work apart from others that often rely on the analysis of the nervous system balance based on the quantification of frequency domain parameters based on FFT. It is important to note that the tests were conducted in an experimental setting that closely resembles a home environment, providing more real-world relevance and practicality.

4.2.6. Remarks

The relations between musical stimuli and noise stress and autonomic nervous system balance were studied, providing interesting results. A preliminary study phase to ascertain the effects of music sound stimulation based on three different music genres – ambient, classic, and metal - on PRV in healthy volunteers was carried out. It was observed that there is an increase of sympathetic activity during metal music session, when compared with classical music. The preliminary results showed that further studies were needed with the inclusion of a no-music rest period, a stress inducing experience based on unwanted noise sounds exposure, an extended number of volunteers and the monitoring of additional physiological parameters. In this way, a more comprehensive study was made with ten volunteers, which involved short-duration sound noise stimulation – 200Hz, 500Hz and White Noise - as well as musical stimulation. New physiological parameters characterized by skin conductivity were acquired to better understand emotional changes that may occur during sound exposures and better comprehend sympathetic nervous system modulation. The findings showed that stress noise contributes to an increase in sympathetic activity. Ambient music, on the other hand, was shown to be particularly beneficial in enhancing parasympathetic activity and regulating comfort levels. Moreover, it was possible to conclude that the activation of the sympathetic branch and the possible emergence of some type of stress is mostly related to the music genre itself, rather than the tempo. The study also addressed the use of supervised ML classification algorithms to create a model that could estimate feelings of stress induced by auditory stimulus. The HRV parameters were used as inputs and the best results were achieved with the RF classification algorithm, with 71,18% accuracy. Finally, the development of a wearable wireless sensor node based on the PPG acquisition technique for real-time monitoring of PRV parameters in the time domain was studied and reported. Its validation was performed using a reference ECG smart sensor, and good correlation results for the PRV parameters of both devices were obtained, enabling its use in AAL scenarios.

The study presented in this sub-chapter led to the publication of an article in a scientific journal:
M. Jacob Rodrigues, O. Postolache and F. Cercas, (2023) "The Influence of Stress Noise and Music Stimulation on the Autonomous Nervous System," in IEEE Transactions on Instrumentation and Measurement, vol. 72, pp. 1-19, 2023, Art no. 4006819 | https://doi.org/10.1109/TIM.2023.3279881

4.3. The Influence of Virtual Reality Serious Games on the Autonomic Nervous System

4.3.1. Overview

The acquisition of vital signs throughout the practice of physical exercise has served as an important measure that follows the subject's physical performance avoiding accidents related to high level of exercise intensity.

Since it is possible to have a robust assessment of a patient's health status using wearable sensors, its use during physical exercising has been extensively studied. In the current context, and due to COVID-19 pandemic and the corresponding containment measures adopted during 2021, the year where this study was made, the practice of physical exercise at home was especially valued. Moreover, physical therapy sessions were suspended in clinics due to coronavirus lockdown, so the patients requiring physical training (e.g., limb strength, resistance, body balance) should practice rehabilitation exercises at-home. In this context, exergaming – a system that combines physical exercise with digital gaming – has been shown to bring positive benefits to a patient's physical and cognitive conditions, and help individuals maintain the recommended levels of physical activity. In addition, virtual reality (VR) serious exergames that are focused on physical rehabilitation may constitute a complementary tool of physiotherapy sessions. The highly engaging and immersive scenarios help patients to stay motivated while executing rehabilitation exercises imposed by the game.

4.3.2. Study Contributions

This study addresses the monitoring of HRV changes in adults while experiencing VR serious gaming of different time duration and exercise intensity. Moreover, the application of artificial intelligence algorithms to classify the VR serious game intensity levels is also considered.

More specifically, the present study sought to investigate:

(1) The variance in HRV indices during a VR rehabilitation serious game considering different intensity levels.

(2) The variance of HR levels characterized by a more complex gameplay session of different time durations.

(3) How artificial intelligence methods can be used to estimate the different intensity levels of the game based on wearable sensor data and subjective measures.

4.3.3. Methods

A VR serious game specifically tailored for upper limb rehabilitation was used for this investigation. This system has been developed and reported by Postolache et al. [262]. It was developed using the Unity3D game engine and relies on a Microsoft Kinect platform for real time detection of the upper limbs' joint angles, thus allowing the user to interact with the VR scenario. The Kinect platform has been shown to be a highly reliable rehabilitation platform, as it can accurately measure upper and lower limbs' joint angles during rehabilitation exercises [21] – [23]. The virtual scenario of this game is expressed by a virtual farm. The main objective of this game is to pick-up fruits placed randomly at different heights from surrounding trees and shrubs, which assures different ranges for the upper limb motion. The objects can be reached by left hand, right hand, or both, depending on the chosen game settings for the training session. The upper limb movements executed by the player are detected by the Kinect platform and reproduced in the game's avatar (Figure 4.28).

The game has two different gameplay modes: a) high-angles (90°-180°), with apples being placed on trees and 2) low-angles (0°-90°), with raspberries being placed on shrubs. Different difficulty levels, namely higher or lower intensity, can be implemented based on the gameplay mode, the movement speed of the avatar and the number of fruits to be harvested. Different audio-visual stimuli are available during gameplay to motivate players, including different immersion levels, such as farm sounds, animals, and other elements, and performance feedback, like a positive sound when a fruit is picked.

FIGURE 4.28. Gameplay of the used VR serious game for upper limb rehabilitation

The participants of this study were 6 healthy adults, 3 males and 3 females aged 24.6 ± 1.9 years old, weighting 64 ± 16 kg, with heights around 176 ± 9 cm and body mass indexes (BMI) 20.3 ± 3 kg/m^2. All participants enrolled in the gaming sessions after informed consent. 4 volunteers were already familiar with the game mechanics and the Kinect platform. Details regarding the purpose and procedures involved in this study, as well as an explanation of the game's instructions and objectives were given before the gameplay session. A Borg rating of perceived exertion (RPE) scale was used as a subjective measure to assess exercise intensity during each game session, along with a Subjective Units of Distress Scale (SUDS) with a scale of 0-100 for measuring the level of distress and anxiety felt during each game session.

The participants enrolled in two sessions of this serious exergame. Each session presented different difficulty/intensity levels. The first was based on a higher intensity level, in which game configurations were set for the high angles' mode, increased number of fruits to pick up, large number of stimuli and the need to stay in a standing position during all gameplay (Figure 4.29 a)). The second session was based on a less intense level, in which game settings were set to a lower angles' mode, slow-paced avatar, less stimuli and finally, participants were seated during gameplay (Figure 4.29 b)).

a) b)

FIGURE 4.29. Gameplay of the VR serious game in a) high angles mode and b) low angles mode.

Physiological measurements were collected for different experimental conditions (Figure 4.30). Prior to the first game session, all participants sat in a relaxed upright position under spontaneous breathing for 5 minutes. In order to investigate the effects that a gameplay of different time durations has on HR levels, participants consecutively played the higher intensity game mode 3 times: the first one for 1 minute, the second for 2 minutes and the third for 4 minutes.

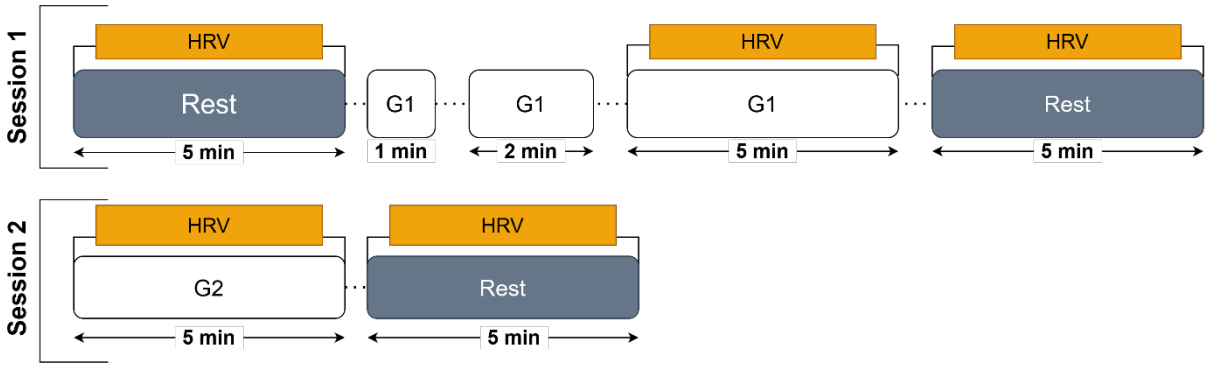

FIGURE 4.30. Experimental schedule for Session 1 (higher intensity level) and Session 2 (lower intensity level), and the respective HRV recording periods.

These 3 conditions were only applied for the first session, since this is the session intended to induce higher exertion levels and fatigue. After the 4 minutes gameplay, participants were asked to sit and stay calm and silent for 5 minutes, so that physiological signals could return to a resting-state. The second session took place 5 minutes after the first one, and all participants were invited to sit and play the low-angles game mode for 4 minutes. While they were seated, 5 minutes of physiological data was acquired after the game ended. HRV analysis was performed during periods of 5 minutes, according to the standard of short-term recordings [263].

Physiological data was collected using an ECG sensing module based on the wearable Shimmer 3 ECG sensor, described in Chapter 3. This compact and small module facilitates its usage as a wearable module without compromising the comfort and movements of the participants while experiencing the games. LabVIEW software was used to configure the Shimmer module and collect the ECG data, which was then saved in a local file for later processing. Figure 4.31 shows the VR serious game setup (high-angles gameplay mode), as well as the placement of the AgCl electrodes (RA, RL, LA, LL and V1).

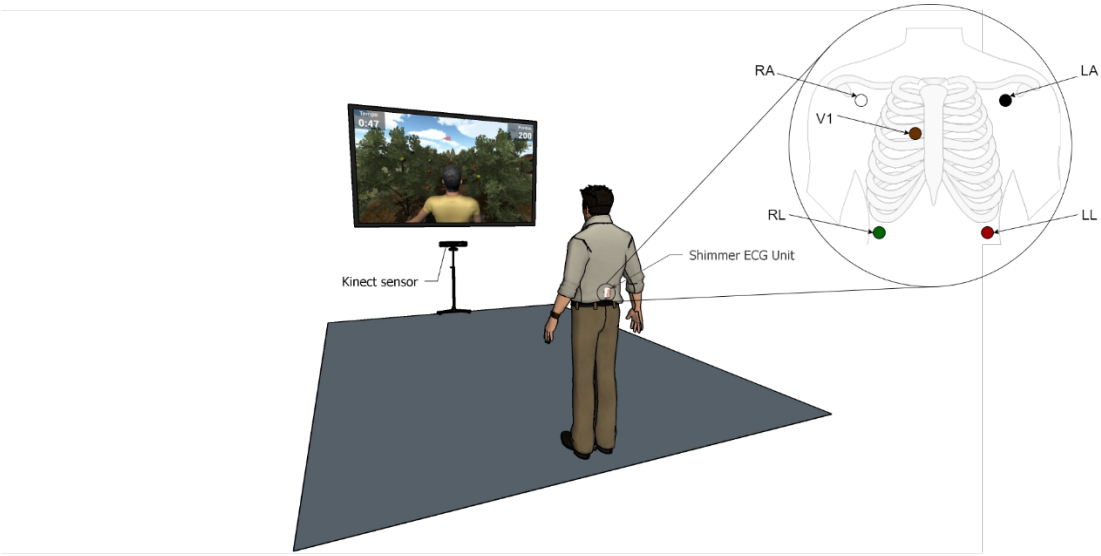

FIGURE 4.31. VR serious game setup including a Kinect sensor and a physiological wearable sensor (Shimmer ECG unit). Positioning of the electrodes for a 5-lead ECG measurement.

The ECG signal pre-processing was made offline on a personal computer using an open-source Python library [264], as was already mentioned in Chapter 3. For this specific study, the data analysis based on HRV was performed with the Kubios HRV Software (ver. 3.3) [265]. Time-domain and Frequency-domain parameters were considered in this study, as well as the quantification of the Stress Index. The time-domain variables included were mean R-R interval, mean HR, SDNN and RMSSD. For the frequency-domain analysis, low frequency (LF, 0.04-0.15 Hz) and high frequency (HF, 0.15-0.40 Hz) components were selected. The Baevsky's stress index (SI), a geometric measure of HRV, was also assessed using Kubios.

4.3.4. Experimental Results and Discussion

A. Variance in HRV indices during different intensity levels

The obtained HRV values for the different experimental sessions are presented in Table I. A one-way analysis of the variance (ANOVA) was separately performed to compare the means and to identify significant changes in HRV measures between different conditions: the higher difficulty gameplay versus easier level gameplay; between resting-period after the gameplay or both difficulty levels, as presented in Table 4.14; and between rest-period (Control) and the gameplay period of each session. A p-value of ≤ 0.05 was considered statistically significant.

TABLE 4.14. Mean and standard deviation (SD) of HRV parameters for each game session and one-way ANOVA results

HRV Parameters		**Control (Pre-Game)**	**Session 1 (Higher Intensity)**	**Session 2 (Lower Intensity)**	***P*-value**
Time – Domain Analysis					
Mean HR (bpm)	*during*	82 ± 5	99 ± 9	86 ± 9	**≤ 0.05**
	post		86 ± 10	83 ± 6	0.59
Max HR (bpm)	*during*	93 ± 6	112 ± 8	97 ± 9	**≤ 0.05**
	post		101 ± 11	97 ± 7	0.53
Mean RR (ms)	*during*	737 ± 44	613 ± 51	709 ± 67	**≤ 0.05**
	post		706 ± 79	726 ± 47	0.65
SDNN (ms)	*during*	52 ± 14	42 ± 28	47 ± 12	0.86
	post		46 ± 13	51 ± 20	0.55
RMSSD (ms)	*during*	49 ± 30	45 ± 51	36 ± 19	0.72
	post		37 ± 20	46 ± 34	0.62
Frequency - Domain Analysis					
LF/HF	*during*	2.6 ± 1.7	4.8 ± 3	5.4 ± 4	0.78
	post		2.9 ± 2	2.7 ± 1.4	0.92
Stress Index	*during*	8.9 ± 2	11.5 ± 4	8.2 ± 3	0.22
	post		9.4 ± 4	8.3 ± 3	0.62

These tests revealed that the gameplay of higher difficulty and intensity (Session 1) induced significant alterations on the average HR levels ($p = 0.004$) and maximum HR ($p = 0.001$) when compared with rest-period (Control) measures. Such significant alterations are observable in the boxplots of Figure 4.32. Low and high frequencies did not show any statistically significant changes (LF: $p = 0.06$, HF: $p = 0.07$). The HR response during the exercise of higher difficulty showed an increase of approximately 17 bpm for all volunteers when compared with the Control group. Moreover, the ratio between low and high frequencies (LF/HF) increased twice the value measured in the control group, which indicates sympathetic activation during the exergaming experience.

Regarding the gameplay session of easier difficulty levels (Session 2) and the Control group measures, there were no significant alterations on HRV parameters. This was expected as the volunteers remained in a relaxed sitting position throughout the whole session. Additionally, the game was physically less demanding since it did not present the same levels of complexity, stimuli, and the need for a faster-reaction time as in the higher difficulty mode. However, although not significantly, LF/HF ratio seemed to be higher during gameplay of Session 2 than on Session 1. This may be explained by the protocol followed, as presented in Figure 4.30. The gameplay of Session 2 occurred right after a resting-period, whereas on Session 1 the HRV analysis during gameplay (4 minutes) was performed right after volunteers played the 1 minute and 2 minutes gameplay sessions. Being accustomed with the game's mechanics of that specific difficulty level may also have helped to reduce stress in participants and decrease the sympathetic tone.

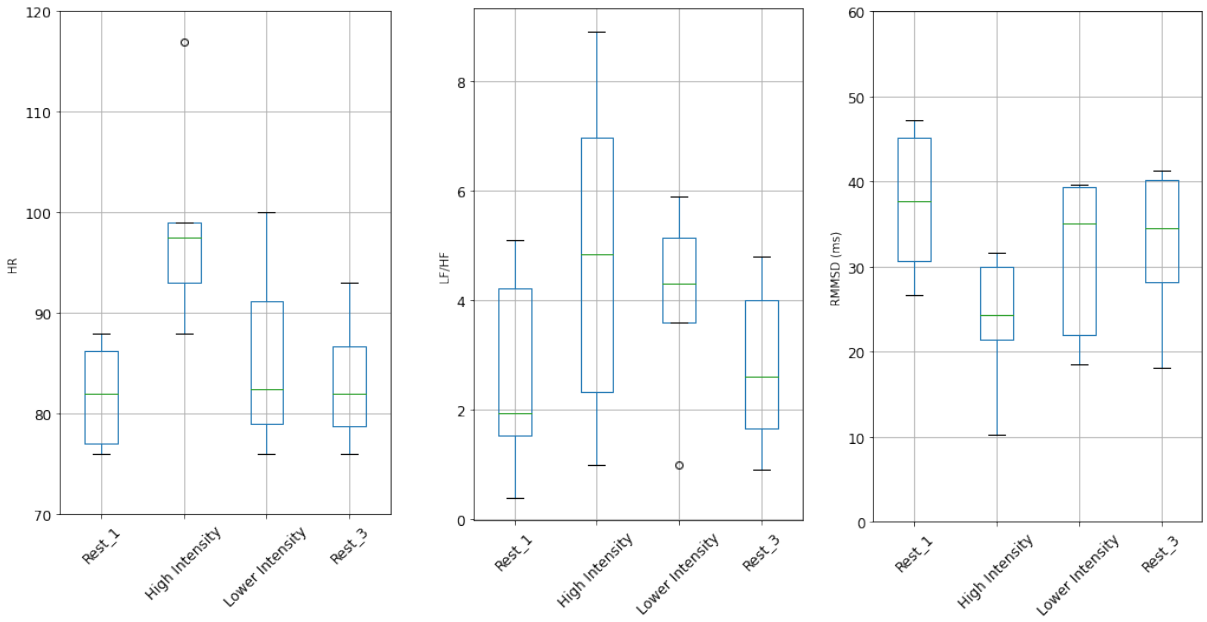

FIGURE 4.32. Box plot of mean HR, LF/HF and RMSSD values for all sessions

One-way ANOVA on the difference between the gameplay of different difficulty levels from both sessions revealed significant main effects on the average HR ($p = 0.04$), maximum HR ($p = 0.02$) and HF power ($p = 0.04$). HF components were much higher during the easier difficulty game level (HF = 597 ± 750 ms^2) than on the higher intensity one (HF = 251 ± 214 ms^2). Thus, parasympathetic stimulation decreased the cardiac output. Moreover, the stress index remained lower and almost at the same level as that obtained for rest periods. No significant interaction of different game complexities on RMSSD ($p = 0.72$) and SDNN ($p = 0.86$) and LF ($p = 0.34$) parameters was found.

During the recovery phase of the lower difficulty/intensity gameplay characterized by a reduced limb motion range, which lasted for 5 minutes, the majority of HRV parameters – HR, SDNN, LF/HF - regained almost the same values registered on pre-exercise/resting periods. On the other hand, the higher intensity gameplay revealed lower parasympathetic recovery after the exercise.

As a complement to the obtained physiological measures, subjective measures were also obtained from volunteers to assess exercise intensity and distress/anxiety levels felt during each gameplay session. Exercise intensity, as assessed by a Borg rating of perceived exertion (RPE) scale, was considered very low for both rehabilitation games (Session 1: 9.8±2; Session 2: 9±3). The volunteer's impression on distress and anxiety assessed by a Subjective Units of Distress Scale (SUDS) was higher for Session 1 (Mean = 28.3) when compared with Session 2 (Mean = 20), which is in accordance with the obtained stress index levels values and LF/HF ratio variation among the different sessions.

B. Variance of HR levels during a more complex gameplay with different time durations

The variance of HR parameter during the more complex gameplay from Session 1 (high-angles gameplay mode) was compared for three different time intervals of 1 minute, 2 minutes and 4 minutes. This study allowed to verify if gameplays of different time periods induce changes on cardiovascular activity and if a longer game duration requires higher levels of effort from the subject. For an HRV analysis of equal time segments, the last 1 minute of each gameplay duration was considered. Only time-domain parameters were examined in this study phase: mean HR, RMSSD and SDNN. As a directly correlated measure of HF power, the RMSSD parameter gives insights of parasympathetic activity during these shorter-term recordings [263].

A one-way ANOVA revealed no significant changes on HRV parameters between 1 minute and 2 minutes gameplay. The same was also verified between the 1 minute and 4 minutes gameplay duration. Heart rate levels remained constant between the three gameplay sessions (Mean=94 bpm). RMSSD levels got slightly higher as the gameplay duration increased, as seen in Figure 4.33 (Mean = 21 ms for 1 min; Mean = 24 ms for 4 min). As a parameter that is correlated with HF power and parasympathetic activity, these values of RMSSD corroborate the explanation given in the previous sub-section, regarding the measurement of a lower LF/HF ratio in Session 1 when compared to session 2.

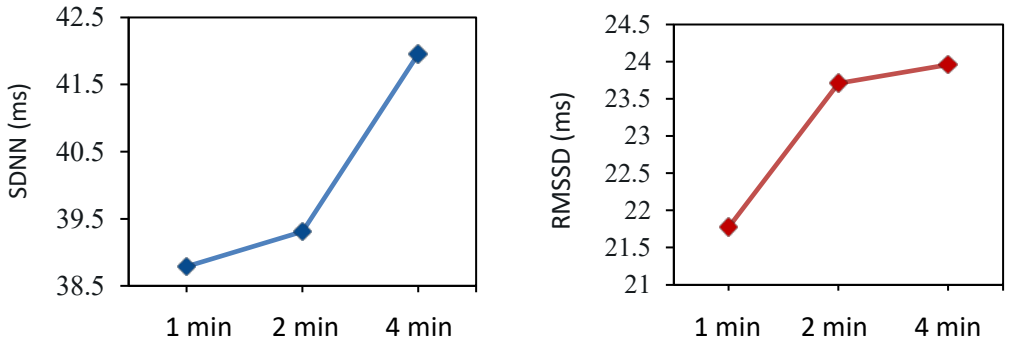

FIGURE 4.33. SDNN and RMSSD values for 3 different gameplay durations: 1 min, 2 min and 4 min

C. Classification of Game Intensity Levels based on Machine Learning Algorithms

Various classification algorithms were investigated for predicting the game complexity/intensity levels according to the participants' HRV. Considering remote physiotherapy sessions based on this VR serious exergame, this classification can help the physiotherapist keep track of the participant's performance and assess which type of upper limb rehabilitation exercises, low angles, or high angles, are being executed, to check whether a patient is following the imposed training plan or not. Moreover, if a certain game intensity level is misclassified, e.g., a lower intensity game is classified as has a high intensity one, it may reveal that HRV levels selected are not at the most appropriate level. Thus, the imposed rehabilitation exercise may not be recommended for a particular patient and the physiotherapist should re-adjust the rehabilitation plan. A set of physiological data from 6 subjects containing HRV measures during a 4-minutes gameplay of two different intensity levels was created. The dataset comprises 8 features (HR, maximum HR, mean RR, SDNN, RMSSD, LF, HF and Stress Index) and a target, which is game intensity. For binary classification purposes, three different machine learning algorithms were considered in this study: SVM, KNN and DT. All classifiers were implemented using the Python programming language and Scikit-learn machine learning library. Pre-processing steps included label encoding of the prediction target, therefore converting categorical values that defined the game intensity into "0" (lower) and "1" (higher). A local outlier factor was (LOF) applied for identifying and removing outliers in the dataset. Considering the limited data samples, a cross-validation technique based on k-fold cross-validation was applied for estimating the performance of our model, since the common train/test split method could exclude data points with useful information during the training phase. A 4-fold cross validation was considered regarding the total number of samples present in the dataset and the achievement of better classification results when compared with other values of k. The obtained performance metrics for our model are presented in Table 4.15. From the three classification models, KNN provided the highest classification accuracy of 81% for the predicting game intensity level, and 0.789 for the best F1-score when compared with the other models.

TABLE 4.15. Accuracy, precision, F1-score and recall values obtained for the three classification algorithms in a 4-fold cross validation

Evaluation Metrics	SVM	KNN	DT
Accuracy	72%	81%	77%
F1-score	0.714	0.789	0.639
Recall	0.729	0.812	0.667
Precision	0.792	0.792	0.575

4.3.5. Remarks

This study aimed to explore how virtual reality exergaming experiences can be related with autonomic nervous system responses, as a highly promising and effective engaging alternative to common physical activity exercises. Firstly, the main results from relevant works that attempted to investigate such influences based on physiological data analysis collected by wearable devices were presented. As a complementary tool for physical rehabilitation exercises, the impact of VR serious games on physical and cognitive performance, as well as on the rehabilitation process were also addressed. More contributions were made in this sense, as this present study sought to evaluate how a VR serious game for rehabilitation modulates physiological responses of younger adults. Two different game complexities were experienced by the subjects, and physiological data collected by biomedical wearable sensors evidenced significant changes in HRV parameters between each game difficulty levels. Stimulation of the parasympathetic branch of the ANS was mostly notable during easier difficulty game levels. On the other hand, it was verified that a higher intensity gameplay induced lower parasympathetic recovery during post-exercise/resting periods. Gameplays of longer time durations did not reveal a significant impact on physio-logical responses of younger adults, when compared with shorter ones.

Finally, this contribution involved the implementation of machine learning algorithms to estimate the different serious game difficulty levels based on HRV measures, and it was verified that the k-NN algorithm achieved the best results amongst other classifiers.

The study presented in this sub-chapter led to the publication of an article in a book chapter: M. Jacob Rodrigues, O. Postolache, F. Cercas, (2021). Autonomic Nervous System Assessment Based on HRV Analysis During Virtual Reality Serious Games. In N. T. Nguyen, L. Iliadis, I. Maglogiannis, & B. Trawiński (Eds.), Computational Collective Intelligence (pp. 756–768). Springer International Publishing | https://doi.org/10.1007/978-3-030-88081-1_57

4.4. Conclusions

This chapter sought to address three different studies that collectively contributed to the measurement of the effects of external stimuli on human physiological status through innovative approaches that relied on the developed biomedical and environmental sensor nodes. The first study aimed to assess indoor environmental quality alongside cardiac and respiratory assessments based on the developed healthcare-IoT system. By analyzing temperature and relative humidity distributions in a non-isothermal office environment, the study demonstrated that changes in ambient conditions affect heart rate variability and respiratory rate, indicating the activation of thermal regulatory reflexes. Machine learning techniques were employed to predict human thermal comfort levels, achieving high accuracy rates.

The second study explored the relationship between musical stimuli and noise stress, with the autonomic nervous system balance. By comparing the effects of different music genres and noise exposure on human physiological parameters, the study revealed that the music type and noise stress directly influence sympathetic and parasympathetic activity of the nervous system. Machine learning algorithms were employed to predict stress induced by auditory stimuli with good accuracy.

The third study focused on the impact of virtual reality exergaming on the autonomic nervous system responses. Through physiological data collected during gameplay, the study identified that game complexity influenced heart rate variability parameters, with easier levels stimulating the parasympathetic branch. Additionally, prolonged intense gameplay affected parasympathetic recovery during rest. Machine learning was employed to predict game difficulty levels based on the heart rate variability measures, achieving good results.

These studies emphasized the interconnections between external *stimuli*, physiological responses, and the autonomic nervous system. They highlighted the usefulness of advanced technologies such as IoT and machine learning, and thus, the utility of the developed system, to understand the complex interaction between environmental factors or *stimuli*, and human physiological well-being.

CHAPTER 5

Indoor Localization and Behavior Monitoring of Users in Ambient Assisted Living Environments

This chapter discusses the utilization and validation of the developed indoor localization and behaviour monitoring layer of the proposed system. It begins with and overview on the importance of integrating this layer in a AAL solution, as well as a reference to the available systems for monitoring such events. It then describes the indoor localization system and its components and presents the artificial intelligence algorithms to classify human activities and detect fall events. A results and discussion session reports the obtained system' performance, and a conclusion section closes the chapter.

5.1. Overview

With the ageing process, several problems arise, namely at the level of physical and motor health. One of the main aspects and challenges of AAL is the accurate localization of individuals within indoor environments and the recognition of their daily life activities. This is a crucial aspect of such assistive technologies since it allows the monitoring of their health conditions by detecting behavior patterns associated with certain daily activities.

Mechanisms to effectively monitor daily life activities and detect falls are indispensable healthcare services in a smart environment, namely in an AAL environment. With the ability to be embedded in smart environments, there are different methods proposed in the literature for indoor localization and fall detection. Such systems can be wearable-based, vision-based, ambient-based or a data fusion between them [266], as addressed in Chapter 2. The recognition of the most common human activities, such as walking, sitting, going upstairs or downstairs and lying, and its fusion with the indoor location information allows a better and more precise estimation of movements and behavior of the individuals within the AAL environment. This recognition can be based on the analysis of acceleration and rotation patterns of the human body, by means of inertial sensors. Supervised ML algorithms are used to estimate these activities based on the 3-axis acceleration signals, and several studies have been reporting very good results on their classification and analyzing human posture by using these methods [267]–[270], as mentioned in Chapter 2.

In this context, this study describes the development of an indoor localization and fall detection system based on a wearable sensor node using ultra-wide band (UWB) technology combined with acceleration and rotation patterns information of the human body. The activities classification and fall detection is performed using different ML models, such as SVM, RF, DT, MLP and recurrent neural networks (RNNs), namely long short-term memory (LSTM) networks.

5.2. Indoor Localization

This study aimed to estimate indoor positioning based on UWB technology, as well as to estimate the type of activity performed by the individual using the wearable sensor node. In the first part, the real-time positioning of the person in the experimental room was tested. Initially, this validation of the positioning given by the UWB system was done by viewing the real-time position of the tag in the web application of the Pozyx® system. Then, after configuring the collection of UWB data by the ESP32 microcontroller and the transmission of X, Y and Z coordinates to the gateway node, a graphical user interface was developed to visualize in real-time the accelerometer and gyroscope signals, as well as the location of the person and the type of activity she/he is performing.

While choosing the right X and Y boundaries, the environment where the experiment took place was divided into different areas that correspond to the various room divisions of a house. Additionally, each division was sub-divided into various small areas corresponding to where specific furniture is located, as demonstrated in Figure 5.1.

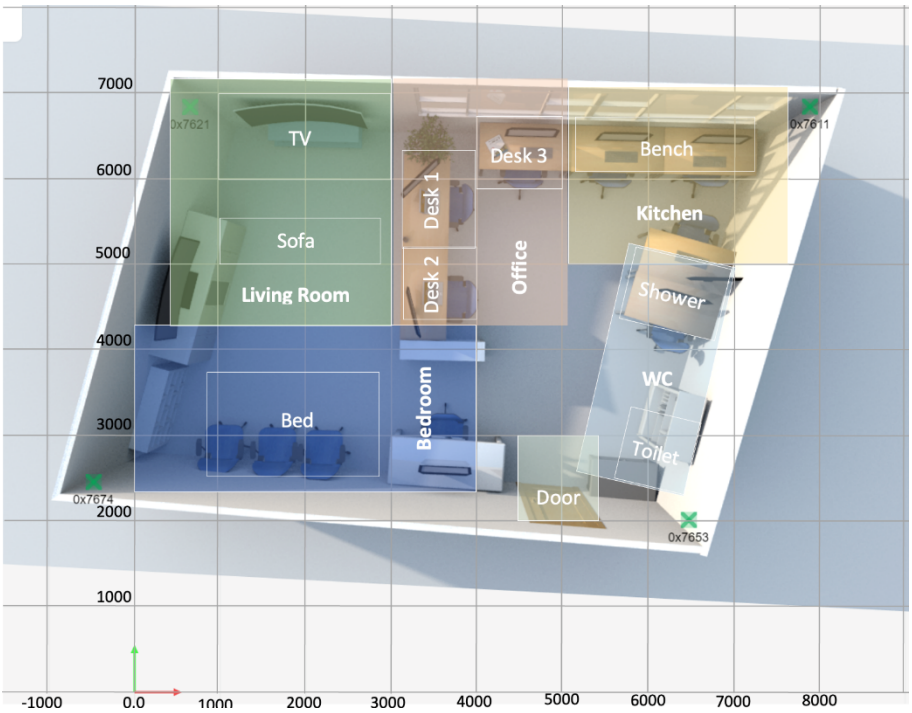

FIGURE 5.1. Floor plan displaying the room divisions and the X and Y coordinates grid

Once the X and Y coordinates have been acquired by the gateway node, the developed user interface indicates which area of the environment the user is at, as the X and Y boundaries of the assigned spaces were adjusted until an ideal configuration was found. This was programmed using a JavaScript function in the Node-RED development tool. The accuracy of the used UWB system is considered to be highly precise, reaching an accuracy of up to 10 cm in a typical indoor environment [271]. The collection of X, Y and Z coordinates from the UWB tag and its association to specific locations in the environment showed no margin of error since this is entirely dependent on the adjustments of the X and Y limits of each room divisions programmed in the gateway node.

Figure 5.2 displays the graphical user interface developed for this system, which aims to provide real-time tracking and monitoring of the wearable tag using the measured X and Y coordinates.

FIGURE 5.2. Graphical user interface for the indoor localization system. Real-time accelerometer and gyro-scope data, UWB coordinates, and the room's divisions are displayed

By knowing the user's location, it is possible to make a correlation between the activity estimated by the ML algorithms with the places where that same activity happens to reduce possible errors in the diagnosis. For example, if the activity "fall" is being detected in the area of the room corresponding to the position where the bed is located, the system disregards the alert. However, if the estimation of a fall is given in any other space, the system will accuse that event.

5.3. Behaviour Monitoring and Fall Detection

5.3.1. Methods

The second part of this study involved activity estimation using the accelerometer and gyroscope data was based on the execution of the 6 most common daily activities: sitting, standing, walking, climbing stairs, walking downstairs, and lying down. In this phase, the participant was asked to perform the above-mentioned activities for approximately 25 seconds. The study included 28 participants aged between 22 and 55 years old. All participants provided informed consent before enrolling in the experiment. The purpose and procedures involved in this study were given before their participation. All participants reported being in good health and had no locomotor problems. The wearable sensor node was placed at the waist, centered in the back of the participants, as it is the body's center of mass that can provide a good estimate of its overall orientation as it is a relatively stable location less prone to movement artifacts.

Lastly, the system was used for fall detection purposes at a third stage of this study. Besides accelerometer and gyroscope data, Z-coordinate obtained with the UWB tag was also used for this classification. Three different activities were examined: falling, sitting, and standing. The sitting and standing activities were contemplated since a distinction must be made between a possible fall event and the person deliberately sitting on the ground. By considering standing as a distinct activity, the machine learning model will be able to identify certain movement patterns that are unique to this activity, helping to reduce false positives in fall detection. The data was acquired from a subject that performed these three activities ten times, with variations in the posture to simulate different scenarios. Each activity was recorded for 20 seconds. As for the sitting position, five recordings were made with the person sitting on the floor, and the remaining five sitting on a chair. The falling activity was considered as a person being already lying on the floor after the occurrence of a fall. By simulating this phase of a fall, the measured variables were better controlled, and the safety of the test participants was better ensured.

5.3.2. Applied AI for Human Activity Classification

The different types of movements performed while doing the previously mentioned activities are characterized by different motion patterns of the x-axis, y-axis and z-axis of the accelerometer and gyroscope. The analysis of the acceleration and rotation patterns of these axis allow to easily distinguish between different types of movements. Walking has a very distinctive periodic pattern in the z-axis and larger movements in the x-axis and y-axis when compared to sitting or standing activities, which are stationary activities. Climbing stairs, for instance, has a similar pattern to walking, but can be distinguished by a more accentuated vertical component in the z-axis. These patterns can be seen in Figures 5.3-5.6, that depict 150 samples of 4 activities (walking, going upstairs, going downstairs, sitting), corresponding to a 6s time window.

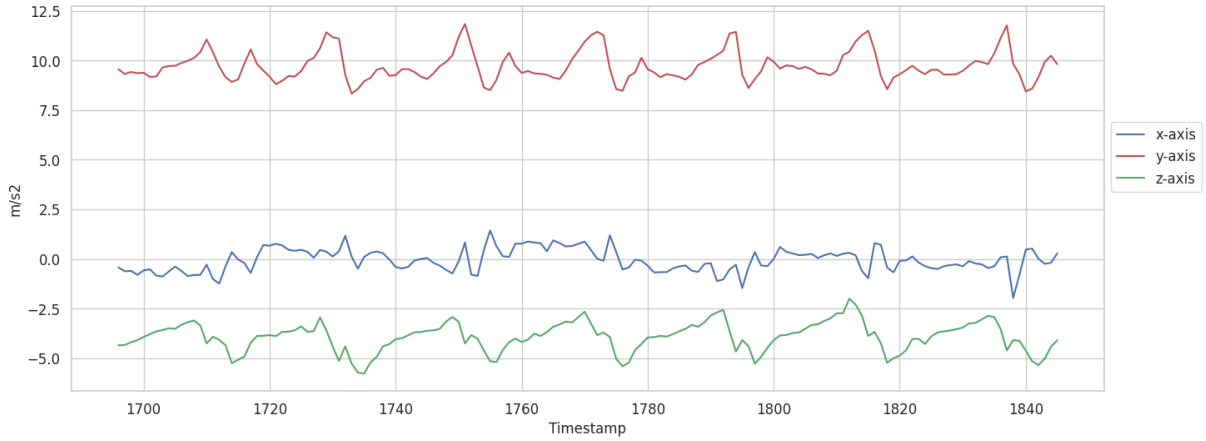

FIGURE 5.3. X, Y and Z-values of acceleration for the walking activity

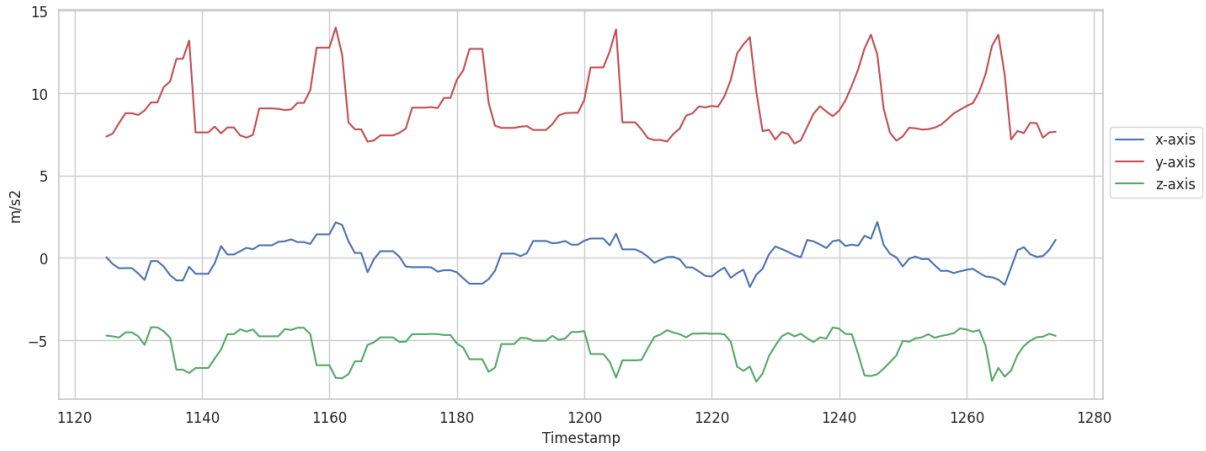

FIGURE 5.4. X, Y and Z-values of acceleration for the activity of going upstairs

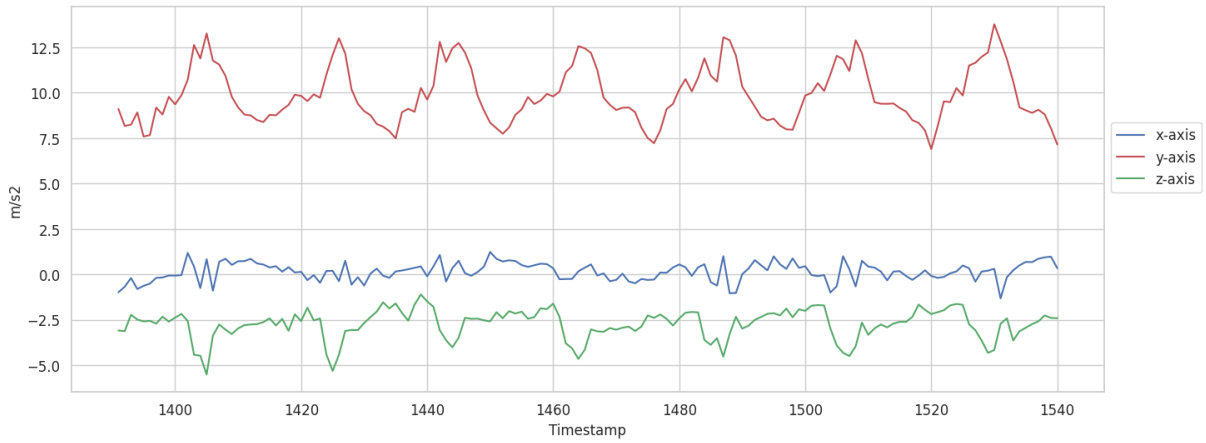

FIGURE 5.5. X, Y and Z-values of acceleration for the activity of going downstairs

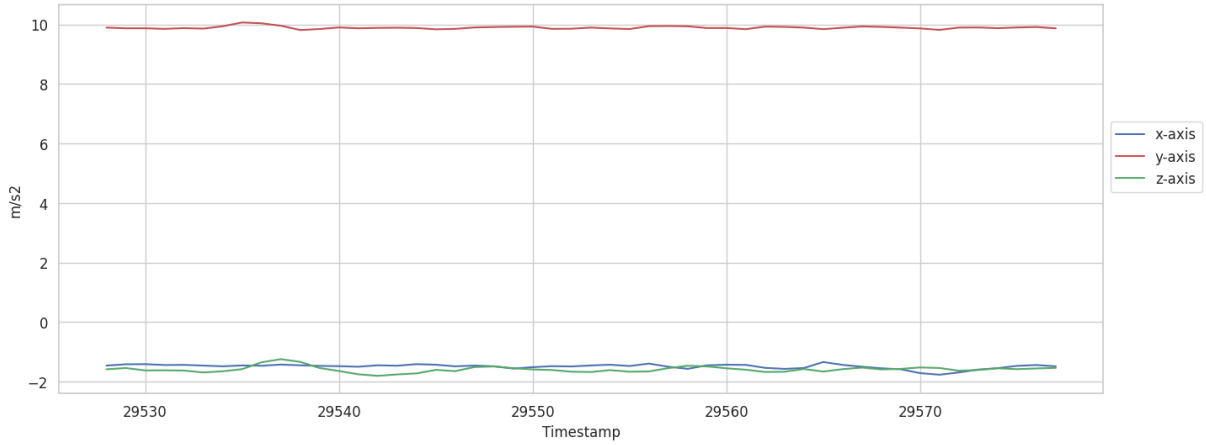

FIGURE 5.6. X, Y and Z-values of acceleration for the sitting activity

The produced dataset has a total of 85923 instances and 6 features: acceleration in the x-axis, y-axis and z-axis, and angular velocity in the x-axis, y-axis and z-axis. The number of samples collected by each participant for all activities are presented in Figure 5.7. For all ML models, 20% of the data was used for testing, and 80% was used for training.

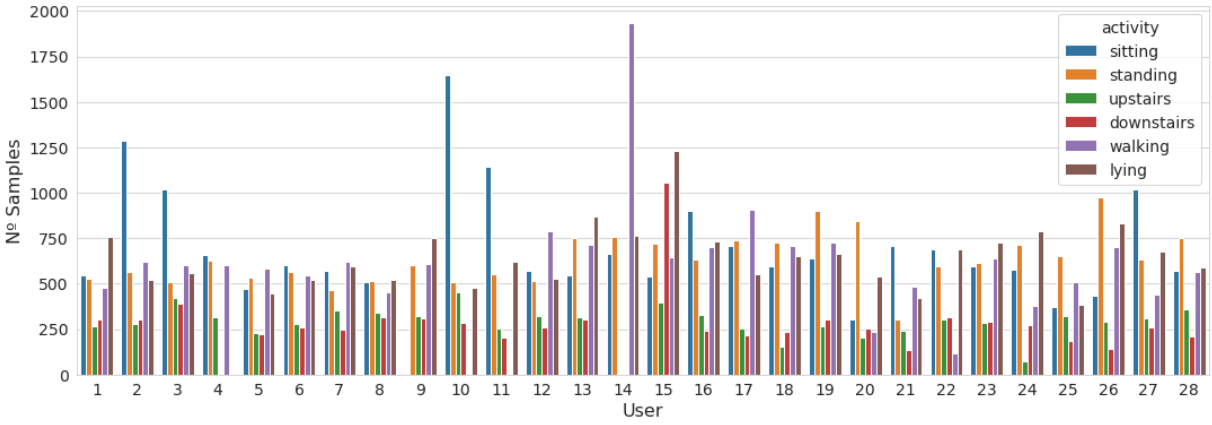

FIGURE. 5.7. Number of samples collected from each participant for all six activities

To achieve better performance levels with the machine learning algorithms, new informative features were generated based on raw accelerometer data. Common time-domain and frequency-domain features used in the literature were selected [267], [268], and calculated using *pandas* and *NumPy* python libraries. These attributes were calculated for each acceleration axis within 5 second segments, which correspond to 120 samples, and using a sliding window of 50 samples. Regarding the time-domain, the following statistical measures were considered: mean value, standard deviation, average absolute deviation, minimum value, maximum value, median, median absolute deviation, negative values count, positive values count, number of values above mean, number of peaks, skewness, kurtosis, energy entropy and signal magnitude area. For the frequency-domain, the Fast-Fourier Transform (FFT) was calculated using *SciPy* python package. As this method retrieves the frequency component of the time-series signal, it provided an additional way for analyzing the data. The above-mentioned measures used for time-domain analysis were also applied for the FFT data. With these feature extraction methods, a total of 90 new features were generated.

After performing the feature extraction, ML classification algorithms were applied to make predictions about the type of activity performed by the participants. The used algorithms were SVM, DT, RF and MLP. *Scikit-learn* machine learning library for Python was used for this purpose. These algorithms were selected based on their ability to learn from complex data patterns. In addition, these are extensively studied algorithms that have demonstrated reaching high levels of accuracy in human activity recognition applications. To ensure the optimal performance of the machine learning algorithms, their hyper-parameters were fine-tuned. We used grid search cross-validation (CV) to systematically explore different combinations of hyperparameters and identify the best performing set for each algorithm [272]. The optimal hyperparameters for each ML model are shown in Table 5.1.

TABLE 5.1. Hyperparameters selection of the ML models

Classifiers	Hyperparameter	Type	Selected value
SVM	*C*	Continuous	10
	kernel	Categorical	rbf
RF	*criterion*	Categorical	entropy
	max_depth	Discrete	8
	n_estimators	Discrete	300
	max_features	Continuous	sqrt
DT	*criterion*	Categorical	gini
	max_depth	Discrete	9
	max_features	Continuous	auto
MLP	*activation*	Categorical	tanh
	alpha	Continuous	0.05
	learning_rate	Categorical	adaptive
	solver	Categorical	adam

Additionally, we explored the use of the Long Short-Term Memory (LSTM) algorithm [273], to predict the 6 activities based on the raw accelerometer and gyroscope data, without performing any of the traditional feature engineering process for human activity recognition. This comes with the thought that this approach may bring some limitations such as the possibility of information loss during feature extraction, and the lack of adaptability to new data. The LSTM is being considered to overcome these limitations by automatically learning the features from the raw sensor data. This algorithm is a type of Recurrent Neural Network (RNN) that can process entire sequences of data and learn long-term dependencies. It introduces the concept of memory cells that can store information for longer periods. The information stored in these cells are controlled by a gating unit which, based on an activation function, will determine which information should be kept or discarded from the cell [273].

This algorithm is considered suitable for time-series data and sequential modeling and can learn the nonlinear relationships between features, which makes it useful for recognizing temporal sequences of activities over time. This approach excludes the need for feature engineering and may result in better performance than conventional techniques. The LSTM algorithm was computed using the Keras deep learning library with TensorFlow as the backend in Python programming language. The hyperparameters for this LSTM model were tuned using grid search cross-validation to find the best performance results and are listed in Table 5.2.

TABLE 5.2. Hyperparameters for the LSTM model for human activity classification

Hyperparameter	**Value**
Input time steps	50
Input feature dimension	6
Batch size	1024
Learning Rate	0.002
Optimization Algorithm	Adam (β_1 = 0.9, β_2=0.999)
Epochs	100
Nodes in LSTM output layer	128
Nodes in the Fully Connected layer	64
Nodes in the softmax layer	6

5.3.3. Applied AI for Fall Detection

As analyzed in subsection 5.3.2, the different movements captured by the IMU are characterized by various motion patterns of the three-dimensional axes of the accelerometer and gyroscope. Moreover, the difference in the elevation (Z coordinate) of the wearable sensor given by the UWB system is what allows the analysis of the patient's waist proximity to the ground, which is observed in the context of a fall. Z values closer to zero will be indicative of a possible fall, as it will be addressed in Section 5.4. B).

This new dataset has a total of 7756 instances. The fall class has a total of 2682 instances (34.58%), the standing class has a total of 2449 (31.58%), and the sitting class has a total of 2625 (33.84%).

The choice of the neural network-based algorithm considered several criteria, namely its ability to deal with raw sensor data and to effectively learn complex time series patterns. Table 5.3 shows the hyperparameters selected for this algorithm.

TABLE 5.3. Hyperparameters for the LSTM model for fall detection

Hyperparameter	**Value**
Input time steps	30
Input feature dimension	7
Batch size	64
Learning Rate	0.002
Optimization Algorithm	Adam (β_1 = 0.9, β_2=0.999)
Epochs	50
Nodes in LSTM output layer	64
Nodes in the Fully Connected layer	64
Nodes in the softmax layer	3

5.4. Results and Discussion

This section reports the results obtained with the machine learning models for classifying human activities and detect fall events using the reported indoor localization wearable node.

5.4.1. Human Activity Classification

The classification of 6 human activities - sitting, standing, walking, climbing stairs, walking downstairs and laying – was done using the accelerometer and gyroscope data. The Random Forest algorithm achieved the highest accuracy of 93.9%, followed by Decision Trees with an accuracy of 86.2%, Multilayer Perceptron with an accuracy of 81.5%, and SVM with an accuracy of 71.2% (Table 5.4).

TABLE 5.4. Accuracy, precision, recall and F1-score values obtained for the RF, DT, SVM and MLP, when classifying human activities

Evaluation Metric	***RF***	***DT***	***SVM***	***MLP***
Accuracy	0.939	0.862	0.712	0.815
Precision	0.938	0.865	0.757	0.817
Recall	0.938	0.863	0.713	0.816
F1 Score	0.938	0.862	0.724	0.815

Furthermore, LSTM was applied only to the raw accelerometer and gyroscope signals without requiring any additional feature engineering. In this case, LSTM achieved an accuracy of 92.6% (Table 5.5), which is comparable to the best performing machine learning algorithms previously tested.

The LSTM training session's progress over the iterations is presented in Figure 5.8. A decreasing trend in the validation and train loss and an increasing trend in accuracy over the course of training shows a good improvement of the model over the epochs.

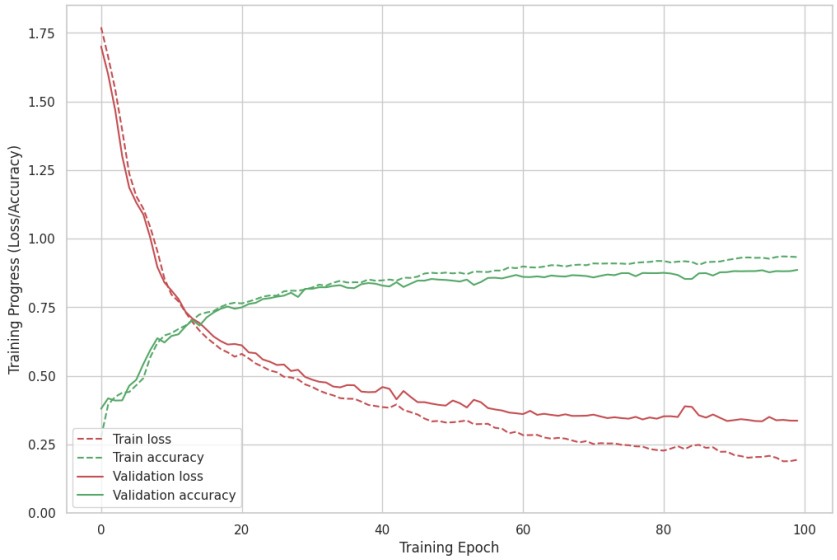

FIGURE 5.8. Logarithmic loss of the LSTM algorithm over 100 epochs

Additionally, the obtained confusion matrix is depicted in Figure 5.9.

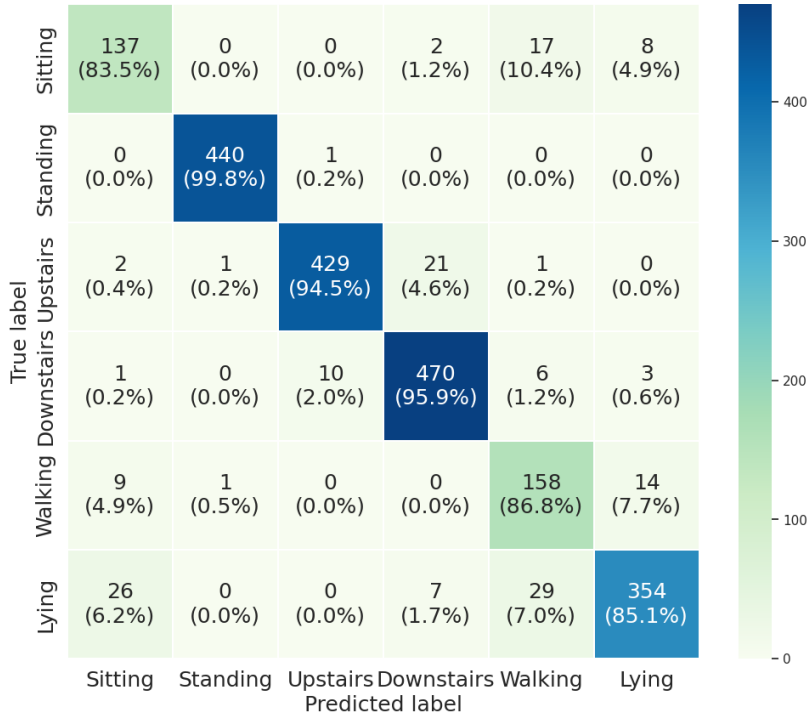

FIGURE 5.9. Confusion matrix for the estimation of 6 activities using LSTM.

A receiver operating characteristic curve (ROC) curve was computed for each class (i.e., type of activity), separately. The area under the ROC curve (AUC) showed how well the classifier was able to distinguish between the different activities. The LSTM achieved high AUC values for all six classes, which ranged from 0.98 to 1.00, as demonstrated in Figure 5.10. The "standing" activity (class 1) achieved the perfect score, while the "lying" activity (class 5) achieved 0.98.

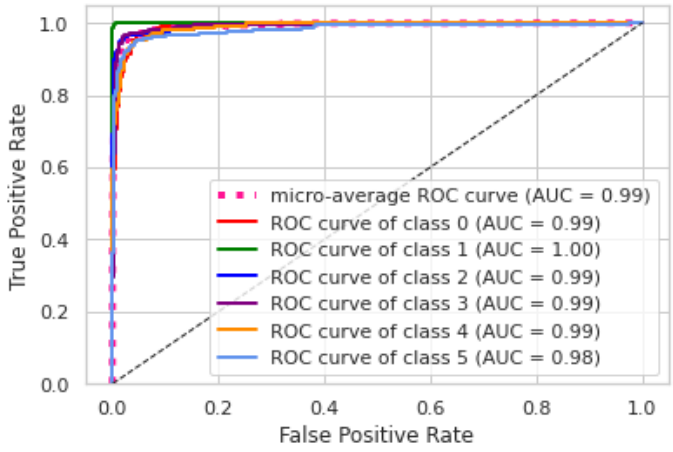

FIGURE 5.10. ROC curve and AUC values for each class using the LSTM algorithm.

These results demonstrate that using accelerometer and gyroscope data with appropriate feature engineering and machine learning algorithms, various types of physical activities can accurately be classified. The Random Forest algorithm had the best performance results, which is consistent with previous studies that have shown this model to be a robust and accurate algorithm for classification tasks, especially with human activity recognition [270].

It was also found that traditional machine learning algorithms, such as Decision Trees and Multilayer Perceptron, can achieve high accuracy with appropriate feature extraction and hyperparameter tuning. SVM, on the other hand, did not perform as well as expected, which may be due to the imbalanced nature of the dataset.

5.4.2. Fall Detection

Regarding the fall detection, which consisted in the use of a new dataset, three different activities were considered for this particular case: fall, sitting and standing. The possibility of adding the information from the UWB location data was tested, namely the elevation given by the Z coordinate, to the data collected by the IMU. An LSTM model was used for this classification task, since there will not be any feature extraction, as the data to be analysed will be raw sensor data. The dataset is composed of acceleration and gyroscope data, as well as the elevation of the wearable sensor node (Z coordinate). The addition of this last parameter is expected to improve the model's performance on detecting fall events.

By conducting data analysis, it was possible to verify that the different activities are relatively well distinguished regarding the Z coordinate measured by the UWB system. Figure 5.11 shows evidence, displaying the density distribution of the different values of the Z coordinate for the different activities, from 0 to 1.

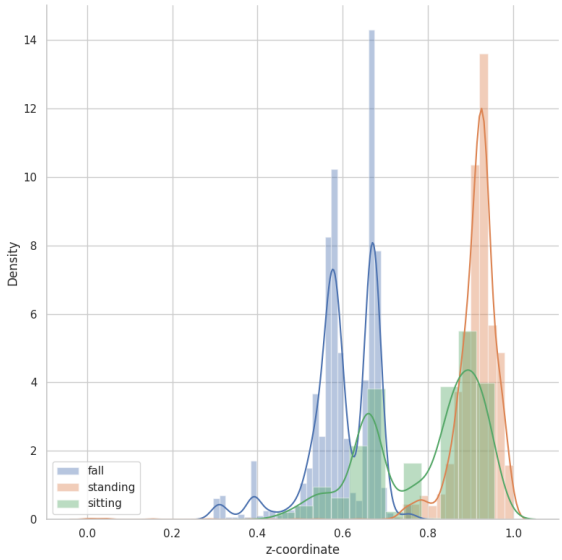

FIGURE 5.11. Density distribution of the z-coordinate for the different activities (fall, sitting and standing)

The activity corresponding to falling presents in fact lower Z values, since the person is on the ground. The sitting activity, which includes both sitting on the floor and sitting on a chair, presents higher average values, and it is possible to distinguish in the figure the occasions when the person was sitting on the floor, whose values are closer to the falling activity, than when the person was sitting on a chair. It should be noted that the values given by the UWB system are not static and suffer fluctuations due to the nature of the transmission as well as a variety of other environmental factors, such as the presence of objects in the transmission path, as well as other wireless signals that cause interference.

The model's performance for this case was evaluated using several metrics (Table 5.5), including accuracy, macro-averaged precision, macro-averaged recall, and macro-averaged F1-score, since it is a multiclass classification problem. TCN and GRU neural network models were also tested to ascertain whether its performance was in fact similar to the LSTM's and thus support the choice of this algorithm. The TCN was able to achieve 93.2% accuracy, while the GRU achieved 85.4% accuracy.

TABLE 5.5. LSTM performance on classifying human activities and estimating fall events

Evaluation Metrics	Activity Classification	Fall Detection
Accuracy	0.926	0.958
Macro-averaged Precision	0.899	0.958
Macro-averaged Recall	0.906	0.954
Macro-averaged F1 Score	0.902	0.955

These algorithms had lower performance than LSTM, so the next results are only about the LSTM's performance.

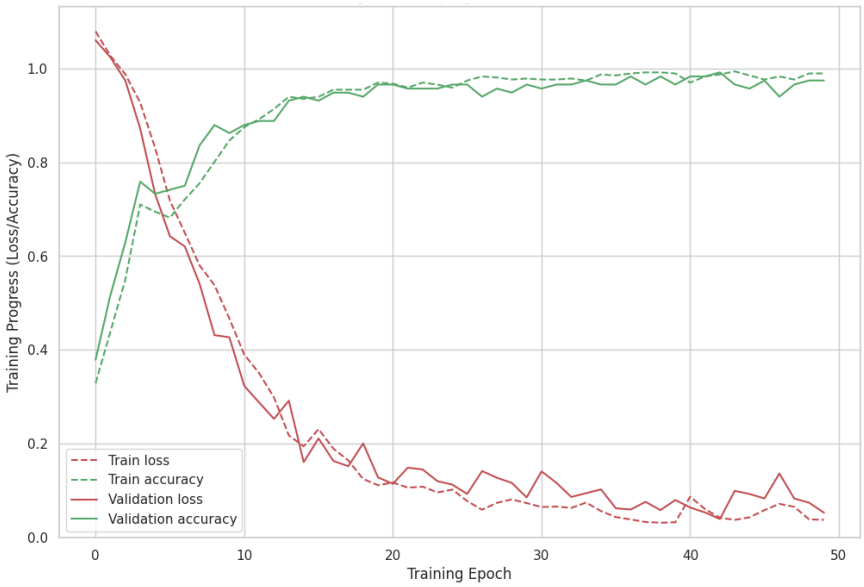

FIGURE 5.12. Logarithmic loss of the LSTM algorithm over 50 epochs

The macro-averaged recall was 0.954, indicating that the model has a good sensitivity to detecting each activity or event. The LSTM training session's progress over the iterations is presented in Figure 5.12. Receiver operating characteristic curves (ROC) were obtained. Figure 5.13 shows the confusion matrix and ROC curves of the LSTM model. The ROC curves show that the model performs well at distinguishing between the three activities, with an area under the curve (AUC) of 1.00 for falling, 1.00 for sitting, and 0.99 for standing.

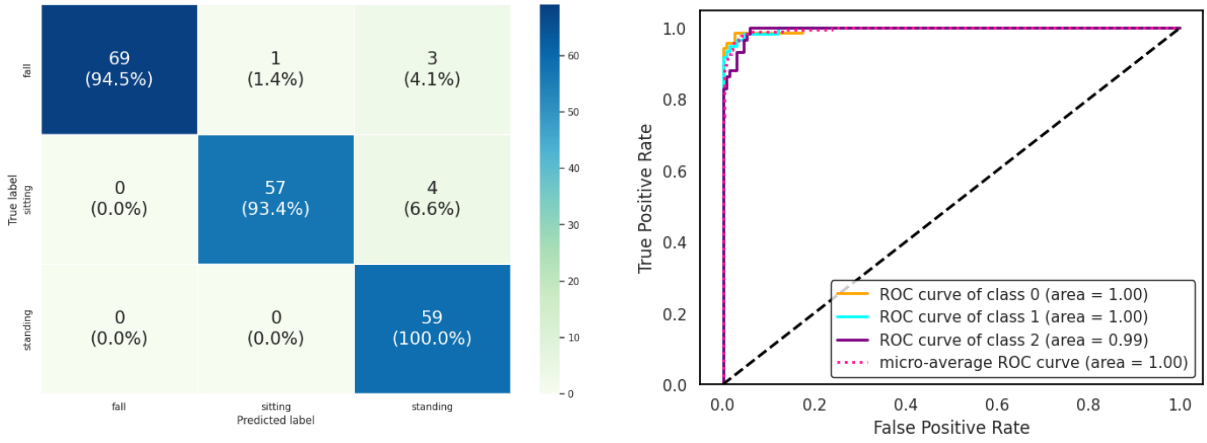

a) b)

FIGURE 5.13. a) Confusion matrix and b) ROC curves for the classification of fall events using LSTM. Class 0: fall, Class 1: sitting, Class 2: standing

5.5. Conclusions

This chapter aimed to report the use of the developed indoor localization sensor node to monitor human behavior and classify fall events in the context of an AAL system. 3D acceleration and rotation data of the human body were obtained for 28 participants to estimate six different types of common human activities, such as sitting, standing, walking, climbing stairs, walking downstairs, and lying. Various machine learning algorithms were used in this classification task. Feature extraction methods based on time-domain and frequency-domain were applied to the raw acceleration data for improving the ML models performance. The RF algorithm achieved the highest accuracy of 93.9%, followed by DT, MLP and SVM. Furthermore, the LSTM algorithm, having as input the raw accelerometer and gyroscope signals, achieved a very good accuracy of 92.6%. Achieving such good performance without requiring feature engineering of the recorded data led us to choose the LSTM algorithm to classify fall events. Therefore, as the final part of the behavior monitoring and indoor localization layer proposed for this thesis, LSTM neural networks were trained to detect fall events using the data measured by the developed wearable sensor. The algorithm achieved a promising accuracy of 95.8 % in classifying fall events as well as sitting and standing activities. For this purpose, not only the acceleration and rotation patterns of the human body were used, but also the coordinates given by the UWB system. In this way, this study allowed us to make the connection between the location where the person is and the type of activity they are performing.

The study presented in this chapter led to the publication of an article in a book chapter: M. Jacob Rodrigues, O. Postolache, F. Cercas, (2023). Wearable Tag for Indoor Localization in the Context of Ambient Assisted Living. In: Nguyen, N.T., et al. Computational Collective Intelligence. ICCCI 2023. Lecture Notes in Computer Science(), vol 14162. Springer International Publishing. https://doi.org/10.1007/978-3-031-41456-5_32

CHAPTER 6

Conclusions and Future Work

As technology advances, there are constantly innovative solutions for assisted living systems and healthcare assessment. The proposal of new architectures is essential to reach healthy, elderly, or disabled individuals and improve their quality of life. Smart tailored environments and AAL systems are based on the architecture of an IoT-based healthcare system and have a special focus on providing personalized and assistive services for their inhabitants. Through the monitoring of several physiological parameters and behavior patterns, these environments have the main purpose of determining a person's physical and mental health status and help to extend the person autonomy for a better quality of life for optimized healthcare costs.

6.1. Conclusions

In response to these challenges, the thesis research work focused on developing of smart tailored environments characterized by healthcare assessment components. These components include biomedical sensor nodes for vital signs monitoring and ambient sensors for evaluating indoor air quality conditions for user wellbeing. The system also involves recognizing behaviors and daily life activities based on artificial intelligence software modules. Moreover, this research work includes a comprehensive study on how several external *stimuli* can affect well-being through the usage of metrics associated with autonomous nervous system.

The first component developed for this AAL system was the physiological parameters acquisition layer. Among the existing techniques for monitoring cardiac activity, photoplethysmography and ballistocardiography were the signal acquisition techniques that were used, not only because of their effectiveness, but primarily because of their non-intrusive and easy-to-use characteristics. A biomedical sensor node based on BCG was developed with the aim of offering measurements of cardiorespiratory activity without the user having to wear any kind of device. To this end, the BCG sensor was installed on the seat of a chair, making the presence of a medical device imperceptible to the user.

Advanced digital signal processing techniques were implemented to improve the signal noise ratio as to extract the heart rate, heart rate variability and respiratory rate in accurate mode. The validation of the BCG based measurements were caried out using certified medical systems.

With the aim to increase the user mobility wearable cardio-respiratory monitoring system expressed by two sensor nodes prototypes characterized by photoplethysmography measurement channel were reported in this thesis. Both sensor nodes are designed to be placed at distinct locations on the body to optimize user mobility. The first prototype consists of a compact wearable node designed for a versatile placement across the body. The research contribution inherent in the development of this wearable system is expressed by optimized algorithms for calculating heart rate variability parameters in real time. The developed algorithm and the calculation of HRV have been validated using ECG measurement reference systems, which is the gold standard technique for measuring cardiac activity. The second prototype consists of an ear-worn sensor node, which runs the same algorithm in optimized embedded form, taking also into account the power consumption.

The second system component was the monitoring of human behavior and daily activities through motion tracking and indoor localization technologies. To this end, an indoor localization and fall detection system that includes a set of new wearable sensor nodes characterized by ultra-wide band technology was developed. The node provides acceleration and rotation patterns information of the human body that are very important on fall detection. The classification of daily human activities as well as fall events were made using ML algorithms, that were able to achieve accuracies of over 95%.

The third system component was the indoor environmental quality layer. This layer is expressed by a portable prototype, which can be used both indoors and outdoors. The developed sensor nodes make it possible to monitor air quality, namely the most common pollutants in urban spaces, such as PM10 and PM2.5, CO, CO2, tVOC and Smoke, as well as temperature, relative humidity, and sound levels.

The devices are interconnected within an IoT framework, referred to as the device layer. An essential component of this system, the gateway node, served as the basis for edge computing. Its main function was to gather and process the information collected from the sensor nodes array. This gateway node was specifically designed to store data locally or transmit it efficiently to remote cloud-based databases. In this way, the system guaranteed greater efficiency in data processing and optimization of edge computing capabilities, enhancing the system's capacity for real-time processing, and ensuring flexibility in the data management of the different sensor nodes.

Specific research work was the validation of the developed system. Thus, all the novel solutions for the smart tailored system were validated in real case scenarios, and several studies were reported throughout this thesis. These studies sought to interconnect the different layers and explore the inter-relations between the measured parameters acquired and processed by each layer. In the first study, a healthcare-IoT system integrated the unobtrusive BCG sensor node to monitor cardiac activity in different indoor environmental conditions of an office environment, employing machine learning to predict thermal comfort levels based on heart rate variability changes. The second study explored the music's impact and stress noise on the autonomic nervous system by using the PPG sensor node, revealing distinct sympathetic responses to different music genres, and using machine learning to accurately predict stress levels induced by auditory stimuli. In the third study, the effects of virtual reality exergaming on physiological and cognitive states were investigated, discovering a varying influence of game complexity on the parasympathetic branch. By employing machine learning models, it was successfully achieved an 81% accuracy rate in predicting game difficulty levels through heart rate variability measurements, which can be used to monitor the subject's physical performance and adjust the game's difficulty levels automatically. This adaptive feature serves to mitigate potential accidents resulting from excessively high exercise intensity during gameplay.

Human daily activities, fall events and real-time location were estimated by using the developed wearable indoor localization sensor node with UWB communication capabilities, achieving very good accuracy rates above 92%.

The obtained results show the efficiency and accuracy of the developed sensor networks and implemented algorithms. Based on these evaluations and on the positive user feedback, the proposed system effectively addressed all the relevant components and healthcare assistive services, such as vital signs monitoring, indoor environmental assessment, human activity recognition and cognitive stimulation. This comprehensive approach facilitated the implementation of a smart tailored environment for AAL, specifically designed to address the needs of elderly populations, individuals with chronic diseases, and even those in good health.

6.2 Future Work

Although everything that was proposed in the planning of this thesis has been accomplished, including the integration of different assistive services essential for AAL environments, there are still some remaining steps that are part of future work. These improvements consist of:

- Improving the design of wearable sensor nodes to create optimized models, with the aim of improving comfort and usability when using them. To achieve this goal acquisition platforms with lower power consumption and lower computation load will be incorporated, along with the development of a more ergonomic design.
- Implementation of novel federated embedded processing for extended scalability according to the future AAL architecture requirements.
- Integration of an AAL smart sensing solution with virtual reality and mixed reality scenarios.
- Construction of a larger dataset for the machine learning algorithms to achieve even more promising results in the classification tasks. This substantial increase is essential to allow the system to be personalised and adapted to the unique needs of everyone.

References

[1] A. Whitmore, A. Agarwal, and L. Da Xu, “The Internet of Things—A survey of topics and trends,” *Inf. Syst. Front.*, vol. 17, no. 2, pp. 261–274, Apr. 2015, doi: 10.1007/s10796-014-9489-2.

[2] A. Dohr, R. Modre-Opsrian, M. Drobics, D. Hayn, and G. Schreier, “The Internet of Things for Ambient Assisted Living,” in *2010 Seventh International Conference on Information Technology: New Generations*, Las Vegas, NV, USA: IEEE, 2010, pp. 804–809. doi: 10.1109/ITNG.2010.104.

[3] J. Cahill, R. Portales, S. McLoughin, N. Nagan, B. Henrichs, and S. Wetherall, “IoT/Sensor-Based Infrastructures Promoting a Sense of Home, Independent Living, Comfort and Wellness,” *Sensors*, vol. 19, no. 3, p. 485, Jan. 2019, doi: 10.3390/s19030485.

[4] M. Saleemi, M. Anjum, and M. Rehman, “Ubiquitous healthcare: a systematic mapping study,” *J. Ambient Intell. Humaniz. Comput.*, Sep. 2020, doi: 10.1007/s12652-020-02513-x.

[5] M. Jacob Rodrigues, O. Postolache, and F. Cercas, “Physiological and Behavior Monitoring Systems for Smart Healthcare Environments: A Review,” *Sensors*, vol. 20, no. 8, p. 2186, Apr. 2020, doi: 10.3390/s20082186.

[6] S. Majumder, T. Mondal, and M. Deen, “Wearable Sensors for Remote Health Monitoring,” *Sensors*, vol. 17, no. 12, p. 130, Jan. 2017, doi: 10.3390/s17010130.

[7] M. Elliott and A. Coventry, “Critical care: the eight vital signs of patient monitoring,” *Br. J. Nurs.*, vol. 21, no. 10, pp. 621–625, May 2012, doi: 10.12968/bjon.2012.21.10.621.

[8] M. J. Deen, “Information and communications technologies for elderly ubiquitous healthcare in a smart home,” *Pers. Ubiquitous Comput.*, vol. 19, no. 3–4, pp. 573–599, Jul. 2015, doi: 10.1007/s00779-015-0856-x.

[9] T. F. of the E. S. Electrophysiology, “Heart Rate Variability: Standards of Measurement, Physiological Interpretation, and Clinical Use,” *Circulation*, vol. 93, no. 5, pp. 1043–1065, Mar. 1996, doi: 10.1161/01.CIR.93.5.1043.

[10] U. Rajendra Acharya, K. Paul Joseph, N. Kannathal, C. M. Lim, and J. S. Suri, “Heart rate variability: a review,” *Med. Biol. Eng. Comput.*, vol. 44, no. 12, pp. 1031–1051, Dec. 2006, doi: 10.1007/s11517-006-0119-0.

[11] P. K. D. Pramanik, B. K. Upadhyaya, S. Pal, and T. Pal, “Internet of things, smart sensors, and pervasive systems: Enabling connected and pervasive healthcare,” in *Healthcare Data Analytics and Management*, Elsevier, 2019, pp. 1–58. doi: 10.1016/B978-0-12-815368-0.00001-4.

[12] Y. T. Tsukada *et al.*, “Validation of wearable textile electrodes for ECG monitoring,” *Heart Vessels*, vol. 34, no. 7, pp. 1203–1211, Jul. 2019, doi: 10.1007/s00380-019-01347-8.

[13] T. Machino *et al.*, “Dry textile electrode for ambulatory monitoring after catheter ablation of atrial fibrillation: A pilot study of simultaneous comparison to the Holter electrocardiogram,” *F1000Research*, vol. 11, p. 97, Jun. 2022, doi: 10.12688/f1000research.75712.2.

[14] Toray Industries, Inc, “hitoe,” *“Toray”, Innovation by Chemestry*. https://www.hitoe.toray/en/ (accessed Aug. 06, 2023).

[15] X. An and G. Stylios, “A Hybrid Textile Electrode for Electrocardiogram (ECG) Measurement and Motion Tracking,” *Materials*, vol. 11, no. 10, p. 1887, Oct. 2018, doi: 10.3390/ma11101887.

[16] Y. Zhou, X. Ding, J. Zhang, Y. Duan, J. Hu, and X. Yang, “Fabrication of conductive fabric as textile electrode for ECG monitoring,” *Fibers Polym.*, vol. 15, no. 11, pp. 2260–2264, Nov. 2014, doi: 10.1007/s12221-014-2260-y.

[17] A. Ankhili, X. Tao, C. Cochrane, D. Coulon, and V. Koncar, “Washable and Reliable Textile Electrodes Embedded into Underwear Fabric for Electrocardiography (ECG) Monitoring,” *Materials*, vol. 11, no. 2, p. 256, Feb. 2018, doi: 10.3390/ma11020256.

[18] P. S. Das, J. W. Kim, and J. Y. Park, “Fashionable wrist band using highly conductive fabric for electrocardiogram signal monitoring,” *J. Ind. Text.*, vol. 49, no. 2, pp. 243–261, Aug. 2019, doi: 10.1177/1528083718779427.

[19] A. Soroudi, N. Hernández, J. Wipenmyr, and V. Nierstrasz, “Surface modification of textile electrodes to improve electrocardiography signals in wearable smart garment,” *J. Mater. Sci. Mater. Electron.*, vol. 30, no. 17, pp. 16666–16675, Sep. 2019, doi: 10.1007/s10854-019-02047-9.
[20] D. L. Presti *et al.*, “Cardiac monitoring with a smart textile based on polymer-encapsulated FBG: influence of sensor positioning,” in *2019 IEEE International Symposium on Medical Measurements and Applications (MeMeA)*, Istanbul, Turkey: IEEE, Jun. 2019, pp. 1–6. doi: 10.1109/MeMeA.2019.8802157.
[21] G. Lu, F. Yang, J. A. Taylor, and J. F. Stein, “A comparison of photoplethysmography and ECG recording to analyse heart rate variability in healthy subjects,” *J. Med. Eng. Technol.*, pp. 1–8, 2009, doi: 10.1080/03091900903150998.
[22] N. Pinheiro *et al.*, “Can PPG be used for HRV analysis?,” in *2016 38th Annual International Conference of the IEEE Engineering in Medicine and Biology Society (EMBC)*, Orlando, FL, USA: IEEE, Aug. 2016, pp. 2945–2949. doi: 10.1109/EMBC.2016.7591347.
[23] M. Ghamari, D. Castaneda, A. Esparza, C. Soltanpur, and H. Nazeran, “A review on wearable photoplethysmography sensors and their potential future applications in health care,” *Int. J. Biosens. Bioelectron.*, vol. 4, no. 4, 2018, doi: 10.15406/ijbsbe.2018.04.00125.
[24] M. Elgendi *et al.*, “The use of photoplethysmography for assessing hypertension,” *Npj Digit. Med.*, vol. 2, no. 1, p. 60, Dec. 2019, doi: 10.1038/s41746-019-0136-7.
[25] K. Malhi, S. C. Mukhopadhyay, J. Schnepper, M. Haefke, and H. Ewald, “A Zigbee-Based Wearable Physiological Parameters Monitoring System,” *IEEE Sens. J.*, vol. 12, no. 3, pp. 423–430, Mar. 2012, doi: 10.1109/JSEN.2010.2091719.
[26] O. Postolache, P. S. Girão, and G. Postolache, “Pervasive Sensing and M-Health: Vital Signs and Daily Activity Monitoring,” in *Pervasive and Mobile Sensing and Computing for Healthcare*, S. C. Mukhopadhyay and O. A. Postolache, Eds., Berlin, Heidelberg: Springer Berlin Heidelberg, 2013, pp. 1–49. doi: 10.1007/978-3-642-32538-0_1.
[27] X. A. Mary, S. Mohan, S. Evangeline, and K. Rajasekaran, “Physiological parameter measurement using wearable sensors and cloud computing,” in *Systems Simulation and Modeling for Cloud Computing and Big Data Applications*, Elsevier, 2020, pp. 15–27. doi: 10.1016/B978-0-12-819779-0.00002-2.
[28] T. Pereira *et al.*, “Photoplethysmography based atrial fibrillation detection: a review,” *Npj Digit. Med.*, vol. 3, no. 1, p. 3, Dec. 2020, doi: 10.1038/s41746-019-0207-9.
[29] E. J. Pino, J. A. P. Chavez, and P. Aqueveque, “BCG algorithm for unobtrusive heart rate monitoring,” in *2017 IEEE Healthcare Innovations and Point of Care Technologies (HI-POCT)*, Bethesda, MD: IEEE, Nov. 2017, pp. 180–183. doi: 10.1109/HIC.2017.8227614.
[30] J. Kranjec, S. Beguš, G. Geršak, M. Šinkovec, J. Drnovšek, and D. Hudoklin, “Design and Clinical Evaluation of a Non-Contact Heart Rate Variability Measuring Device,” *Sensors*, vol. 17, no. 11, p. 2637, Nov. 2017, doi: 10.3390/s17112637.
[31] O. Postolache, P. S. Girao, G. Postolache, and J. Gabriel, “Cardio-respiratory and daily activity monitor based on FMCW Doppler radar embedded in a wheelchair,” in *2011 Annual International Conference of the IEEE Engineering in Medicine and Biology Society*, Boston, MA: IEEE, Aug. 2011, pp. 1917–1920. doi: 10.1109/IEMBS.2011.6090542.
[32] E. J. Pino, C. Larsen, J. Chavez, and P. Aqueveque, “Non-invasive BCG monitoring for non-traditional settings,” in *2016 38th Annual International Conference of the IEEE Engineering in Medicine and Biology Society (EMBC)*, Orlando, FL, USA: IEEE, Aug. 2016, pp. 4776–4779. doi: 10.1109/EMBC.2016.7591795.
[33] O. A. Postolache, P. M. B. S. Girao, J. Mendes, E. C. Pinheiro, and G. Postolache, “Physiological Parameters Measurement Based on Wheelchair Embedded Sensors and Advanced Signal Processing,” *IEEE Trans. Instrum. Meas.*, vol. 59, no. 10, pp. 2564–2574, Oct. 2010, doi: 10.1109/TIM.2010.2057590.
[34] S. Gilaberte, J. Gómez-Clapers, R. Casanella, and R. Pallas-Areny, “Heart and respiratory rate detection on a bathroom scale based on the ballistocardiogram and the continuous wavelet

transform," in *2010 Annual International Conference of the IEEE Engineering in Medicine and Biology*, Buenos Aires: IEEE, Aug. 2010, pp. 2557–2560. doi: 10.1109/IEMBS.2010.5626866.
[35] D.-H. Kim *et al.*, "Epidermal Electronics," *Science*, vol. 333, no. 6044, pp. 838–843, Aug. 2011, doi: 10.1126/science.1206157.
[36] S. Xu *et al.*, "Soft Microfluidic Assemblies of Sensors, Circuits, and Radios for the Skin," *Science*, vol. 344, no. 6179, pp. 70–74, Apr. 2014, doi: 10.1126/science.1250169.
[37] R. C. Webb *et al.*, "Epidermal devices for noninvasive, precise, and continuous mapping of macrovascular and microvascular blood flow," *Sci. Adv.*, vol. 1, no. 9, p. e1500701, Oct. 2015, doi: 10.1126/sciadv.1500701.
[38] T. Ha *et al.*, "A Chest-Laminated Ultrathin and Stretchable E-Tattoo for the Measurement of Electrocardiogram, Seismocardiogram, and Cardiac Time Intervals," *Adv. Sci.*, p. 1900290, May 2019, doi: 10.1002/advs.201900290.
[39] Z. Popovic, P. Momenroodaki, and R. Scheeler, "Toward wearable wireless thermometers for internal body temperature measurements," *IEEE Commun. Mag.*, vol. 52, no. 10, pp. 118–125, Oct. 2014, doi: 10.1109/MCOM.2014.6917412.
[40] C. A. Boano, M. Lasagni, K. Romer, and T. Lange, "Accurate Temperature Measurements for Medical Research Using Body Sensor Networks," in *2011 14th IEEE International Symposium on Object/Component/Service-Oriented Real-Time Distributed Computing Workshops*, Newport Beach, CA, USA: IEEE, Mar. 2011, pp. 189–198. doi: 10.1109/ISORCW.2011.28.
[41] R. Chad Webb, S. Krishnan, and J. A. Rogers, "Ultrathin, Skin-Like Devices for Precise, Continuous Thermal Property Mapping of Human Skin and Soft Tissues," in *Stretchable Bioelectronics for Medical Devices and Systems*, J. A. Rogers, R. Ghaffari, and D.-H. Kim, Eds., Cham: Springer International Publishing, 2016, pp. 117–132. doi: 10.1007/978-3-319-28694-5_6.
[42] C. Miozzi, S. Amendola, A. Bergamini, and G. Marrocco, "Reliability of a re-usable wireless Epidermal temperature sensor in real conditions," in *2017 IEEE 14th International Conference on Wearable and Implantable Body Sensor Networks (BSN)*, Eindhoven, Netherlands: IEEE, May 2017, pp. 95–98. doi: 10.1109/BSN.2017.7936016.
[43] C. Sugimoto and R. Kohno, "Wireless Sensing System for Healthcare Monitoring Thermal Physiological State and Recognizing Behavior," in *2011 International Conference on Broadband and Wireless Computing, Communication and Applications*, Barcelona, Spain: IEEE, Oct. 2011, pp. 285–291. doi: 10.1109/BWCCA.2011.44.
[44] G. G. Berntson *et al.*, "Heart rate variability: Origins, methods, and interpretive caveats," *Psychophysiology*, vol. 34, no. 6, pp. 623–648, Nov. 1997, doi: 10.1111/j.1469-8986.1997.tb02140.x.
[45] M. Malik, "Heart Rate Variability.: Standards of Measurement, Physiological Interpretation, and Clinical Use: Task Force of The European Society of Cardiology and the North American Society for Pacing and Electrophysiology," *Ann. Noninvasive Electrocardiol.*, vol. 1, no. 2, pp. 151–181, Apr. 1996, doi: 10.1111/j.1542-474X.1996.tb00275.x.
[46] L. C. M. Vanderlei, C. M. Pastre, R. A. Hoshi, T. D. de Carvalho, and M. F. de Godoy, "Noções básicas de variabilidade da frequência cardíaca e sua aplicabilidade clínica," *Rev. Bras. Cir. Cardiovasc.*, vol. 24, no. 2, pp. 205–217, Jun. 2009, doi: 10.1590/S0102-76382009000200018.
[47] B. Becerra-Luna *et al.*, "Heart Rate Variability Assessment Using Time–Frequency Analysis in Hypotensive and Non-Hypotensive Patients in Hemodialysis," *Appl. Sci.*, vol. 10, no. 17, p. 6074, Sep. 2020, doi: 10.3390/app10176074.
[48] L. Capdevila, E. Parrado, J. Ramos-Castro, R. Zapata-Lamana, and J. F. Lalanza, "Resonance frequency is not always stable over time and could be related to the inter-beat interval," *Sci. Rep.*, vol. 11, no. 1, p. 8400, Apr. 2021, doi: 10.1038/s41598-021-87867-8.
[49] E. E. Solís-Montufar, G. Gálvez-Coyt, and A. Muñoz-Diosdado, "Entropy Analysis of RR-Time Series From Stress Tests," *Front. Physiol.*, vol. 11, p. 981, Aug. 2020, doi: 10.3389/fphys.2020.00981.
[50] J.-Y. Chiang *et al.*, "Detrended Fluctuation Analysis of Heart Rate Dynamics Is an Important Prognostic Factor in Patients with End-Stage Renal Disease Receiving Peritoneal Dialysis," *PLOS ONE*, vol. 11, no. 2, p. e0147282, Feb. 2016, doi: 10.1371/journal.pone.0147282.

[51] M. Umemura and K. Honda, “Influence of music on heart rate variability and comfort--a consideration through comparison of music and noise,” *J. Hum. Ergol. (Tokyo)*, vol. 27, no. 1–2, pp. 30–38, Dec. 1998.
[52] X. Tan, C. J. Yowler, D. M. Super, and R. B. Fratianne, “The Interplay of Preference, Familiarity and Psychophysical Properties in Defining Relaxation Music,” *J. Music Ther.*, vol. 49, no. 2, pp. 150–179, Jun. 2012, doi: 10.1093/jmt/49.2.150.
[53] W.-C. Wang, “A study of the type and characteristics of relaxing music for college students,” presented at the 162nd Meeting Acoustical Society of America, San Diego, California, 2014, p. 035001. doi: 10.1121/1.4902001.
[54] L. Bernardi *et al.*, “Dynamic Interactions Between Musical, Cardiovascular, and Cerebral Rhythms in Humans,” *Circulation*, vol. 119, no. 25, pp. 3171–3180, Jun. 2009, doi: 10.1161/CIRCULATIONAHA.108.806174.
[55] U. Kirk, C. Ngnoumen, A. Clausel, and C. K. Purvis, “Effects of Three Genres of Focus Music on Heart Rate Variability and Sustained Attention,” *J. Cogn. Enhanc.*, Sep. 2021, doi: 10.1007/s41465-021-00226-3.
[56] H.-J. Trappe and G. Voit, “The Cardiovascular Effect of Musical Genres,” *Dtsch Arztebl Int.*, vol. 113, no. 20, pp. 347–352, 2016, doi: 10.3238/arztebl.2016.0347.
[57] J. A. T. do Amaral, H. L. Guida, L. C. de Abreu, V. Barnabé, F. M. Vanderlei, and V. E. Valenti, “Effects of auditory stimulation with music of different intensities on heart period,” *J. Tradit. Complement. Med.*, vol. 6, no. 1, pp. 23–28, Jan. 2016, doi: 10.1016/j.jtcme.2014.11.032.
[58] J. Amaral, “Cardiac autonomic regulation during exposure to auditory stimulation with classical baroque or heavy metal music of different intensities,” *Turk Kardiyol. Dernegi Arsivi-Arch. Turk. Soc. Cardiol.*, vol. 42, no. 2, pp. 139–146, 2014, doi: 10.5543/tkda.2014.39000.
[59] J. Bradt, C. Dileo, and N. Potvin, “Music for stress and anxiety reduction in coronary heart disease patients,” *Cochrane Database Syst. Rev.*, vol. 2021, no. 9, Dec. 2013, doi: 10.1002/14651858.CD006577.pub3.
[60] R. U. Krabs, R. Enk, N. Teich, and S. Koelsch, “Autonomic Effects of Music in Health and Crohn’s Disease: The Impact of Isochronicity, Emotional Valence, and Tempo,” *PLOS ONE*, vol. 10, no. 5, p. e0126224, May 2015, doi: 10.1371/journal.pone.0126224.
[61] E. C. Martiniano *et al.*, “Musical auditory stimulus acutely influences heart rate dynamic responses to medication in subjects with well-controlled hypertension,” *Sci. Rep.*, vol. 8, no. 1, p. 958, Dec. 2018, doi: 10.1038/s41598-018-19418-7.
[62] I. A. Mir *et al.*, “Relaxing music reduces blood pressure and heart rate among pre-hypertensive young adults: A randomized control trial,” *J. Clin. Hypertens.*, vol. 23, no. 2, pp. 317–322, Feb. 2021, doi: 10.1111/jch.14126.
[63] H.-G. Kim, E.-J. Cheon, D.-S. Bai, Y. H. Lee, and B.-H. Koo, “Stress and Heart Rate Variability: A Meta-Analysis and Review of the Literature,” *Psychiatry Investig.*, vol. 15, no. 3, pp. 235–245, Mar. 2018, doi: 10.30773/pi.2017.08.17.
[64] D. Ayata, Y. Yaslan, and M. E. Kamasak, “Emotion Based Music Recommendation System Using Wearable Physiological Sensors,” *IEEE Trans. Consum. Electron.*, vol. 64, no. 2, pp. 196–203, May 2018, doi: 10.1109/TCE.2018.2844736.
[65] S. Paszkiel, P. Dobrakowski, and A. Łysiak, “The Impact of Different Sounds on Stress Level in the Context of EEG, Cardiac Measures and Subjective Stress Level: A Pilot Study,” *Brain Sci.*, vol. 10, no. 10, p. 728, Oct. 2020, doi: 10.3390/brainsci10100728.
[66] A. Maseda *et al.*, “Multisensory Stimulation and Individualized Music Sessions on Older Adults with Severe Dementia: Effects on Mood, Behavior, and Biomedical Parameters,” *J. Alzheimers Dis.*, vol. 63, no. 4, pp. 1415–1425, May 2018, doi: 10.3233/JAD-180109.
[67] H. L. Lam, W. T. V. Li, I. Laher, and R. Y. Wong, “Effects of Music Therapy on Patients with Dementia—A Systematic Review,” *Geriatrics*, vol. 5, no. 4, p. 62, Sep. 2020, doi: 10.3390/geriatrics5040062.

[68] C. S. Sim, J. H. Sung, S. H. Cheon, J. M. Lee, J. W. Lee, and J. Lee, “The effects of different noise types on heart rate variability in men,” *Yonsei Med. J.*, vol. 56, no. 1, pp. 235–243, Jan. 2015, doi: 10.3349/ymj.2015.56.1.235.
[69] G.-S. Lee, M.-L. Chen, and G.-Y. Wang, “Evoked response of heart rate variability using short-duration white noise,” *Auton. Neurosci. Basic Clin.*, vol. 155, no. 1–2, pp. 94–97, Jun. 2010, doi: 10.1016/j.autneu.2009.12.008.
[70] E. D. Walker, A. Brammer, M. G. Cherniack, F. Laden, and J. M. Cavallari, “Cardiovascular and stress responses to short-term noise exposures-A panel study in healthy males,” *Environ. Res.*, vol. 150, pp. 391–397, Oct. 2016, doi: 10.1016/j.envres.2016.06.016.
[71] Y. Nakajima, N. Tanaka, T. Mima, and S.-I. Izumi, “Stress Recovery Effects of High- and Low-Frequency Amplified Music on Heart Rate Variability,” *Behav. Neurol.*, vol. 2016, pp. 1–8, 2016, doi: 10.1155/2016/5965894.
[72] W. Pirker and R. Katzenschlager, “Gait disorders in adults and the elderly: A clinical guide,” *Wien. Klin. Wochenschr.*, vol. 129, no. 3–4, pp. 81–95, Feb. 2017, doi: 10.1007/s00508-016-1096-4.
[73] “Falls.” https://www.who.int/news-room/fact-sheets/detail/falls (accessed Apr. 17, 2023).
[74] “Falls and Fractures in Older Adults: Causes and Prevention,” *National Institute on Aging*. https://www.nia.nih.gov/health/falls-and-fractures-older-adults-causes-and-prevention (accessed Apr. 17, 2023).
[75] V.-R. Xefteris, A. Tsanousa, G. Meditskos, S. Vrochidis, and I. Kompatsiaris, “Performance, Challenges, and Limitations in Multimodal Fall Detection Systems: A Review,” *IEEE Sens. J.*, vol. 21, no. 17, pp. 18398–18409, Sep. 2021, doi: 10.1109/JSEN.2021.3090454.
[76] S. Usmani, A. Saboor, M. Haris, M. A. Khan, and H. Park, “Latest Research Trends in Fall Detection and Prevention Using Machine Learning: A Systematic Review,” *Sensors*, vol. 21, no. 15, p. 5134, Jul. 2021, doi: 10.3390/s21155134.
[77] W. Saadeh, S. A. Butt, and M. A. B. Altaf, “A Patient-Specific Single Sensor IoT-Based Wearable Fall Prediction and Detection System,” *IEEE Trans. Neural Syst. Rehabil. Eng.*, vol. 27, no. 5, pp. 995–1003, May 2019, doi: 10.1109/TNSRE.2019.2911602.
[78] J.-S. Lee and H.-H. Tseng, “Development of an Enhanced Threshold-Based Fall Detection System Using Smartphones With Built-In Accelerometers,” *IEEE Sens. J.*, vol. 19, no. 18, pp. 8293–8302, Sep. 2019, doi: 10.1109/JSEN.2019.2918690.
[79] A. Shahzad and K. Kim, “FallDroid: An Automated Smart-Phone-Based Fall Detection System Using Multiple Kernel Learning,” *IEEE Trans. Ind. Inform.*, vol. 15, no. 1, pp. 35–44, Jan. 2019, doi: 10.1109/TII.2018.2839749.
[80] J. Silva, D. Gomes, I. Sousa, and J. S. Cardoso, “Automated Development of Custom Fall Detectors: Position, Model and Rate Impact in Performance,” *IEEE Sens. J.*, vol. 20, no. 10, pp. 5465–5472, May 2020, doi: 10.1109/JSEN.2020.2970994.
[81] W. Lu, M. C. Stevens, C. Wang, S. J. Redmond, and N. H. Lovell, “Smart Triggering of the Barometer in a Fall Detector Using a Semi-Permeable Membrane,” *IEEE Trans. Biomed. Eng.*, vol. 67, no. 1, pp. 146–157, Jan. 2020, doi: 10.1109/TBME.2019.2909907.
[82] J. C. Ayena, H. Zaibi, M. J.-D. Otis, and B.-A. J. Menelas, “Home-Based Risk of Falling Assessment Test Using a Closed-Loop Balance Model,” *IEEE Trans. Neural Syst. Rehabil. Eng.*, vol. 24, no. 12, pp. 1351–1362, Dec. 2016, doi: 10.1109/TNSRE.2015.2508960.
[83] H. Ponce, L. Martinez-Villasenor, and J. Nunez-Martinez, “Sensor Location Analysis and Minimal Deployment for Fall Detection System,” *IEEE Access*, vol. 8, pp. 166678–166691, 2020, doi: 10.1109/ACCESS.2020.3022971.
[84] eugeria, “Have you heard of ADLs?” https://info.eugeria.ca/en/have-you-heard-of-adls/
[85] N. Lee, S. Ahn, and D. Han, “AMID: Accurate Magnetic Indoor Localization Using Deep Learning,” *Sensors*, vol. 18, no. 5, p. 1598, May 2018, doi: 10.3390/s18051598.
[86] I. Ashraf, S. Hur, and Y. Park, “mPILOT-Magnetic Field Strength Based Pedestrian Indoor Localization,” *Sensors*, vol. 18, no. 7, p. 2283, Jul. 2018, doi: 10.3390/s18072283.

[87] G. Wang, X. Wang, J. Nie, and L. Lin, “Magnetic-Based Indoor Localization Using Smartphone via a Fusion Algorithm,” *IEEE Sens. J.*, vol. 19, no. 15, pp. 6477–6485, Aug. 2019, doi: 10.1109/JSEN.2019.2909195.
[88] I. Ashraf, S. Hur, and Y. Park, “MagIO: Magnetic Field Strength Based Indoor- Outdoor Detection with a Commercial Smartphone,” *Micromachines*, vol. 9, no. 10, p. 534, Oct. 2018, doi: 10.3390/mi9100534.
[89] J. Qi and G.-P. Liu, “A Robust High-Accuracy Ultrasound Indoor Positioning System Based on a Wireless Sensor Network,” *Sensors*, vol. 17, no. 11, p. 2554, Nov. 2017, doi: 10.3390/s17112554.
[90] C. Medina, J. Segura, and Á. De la Torre, “Ultrasound Indoor Positioning System Based on a Low-Power Wireless Sensor Network Providing Sub-Centimeter Accuracy,” *Sensors*, vol. 13, no. 3, pp. 3501–3526, Mar. 2013, doi: 10.3390/s130303501.
[91] S. Holm and C.-I. C. Nilsen, “Robust ultrasonic indoor positioning using transmitter arrays,” in *2010 International Conference on Indoor Positioning and Indoor Navigation*, Zurich, Switzerland: IEEE, Sep. 2010, pp. 1–5. doi: 10.1109/IPIN.2010.5646198.
[92] J. Li, G. Han, C. Zhu, and G. Sun, “An Indoor Ultrasonic Positioning System Based on TOA for Internet of Things,” *Mob. Inf. Syst.*, vol. 2016, pp. 1–10, 2016, doi: 10.1155/2016/4502867.
[93] A. Fleury, M. Vacher, and N. Noury, “SVM-Based Multimodal Classification of Activities of Daily Living in Health Smart Homes: Sensors, Algorithms, and First Experimental Results,” *IEEE Trans. Inf. Technol. Biomed.*, vol. 14, no. 2, pp. 274–283, Mar. 2010, doi: 10.1109/TITB.2009.2037317.
[94] A. Fleury, N. Noury, M. Vacher, H. Glasson, and J.-F. Seri, “Sound and speech detection and classification in a Health Smart Home,” in *2008 30th Annual International Conference of the IEEE Engineering in Medicine and Biology Society*, Vancouver, BC: IEEE, Aug. 2008, pp. 4644–4647. doi: 10.1109/IEMBS.2008.4650248.
[95] S. Junnila *et al.*, “Wireless, Multipurpose In-Home Health Monitoring Platform: Two Case Trials,” *IEEE Trans. Inf. Technol. Biomed.*, vol. 14, no. 2, pp. 447–455, Mar. 2010, doi: 10.1109/TITB.2009.2037615.
[96] P. N. Dawadi, D. J. Cook, and M. Schmitter-Edgecombe, “Automated Cognitive Health Assessment Using Smart Home Monitoring of Complex Tasks,” *IEEE Trans. Syst. Man Cybern. Syst.*, vol. 43, no. 6, pp. 1302–1313, Nov. 2013, doi: 10.1109/TSMC.2013.2252338.
[97] C. Debes, A. Merentitis, S. Sukhanov, M. Niessen, N. Frangiadakis, and A. Bauer, “Monitoring Activities of Daily Living in Smart Homes: Understanding human behavior,” *IEEE Signal Process. Mag.*, vol. 33, no. 2, pp. 81–94, Mar. 2016, doi: 10.1109/MSP.2015.2503881.
[98] D. J. Cook, A. S. Crandall, B. L. Thomas, and N. C. Krishnan, “CASAS: A Smart Home in a Box,” *Computer*, vol. 46, no. 7, pp. 62–69, Jul. 2013, doi: 10.1109/MC.2012.328.
[99] N. ElHady and J. Provost, “A Systematic Survey on Sensor Failure Detection and Fault-Tolerance in Ambient Assisted Living,” *Sensors*, vol. 18, no. 7, p. 1991, Jun. 2018, doi: 10.3390/s18071991.
[100] J. Ye, G. Stevenson, and S. Dobson, “Fault detection for binary sensors in smart home environments,” in *2015 IEEE International Conference on Pervasive Computing and Communications (PerCom)*, St. Louis, MO, USA: IEEE, Mar. 2015, pp. 20–28. doi: 10.1109/PERCOM.2015.7146505.
[101] D. De, P. Bharti, S. K. Das, and S. Chellappan, “Multimodal Wearable Sensing for Fine-Grained Activity Recognition in Healthcare,” *IEEE Internet Comput.*, vol. 19, no. 5, pp. 26–35, Sep. 2015, doi: 10.1109/MIC.2015.72.
[102] H. Zou, H. Jiang, Y. Luo, J. Zhu, X. Lu, and L. Xie, “BlueDetect: An iBeacon-Enabled Scheme for Accurate and Energy-Efficient Indoor-Outdoor Detection and Seamless Location-Based Service,” *Sensors*, vol. 16, no. 2, p. 268, Feb. 2016, doi: 10.3390/s16020268.
[103] G. Mokhtari, Q. Zhang, and M. Karunanithi, “Modeling of human movement monitoring using Bluetooth Low Energy technology,” in *2015 37th Annual International Conference of the IEEE Engineering in Medicine and Biology Society (EMBC)*, Milan: IEEE, Aug. 2015, pp. 5066–5069. doi: 10.1109/EMBC.2015.7319530.

[104] J.-H. Huh, Y. Bu, and K. Seo, “Bluetooth-Tracing RSSI Sampling Method as Basic Technology of Indoor Localization for Smart Homes,” *Int. J. Smart Home*, vol. 10, no. 10, pp. 9–22, Oct. 2016, doi: 10.14257/ijsh.2016.10.10.02.

[105] Y. Peng, W. Fan, X. Dong, and X. Zhang, “An Iterative Weighted KNN (IW-KNN) Based Indoor Localization Method in Bluetooth Low Energy (BLE) Environment,” in *2016 Intl IEEE Conferences on Ubiquitous Intelligence & Computing, Advanced and Trusted Computing, Scalable Computing and Communications, Cloud and Big Data Computing, Internet of People, and Smart World Congress (UIC/ATC/ScalCom/CBDCom/IoP/SmartWorld)*, Toulouse: IEEE, Jul. 2016, pp. 794–800. doi: 10.1109/UIC-ATC-ScalCom-CBDCom-IoP-SmartWorld.2016.0127.

[106] S. Viswanathan and S. Srinivasan, “Improved path loss prediction model for short range indoor positioning using bluetooth low energy,” in *2015 IEEE SENSORS*, Busan: IEEE, Nov. 2015, pp. 1–4. doi: 10.1109/ICSENS.2015.7370397.

[107] J. Tosi, F. Taffoni, M. Santacatterina, R. Sannino, and D. Formica, “Performance Evaluation of Bluetooth Low Energy: A Systematic Review,” *Sensors*, vol. 17, no. 12, p. 2898, Dec. 2017, doi: 10.3390/s17122898.

[108] Xin-Yu Lin, Te-Wei Ho, Cheng-Chung Fang, Zui-Shen Yen, Bey-Jing Yang, and Feipei Lai, “A mobile indoor positioning system based on iBeacon technology,” in *2015 37th Annual International Conference of the IEEE Engineering in Medicine and Biology Society (EMBC)*, Milan: IEEE, Aug. 2015, pp. 4970–4973. doi: 10.1109/EMBC.2015.7319507.

[109] S. S. Saab and Z. S. Nakad, “A Standalone RFID Indoor Positioning System Using Passive Tags,” *IEEE Trans. Ind. Electron.*, vol. 58, no. 5, pp. 1961–1970, May 2011, doi: 10.1109/TIE.2010.2055774.

[110] S. Subedi, E. Pauls, and Y. D. Zhang, “Accurate Localization and Tracking of a Passive RFID Reader Based on RSSI Measurements,” *IEEE J. Radio Freq. Identif.*, vol. 1, no. 2, pp. 144–154, Jun. 2017, doi: 10.1109/JRFID.2017.2765618.

[111] S.-C. Kim, Y.-S. Jeong, and S.-O. Park, “RFID-based indoor location tracking to ensure the safety of the elderly in smart home environments,” *Pers. Ubiquitous Comput.*, vol. 17, no. 8, pp. 1699–1707, Dec. 2013, doi: 10.1007/s00779-012-0604-4.

[112] P.-C. Huang, S.-S. Lee, Y.-H. Kuo, and K.-R. Lee, “A flexible sequence alignment approach on pattern mining and matching for human activity recognition,” *Expert Syst. Appl.*, vol. 37, no. 1, pp. 298–306, Jan. 2010, doi: 10.1016/j.eswa.2009.05.057.

[113] F. Zafari, A. Gkelias, and K. K. Leung, “A Survey of Indoor Localization Systems and Technologies,” *IEEE Commun. Surv. Tutor.*, vol. 21, no. 3, pp. 2568–2599, 2019, doi: 10.1109/COMST.2019.2911558.

[114] E. Borelli *et al.*, “HABITAT: An IoT Solution for Independent Elderly,” *Sensors*, vol. 19, no. 5, p. 1258, Mar. 2019, doi: 10.3390/s19051258.

[115] H. Zhang, Z. Zhang, N. Gao, Y. Xiao, Z. Meng, and Z. Li, “Cost-Effective Wearable Indoor Localization and Motion Analysis via the Integration of UWB and IMU,” *Sensors*, vol. 20, no. 2, p. 344, Jan. 2020, doi: 10.3390/s20020344.

[116] A. Alarifi *et al.*, “Ultra Wideband Indoor Positioning Technologies: Analysis and Recent Advances,” *Sensors*, vol. 16, no. 5, p. 707, May 2016, doi: 10.3390/s16050707.

[117] A. Fujii, H. Sekiguchi, M. Asai, S. Kurashima, H. Ochiai, and R. Kohno, “Impulse Radio UWB Positioning System,” in *2007 IEEE Radio and Wireless Symposium*, Long Beach, CA, USA: IEEE, 2007, pp. 55–58. doi: 10.1109/RWS.2007.351756.

[118]M. Deputter, “UWB versus other location technologies,” *Pozyx*. https://www.pozyx.io/newsroom/uwb-versus-other-technologies (accessed Aug. 08, 2023).

[119]M. Abdul Mujeebu, “Introductory Chapter: Indoor Environmental Quality,” in *Indoor Environmental Quality*, M. Abdul Mujeebu, Ed., IntechOpen, 2019. doi: 10.5772/intechopen.83612.

[120] United States Environmental Protection Agency (EPA), “Indoor Air Quality,” Jul. 16, 2018. https://www.epa.gov/report-environment/indoor-air-quality (accessed Jan. 12, 2020).

[121] O. K. Kurt, J. Zhang, and K. E. Pinkerton, “Pulmonary health effects of air pollution:,” *Curr. Opin. Pulm. Med.*, vol. 22, no. 2, pp. 138–143, Mar. 2016, doi: 10.1097/MCP.0000000000000248.
[122] I. Galán, A. Tobías, J. R. Banegas, and E. Aránguez, “Short-term effects of air pollution on daily asthma emergency room admissions,” *Eur. Respir. J.*, vol. 22, no. 5, pp. 802–808, Nov. 2003, doi: 10.1183/09031936.03.00013003.
[123] D. Y. C. Leung, “Outdoor-indoor air pollution in urban environment: challenges and opportunity,” *Front. Environ. Sci.*, vol. 2, Jan. 2015, doi: 10.3389/fenvs.2014.00069.
[124] World Health Organization, Ed., *Who guidelines for indoor air quality: selected pollutants*. Copenhagen: WHO, 2010.
[125]“A Guide on Volatile Organic Compounds (VOCs),” *TSI.com*. https://tsi.com//Microsites/IEQ/Resources/Blog/May-2023/A-Guide-on-Volatile-Organic-Compounds-(VOCs) (accessed Aug. 28, 2023).
[126] A. V. Arundel, E. M. Sterling, J. H. Biggin, and T. D. Sterling, “Indirect Health Effects of Relative Humidity in Indoor Environments,” *Environ. Health Perspect.*, vol. 65, p. 351, Mar. 1986, doi: 10.2307/3430203.
[127] S. Watson, “Humidity and Asthma: Effects of Humidity on Asthma & How to Prevent It,” *Healthline*, Apr. 05, 2018. https://www.healthline.com/health/humidity-and-asthma (accessed Feb. 12, 2020).
[128] O. Postolache, J. Miguel, P. Silva, and Gabriela, “Distributed Smart Sensing Systems for Indoor Monitoring of Respiratory Distress Triggering Factors,” in *Chemistry, Emission Control, Radioactive Pollution and Indoor Air Quality*, N. Mazzeo, Ed., InTech, 2011. doi: 10.5772/16929.
[129] F. Salamone, L. Belussi, L. Danza, T. Galanos, M. Ghellere, and I. Meroni, “Design and Development of a Nearable Wireless System to Control Indoor Air Quality and Indoor Lighting Quality,” *Sensors*, vol. 17, no. 5, p. 1021, May 2017, doi: 10.3390/s17051021.
[130] N. Vidakis, M. A. Lasithiotakis, and E. Karapidakis, “Recodify: an intelligent environment and space hazard condition monitoring system based on WSN and IoT technology,” in *Proceedings of the 22nd Pan-Hellenic Conference on Informatics - PCI ’18*, Athens, Greece: ACM Press, 2018, pp. 300–305. doi: 10.1145/3291533.3291554.
[131] S. Abraham and X. Li, “A Cost-effective Wireless Sensor Network System for Indoor Air Quality Monitoring Applications,” *Procedia Comput. Sci.*, vol. 34, pp. 165–171, 2014, doi: 10.1016/j.procs.2014.07.090.
[132] J.-Y. Kim, C.-H. Chu, and S.-M. Shin, “ISSAQ: An Integrated Sensing Systems for Real-Time Indoor Air Quality Monitoring,” *IEEE Sens. J.*, vol. 14, no. 12, pp. 4230–4244, Dec. 2014, doi: 10.1109/JSEN.2014.2359832.
[133] “Recommended Light Levels (Illuminance) for Outdoor and Indoor Venues.” The National Optical Astronomy Observatory (NOAO). Accessed: Mar. 12, 2020. [Online]. Available: https://www.noao.edu/education/QLTkit/ACTIVITY_Documents/Safety/LightLevels_outdoor+indoor.pdf
[134]L. Knoerzer, “What Is Circadian Ligthing?,” *The Lighting Practice*. https://www.thelightingpractice.com/what-is-circadian-lighting/ (accessed Mar. 12, 2020).
[135]“What is Circadian Rhythm?,” *National Sleep Foundation*. https://www.sleepfoundation.org/articles/what-circadian-rhythm (accessed Jul. 29, 2019).
[136] M. Jacob Rodrigues, O. Postolache, and F. Cercas, “Indoor Air Quality Monitoring System to Prevent the Triggering of Respiratory Distress,” Lisbon, Portugal, Aug. 2019.
[137] Yeelight, “LED Bulb (Color).” https://www.yeelight.com/en_US/product/wifi-led-c
[138]Philips Hue, “The official site of Philips Hue | Meethue.com.” https://www2.meethue.com/en-us
[139] Weltgesundheitsorganisation and Regionalbüro für Europa, *Environmental noise guidelines for the European Region*. 2018. Accessed: Feb. 18, 2020. [Online]. Available: http://www.euro.who.int/__data/assets/pdf_file/0008/383921/noise-guidelines-eng.pdf?ua=1
[140] A. Muzet, “Environmental noise, sleep and health,” *Sleep Med. Rev.*, vol. 11, no. 2, pp. 135–142, Apr. 2007, doi: 10.1016/j.smrv.2006.09.001.

[141] D. Halperin, “Environmental noise and sleep disturbances: A threat to health?,” *Sleep Sci.*, vol. 7, no. 4, pp. 209–212, Dec. 2014, doi: 10.1016/j.slsci.2014.11.003.
[142] C. Gomez, S. Chessa, A. Fleury, G. Roussos, and D. Preuveneers, “Internet of Things for enabling smart environments: A technology-centric perspective,” *J. Ambient Intell. Smart Environ.*, vol. 11, no. 1, pp. 23–43, Jan. 2019, doi: 10.3233/AIS-180509.
[143] S. Zhang, Z. Wei, J. Nie, L. Huang, S. Wang, and Z. Li, “A Review on Human Activity Recognition Using Vision-Based Method,” *J. Healthc. Eng.*, vol. 2017, pp. 1–31, 2017, doi: 10.1155/2017/3090343.
[144] L. Chen, C. D. Nugent, and H. Wang, “A Knowledge-Driven Approach to Activity Recognition in Smart Homes,” *IEEE Trans. Knowl. Data Eng.*, vol. 24, no. 6, pp. 961–974, Jun. 2012, doi: 10.1109/TKDE.2011.51.
[145] A. Y. Ng and M. I. Jordan, “On discriminative vs. generative classifiers: A comparison of logistic regression and naive bayes,” 2002, pp. 841–848.
[146] “CASAS Datasets.” http://casas.wsu.edu/datasets/ (accessed Feb. 17, 2020).
[147] “MavHome Datasets.” http://ailab.wsu.edu/mavhome/research.html (accessed Feb. 17, 2020).
[148] “ARAS Datasets.” http://aras.cmpe.boun.edu.tr/# (accessed Feb. 17, 2020).
[149] “MIT Activity Dataset.” https://courses.media.mit.edu/2004fall/mas622j/04.projects/home/ (accessed Feb. 17, 2020).
[150] “Kasteren Datasets.” https://sites.google.com/site/tim0306/datasets (accessed Feb. 17, 2020).
[151] Du, Lim, and Tan, “A Novel Human Activity Recognition and Prediction in Smart Home Based on Interaction,” *Sensors*, vol. 19, no. 20, p. 4474, Oct. 2019, doi: 10.3390/s19204474.
[152] S. Chernbumroong, S. Cang, A. Atkins, and H. Yu, “Elderly activities recognition and classification for applications in assisted living,” *Expert Syst. Appl.*, vol. 40, no. 5, pp. 1662–1674, Apr. 2013, doi: 10.1016/j.eswa.2012.09.004.
[153] S. Chernbumroong, S. Cang, and H. Yu, “A practical multi-sensor activity recognition system for home-based care,” *Decis. Support Syst.*, vol. 66, pp. 61–70, Oct. 2014, doi: 10.1016/j.dss.2014.06.005.
[154] K. Davis *et al.*, “Activity recognition based on inertial sensors for Ambient Assisted Living,” Heidelberg, Germany, Jul. 2016, p. pp.371-378.
[155] M. Prossegger and A. Bouchachia, “Multi-resident Activity Recognition Using Incremental Decision Trees,” in *Adaptive and Intelligent Systems*, A. Bouchachia, Ed., Cham: Springer International Publishing, 2014, pp. 182–191. doi: 10.1007/978-3-319-11298-5_19.
[156] N. Melo and J. Lee, “Environment aware ADL recognition system based on decision tree and activity frame,” *Paladyn J. Behav. Robot.*, vol. 9, no. 1, pp. 155–167, Jul. 2018, doi: 10.1515/pjbr-2018-0011.
[157] V. G. Sánchez and N.-O. Skeie, “Decision Trees for Human Activity Recognition in Smart House Environments,” Nov. 2018, pp. 222–229. doi: 10.3384/ecp18153222.
[158] E. García, M. Villar, M. Fáñez, J. R. Villar, E. De La Cal, and S.-B. Cho, “Towards effective detection of elderly falls with CNN-LSTM neural networks,” *Neurocomputing*, vol. 500, pp. 231–240, Aug. 2022, doi: 10.1016/j.neucom.2021.06.102.
[159] J. Wu, J. Wang, A. Zhan, and C. Wu, “Fall Detection with CNN-Casual LSTM Network,” *Information*, vol. 12, no. 10, p. 403, Sep. 2021, doi: 10.3390/info12100403.
[160] A. Butt, S. Narejo, M. R. Anjum, M. U. Yonus, M. Memon, and A. A. Samejo, “Fall Detection Using LSTM and Transfer Learning,” *Wirel. Pers. Commun.*, vol. 126, no. 2, pp. 1733–1750, Sep. 2022, doi: 10.1007/s11277-022-09819-3.
[161] H. Sak, A. Senior, and F. Beaufays, “Long Short-Term Memory Based Recurrent Neural Network Architectures for Large Vocabulary Speech Recognition,” 2014, doi: 10.48550/ARXIV.1402.1128.
[162] T. Buz, “Comparing RNN and CNN models on invoice extraction: LSTM vs GRU vs TCN,” *Hypatos_Insights*, May 29, 2019. https://medium.com/hypatos-insights/comparing-rnn-and-cnn-models-on-invoice-extraction-lstm-vs-gru-vs-tcn-f2464bf74329 (accessed May 25, 2023).

[163] D. Sarabia-Jácome, R. Usach, C. E. Palau, and M. Esteve, “Highly-efficient fog-based deep learning AAL fall detection system,” *Internet Things*, vol. 11, p. 100185, Sep. 2020, doi: 10.1016/j.iot.2020.100185.
[164] L. Ma, M. Liu, N. Wang, L. Wang, Y. Yang, and H. Wang, “Room-Level Fall Detection Based on Ultra-Wideband (UWB) Monostatic Radar and Convolutional Long Short-Term Memory (LSTM),” *Sensors*, vol. 20, no. 4, p. 1105, Feb. 2020, doi: 10.3390/s20041105.
[165] W. Liu, Z. Lian, and Y. Liu, “Heart rate variability at different thermal comfort levels,” *Eur. J. Appl. Physiol.*, vol. 103, no. 3, pp. 361–366, Jun. 2008, doi: 10.1007/s00421-008-0718-6.
[166] H. Zhu, H. Wang, Z. Liu, D. Li, G. Kou, and C. Li, “Experimental study on the human thermal comfort based on the heart rate variability (HRV) analysis under different environments,” *Sci. Total Environ.*, vol. 616–617, pp. 1124–1133, Mar. 2018, doi: 10.1016/j.scitotenv.2017.10.208.
[167] K. N. Nkurikiyeyezu, Y. Suzuki, and G. F. Lopez, “Heart rate variability as a predictive biomarker of thermal comfort,” *J. Ambient Intell. Humaniz. Comput.*, vol. 9, no. 5, pp. 1465–1477, Oct. 2018, doi: 10.1007/s12652-017-0567-4.
[168] N. Morresi *et al.*, “Sensing physiological and environmental quantities to measure human thermal comfort through Machine Learning techniques,” *IEEE Sens. J.*, pp. 1–1, 2021, doi: 10.1109/JSEN.2021.3064707.
[169] D. Kukolja, S. Popović, M. Horvat, B. Kovač, and K. Ćosić, “Comparative analysis of emotion estimation methods based on physiological measurements for real-time applications,” *Int. J. Hum.-Comput. Stud.*, vol. 72, no. 10–11, pp. 717–727, Oct. 2014, doi: 10.1016/j.ijhcs.2014.05.006.
[170] E. Smets *et al.*, “Comparison of Machine Learning Techniques for Psychophysiological Stress Detection,” in *Pervasive Computing Paradigms for Mental Health*, S. Serino, A. Matic, D. Giakoumis, G. Lopez, and P. Cipresso, Eds., in Communications in Computer and Information Science, vol. 604. Cham: Springer International Publishing, 2016, pp. 13–22. doi: 10.1007/978-3-319-32270-4_2.
[171] J. A. Domínguez-Jiménez, K. C. Campo-Landines, J. C. Martínez-Santos, E. J. Delahoz, and S. H. Contreras-Ortiz, “A machine learning model for emotion recognition from physiological signals,” *Biomed. Signal Process. Control*, vol. 55, p. 101646, Jan. 2020, doi: 10.1016/j.bspc.2019.101646.
[172] E. Smets *et al.*, “Comparison of Machine Learning Techniques for Psychophysiological Stress Detection,” in *Pervasive Computing Paradigms for Mental Health*, S. Serino, A. Matic, D. Giakoumis, G. Lopez, and P. Cipresso, Eds., in Communications in Computer and Information Science, vol. 604. Cham: Springer International Publishing, 2016, pp. 13–22. doi: 10.1007/978-3-319-32270-4_2.
[173] A. O. Akmandor and N. K. Jha, “Keep the Stress Away with SoDA: Stress Detection and Alleviation System,” *IEEE Trans. Multi-Scale Comput. Syst.*, vol. 3, no. 4, pp. 269–282, Oct. 2017, doi: 10.1109/TMSCS.2017.2703613.
[174] A. Salazar-Ramirez, E. Irigoyen, R. Martinez, and U. Zalabarria, “An enhanced fuzzy algorithm based on advanced signal processing for identification of stress,” *Neurocomputing*, vol. 271, pp. 48–57, Jan. 2018, doi: 10.1016/j.neucom.2016.08.153.
[175] I. Bichindaritz, C. Breen, E. Cole, N. Keshan, and P. Parimi, “Feature Selection and Machine Learning Based Multilevel Stress Detection from ECG Signals,” in *Innovation in Medicine and Healthcare 2017*, Y.-W. Chen, S. Tanaka, R. J. Howlett, and L. C. Jain, Eds., in Smart Innovation, Systems and Technologies, vol. 71. Cham: Springer International Publishing, 2018, pp. 202–213. doi: 10.1007/978-3-319-59397-5_22.
[176] F. Al-shargie, T. B. Tang, N. Badruddin, and M. Kiguchi, “Towards multilevel mental stress assessment using SVM with ECOC: an EEG approach,” *Med. Biol. Eng. Comput.*, vol. 56, no. 1, pp. 125–136, Jan. 2018, doi: 10.1007/s11517-017-1733-8.
[177] B. Hwang, J. You, T. Vaessen, I. Myin-Germeys, C. Park, and B.-T. Zhang, “Deep ECGNet: An Optimal Deep Learning Framework for Monitoring Mental Stress Using Ultra Short-Term ECG Signals,” *Telemed. E-Health*, vol. 24, no. 10, pp. 753–772, Oct. 2018, doi: 10.1089/tmj.2017.0250.
[178] G. Giannakakis, K. Marias, and M. Tsiknakis, “A stress recognition system using HRV parameters and machine learning techniques,” in *2019 8th International Conference on Affective Computing*

and Intelligent Interaction Workshops and Demos (ACIIW), Cambridge, United Kingdom: IEEE, Sep. 2019, pp. 269–272. doi: 10.1109/ACIIW.2019.8925142.

[179] A. Oskooei, S. M. Chau, J. Weiss, A. Sridhar, M. R. Martínez, and B. Michel, "DeStress: Deep Learning for Unsupervised Identification of Mental Stress in Firefighters from Heart-rate Variability (HRV) Data," 2019, doi: 10.48550/ARXIV.1911.13213.

[180] Q. V. Le and others, "A tutorial on deep learning part 2: Autoencoders, convolutional neural networks and recurrent neural networks," *Google Brain*, vol. 20, pp. 1–20, 2015.

[181] J. Li, M. Erdt, L. Chen, Y. Cao, S.-Q. Lee, and Y.-L. Theng, "The Social Effects of Exergames on Older Adults: Systematic Review and Metric Analysis," *J. Med. Internet Res.*, vol. 20, no. 6, p. e10486, Jun. 2018, doi: 10.2196/10486.

[182] L. A. Cushman, K. Stein, and C. J. Duffy, "Detecting navigational deficits in cognitive aging and Alzheimer disease using virtual reality," *Neurology*, vol. 71, no. 12, pp. 888–895, Sep. 2008, doi: 10.1212/01.wnl.0000326262.67613.fe.

[183] M. Kafri, M. J. Myslinski, V. K. Gade, and J. E. Deutsch, "Energy Expenditure and Exercise Intensity of Interactive Video Gaming in Individuals Poststroke," *Neurorehabil. Neural Repair*, vol. 28, no. 1, pp. 56–65, Jan. 2014, doi: 10.1177/1545968313497100.

[184] J. E. Munoz Cardona, M. S. Cameirao, T. Paulino, S. Bermudez i Badia, and E. Rubio, "Modulation of Physiological Responses and Activity Levels during Exergame Experiences," in *2016 8th International Conference on Games and Virtual Worlds for Serious Applications (VS-GAMES)*, Barcelona, Spain: IEEE, Sep. 2016, pp. 1–8. doi: 10.1109/VS-GAMES.2016.7590353.

[185] C. L. F. Chan, E. K. Y. Ngai, P. K. H. Leung, and S. Wong, "Effect of the adapted virtual reality cognitive training program among Chinese older adults with chronic schizophrenia: a pilot study," *Int. J. Geriatr. Psychiatry*, p. n/a-n/a, 2009, doi: 10.1002/gps.2403.

[186] G. H. Cho, G. Hwangbo, and H. S. Shin, "The Effects of Virtual Reality-based Balance Training on Balance of the Elderly," *J. Phys. Ther. Sci.*, vol. 26, no. 4, pp. 615–617, 2014, doi: 10.1589/jpts.26.615.

[187] L. Donath, R. Rössler, and O. Faude, "Effects of Virtual Reality Training (Exergaming) Compared to Alternative Exercise Training and Passive Control on Standing Balance and Functional Mobility in Healthy Community-Dwelling Seniors: A Meta-Analytical Review," *Sports Med.*, vol. 46, no. 9, pp. 1293–1309, Sep. 2016, doi: 10.1007/s40279-016-0485-1.

[188] J. S. C. de Amorim, R. C. Leite, R. Brizola, and C. Y. Yonamine, "Virtual reality therapy for rehabilitation of balance in the elderly: a systematic review and META-analysis," *Adv. Rheumatol.*, vol. 58, no. 1, p. 18, Dec. 2018, doi: 10.1186/s42358-018-0013-0.

[189] C. Lei *et al.*, "Effects of virtual reality rehabilitation training on gait and balance in patients with Parkinson's disease: A systematic review," *PLOS ONE*, vol. 14, no. 11, p. e0224819, Nov. 2019, doi: 10.1371/journal.pone.0224819.

[190] Q. Fang *et al.*, "Effects of Exergaming on Balance of Healthy Older Adults: A Systematic Review and Meta-analysis of Randomized Controlled Trials," *Games Health J.*, vol. 9, no. 1, pp. 11–23, Feb. 2020, doi: 10.1089/g4h.2019.0016.

[191] E. Wiley, S. Khattab, and A. Tang, "Examining the effect of virtual reality therapy on cognition post-stroke: a systematic review and meta-analysis," *Disabil. Rehabil. Assist. Technol.*, pp. 1–11, May 2020, doi: 10.1080/17483107.2020.1755376.

[192] A. Brachman *et al.*, "The Effects of Exergaming Training on Balance in Healthy Elderly Women—A Pilot Study," *Int. J. Environ. Res. Public. Health*, vol. 18, no. 4, p. 1412, Feb. 2021, doi: 10.3390/ijerph18041412.

[193] J. Bourrelier, J. Ryard, M. Dion, F. Merienne, P. Manckoundia, and F. Mourey, "Use of a Virtual Environment to Engage Motor and Postural Abilities in Elderly Subjects With and Without Mild Cognitive Impairment (MAAMI Project)," *IRBM*, vol. 37, no. 2, pp. 75–80, Apr. 2016, doi: 10.1016/j.irbm.2016.02.007.

[194] R. Stojan and C. Voelcker-Rehage, "A Systematic Review on the Cognitive Benefits and Neurophysiological Correlates of Exergaming in Healthy Older Adults," *J. Clin. Med.*, vol. 8, no. 5, p. 734, May 2019, doi: 10.3390/jcm8050734.

[195] P. Eggenberger, S. Annaheim, K. A. Kündig, R. M. Rossi, T. Münzer, and E. D. de Bruin, “Heart Rate Variability Mainly Relates to Cognitive Executive Functions and Improves Through Exergame Training in Older Adults: A Secondary Analysis of a 6-Month Randomized Controlled Trial,” *Front. Aging Neurosci.*, vol. 12, p. 197, Jul. 2020, doi: 10.3389/fnagi.2020.00197.

[196] E. Vogiatzaki and A. Krukowski, “Maintaining Mental Wellbeing of Elderly at Home,” in *Enhanced Living Environments*, I. Ganchev, N. M. Garcia, C. Dobre, C. X. Mavromoustakis, and R. Goleva, Eds., Cham: Springer International Publishing, 2019, pp. 177–209. doi: 10.1007/978-3-030-10752-9_8.

[197] “Active Assisted Living Programme.” http://www.aal-europe.eu/

[198] G. Goodall *et al.*, “The Use of Virtual and Immersive Technology in Creating Personalized Multisensory Spaces for People Living With Dementia (SENSE-GARDEN): Protocol for a Multisite Before-After Trial,” *JMIR Res. Protoc.*, vol. 8, no. 9, p. e14096, Aug. 2019, doi: 10.2196/14096.

[199] G. Goodall *et al.*, “The Role of Adaptive Immersive Technology in Creating Personalised Environments for Emotional Connection and Preservation of Identity in Dementia Care,” *International Journal on Advances in Life Sciences*.

[200] S. Mallat, *A wavelet tour of signal processing: the sparse way*, 3rd ed. Amsterdam Boston: Elsevier/Academic Press, 2009.

[201] O. Postolache, P. S. Girão, E. Pinheiro, and G. Postolache, “Unobtrusive and Non-invasive Sensing Solutions for On-Line Physiological Parameters Monitoring,” in *Wearable and Autonomous Biomedical Devices and Systems for Smart Environment*, A. Lay-Ekuakille and S. C. Mukhopadhyay, Eds., in Lecture Notes in Electrical Engineering, vol. 75. Berlin, Heidelberg: Springer Berlin Heidelberg, 2010, pp. 277–314. doi: 10.1007/978-3-642-15687-8_15.

[202] A. Burns *et al.*, “SHIMMER^{TM} – A Wireless Sensor Platform for Noninvasive Biomedical Research,” *IEEE Sens. J.*, vol. 10, no. 9, pp. 1527–1534, Sep. 2010, doi: 10.1109/JSEN.2010.2045498.

[203] outsourcing-pharma.com, “Shimmer wearable lands CE certification,” *outsourcing-pharma.com*. https://www.outsourcing-pharma.com/Article/2020/11/25/Shimmer-wearable-sensor-lands-CE-certification (accessed Oct. 01, 2022).

[204] A. Burns *et al.*, “SHIMMER: An extensible platform for physiological signal capture,” in *2010 Annual International Conference of the IEEE Engineering in Medicine and Biology*, Buenos Aires: IEEE, Aug. 2010, pp. 3759–3762. doi: 10.1109/IEMBS.2010.5627535.

[205] iMotions, “Galvanic Skin Response (GSR): The Complete Pocket Guide,” *Research Fundamentals*. https://imotions.com/blog/learning/research-fundamentals/galvanic-skin-response/ (accessed Aug. 28, 2023).

[206] D. Makowski *et al.*, “neuropsychology/NeuroKit: 0.0.6.” Zenodo, Jan. 05, 2020. doi: 10.5281/ZENODO.3597887.

[207] M. Abdul Mujeebu, “Introductory Chapter: Indoor Environmental Quality,” in *Indoor Environmental Quality*, M. Abdul Mujeebu, Ed., IntechOpen, 2019. doi: 10.5772/intechopen.83612.

[208] O. K. Kurt, J. Zhang, and K. E. Pinkerton, “Pulmonary health effects of air pollution:,” *Curr. Opin. Pulm. Med.*, vol. 22, no. 2, pp. 138–143, Mar. 2016, doi: 10.1097/MCP.0000000000000248.

[209] Sensirion, “Particulate Matter Sensor SPS30.” https://www.sensirion.com/en/environmental-sensors/particulate-matter-sensors-pm25/ (accessed Aug. 20, 2021).

[210] CSA Group, “MCERTS Certified Products: Indicative Ambient Particulate Monitors.” https://www.csagroup.org/en-gb/services/mcerts/mcerts-product-certification/mcerts-certified-products/mcerts-certified-products-indicative-ambient-particulate-monitors/ (accessed Aug. 20, 2021).

[211] M. Jacob Rodrigues, O. Postolache, and F. Cercas, “Indoor Air Quality Monitoring System to Prevent the Triggering of Respiratory Distress,” in *2019 International Conference on Sensing and Instrumentation in IoT Era (ISSI)*, Lisbon, Portugal: IEEE, Aug. 2019, pp. 1–6. doi: 10.1109/ISSI47111.2019.9043669.

[212] Silicon Laboratories, “Si7021 - I2C Humidity and Temperature Sensor Datasheet.” Accessed: Aug. 20, 2021. [Online]. Available: https://www.silabs.com/documents/public/data-sheets/Si7021-A20.pdf

[213] “CCS811 Ultra-Low Power Digital Gas Sensor for Monitoring Indoor Air Quality.” ams OSRAM, Dec. 23, 2016.
[214] “Adafruit AGC Electret Microphone Amplifier - MAX9814.” Adafruit Learning System. Accessed: Aug. 28, 2023. [Online]. Available: https://learn.adafruit.com/adafruit-agc-electret-microphone-amplifier-max9814/overview
[215] “Pozyx Academy | How positioning works.” https://www.pozyx.io/pozyx-academy/how-does-positioning-work (accessed Apr. 12, 2023).
[216] “Eclipse Mosquitto,” *Eclipse Mosquitto*, Jan. 08, 2018. https://mosquitto.org/ (accessed Aug. 28, 2023).
[217] J. Schwartz, J. M. Samet, and J. A. Patz, “Hospital Admissions for Heart Disease: The Effects of Temperature and Humidity,” *Epidemiology*, vol. 15, no. 6, pp. 755–761, Nov. 2004, doi: 10.1097/01.ede.0000134875.15919.0f.
[218] N. Fann, *et al.*, “Ch. 3: Air Quality Impacts. The Impacts of Climate Change on Human Health in the United States: A Scientific Assessment,” U.S. Global Change Research Program, 2016. doi: 10.7930/J0GQ6VP6.
[219] W.-C. Lee, L. Shen, P. J. Catalano, L. J. Mickley, and P. Koutrakis, “Effects of future temperature change on PM2.5 infiltration in the Greater Boston area,” *Atmos. Environ.*, vol. 150, pp. 98–105, Feb. 2017, doi: 10.1016/j.atmosenv.2016.11.027.
[220] World Health Organization, *WHO housing and health guidelines*. Geneva: World Health Organization, 2018. Accessed: Nov. 13, 2021. [Online]. Available: https://apps.who.int/iris/handle/10665/276001
[221] K. K. Zander, S. Moss, and S. T. Garnett, “Climate Change–Related Heat Stress and Subjective Well-Being in Australia,” *Weather Clim. Soc.*, vol. 11, no. 3, pp. 505–520, Jul. 2019, doi: 10.1175/WCAS-D-18-0074.1.
[222] I. Manisalidis, E. Stavropoulou, A. Stavropoulos, and E. Bezirtzoglou, “Environmental and Health Impacts of Air Pollution: A Review,” *Front. Public Health*, vol. 8, p. 14, Feb. 2020, doi: 10.3389/fpubh.2020.00014.
[223] K. L. Ebi and J. J. Hess, “Health Risks Due To Climate Change: Inequity In Causes And Consequences: Study examines health risks due to climate change.,” *Health Aff. (Millwood)*, vol. 39, no. 12, pp. 2056–2062, Dec. 2020, doi: 10.1377/hlthaff.2020.01125.
[224] S. Tham, R. Thompson, O. Landeg, K. A. Murray, and T. Waite, “Indoor temperature and health: a global systematic review,” *Public Health*, vol. 179, pp. 9–17, Feb. 2020, doi: 10.1016/j.puhe.2019.09.005.
[225] P. Wolkoff, “Indoor air humidity, air quality, and health – An overview,” *Int. J. Hyg. Environ. Health*, vol. 221, no. 3, pp. 376–390, Apr. 2018, doi: 10.1016/j.ijheh.2018.01.015.
[226] T. Lindgren, D. Norbäck, and G. Wieslander, “Perception of cabin air quality in airline crew related to air humidification, on intercontinental flights,” *Indoor Air*, vol. 17, no. 3, pp. 204–210, Jun. 2007, doi: 10.1111/j.1600-0668.2006.00467.x.
[227] Y. Kim *et al.*, “Effects of relative humidity and particle and surface properties on particle resuspension rates,” *Aerosol Sci. Technol.*, vol. 50, no. 4, pp. 339–352, Apr. 2016, doi: 10.1080/02786826.2016.1152350.
[228] D. Hayes, P. B. Collins, M. Khosravi, R.-L. Lin, and L.-Y. Lee, “Bronchoconstriction Triggered by Breathing Hot Humid Air in Patients with Asthma: Role of Cholinergic Reflex,” *Am. J. Respir. Crit. Care Med.*, vol. 185, no. 11, pp. 1190–1196, Jun. 2012, doi: 10.1164/rccm.201201-0088OC.
[229] A. V. Arundel, E. M. Sterling, J. H. Biggin, and T. D. Sterling, “Indirect health effects of relative humidity in indoor environments.,” *Environ. Health Perspect.*, vol. 65, pp. 351–361, Mar. 1986, doi: 10.1289/ehp.8665351.
[230] M. Malik, “Heart Rate Variability.: Standards of Measurement, Physiological Interpretation, and Clinical Use: Task Force of The European Society of Cardiology and the North American Society for Pacing and Electrophysiology,” *Ann. Noninvasive Electrocardiol.*, vol. 1, no. 2, pp. 151–181, Apr. 1996, doi: 10.1111/j.1542-474X.1996.tb00275.x.

[231] H. J. Baek, C.-H. Cho, J. Cho, and J.-M. Woo, “Reliability of Ultra-Short-Term Analysis as a Surrogate of Standard 5-Min Analysis of Heart Rate Variability,” *Telemed. E-Health*, vol. 21, no. 5, pp. 404–414, May 2015, doi: 10.1089/tmj.2014.0104.

[232] D. Wehler *et al.*, “Reliability of heart-rate-variability features derived from ultra-short ECG recordings and their validity in the assessment of cardiac autonomic neuropathy,” *Biomed. Signal Process. Control*, vol. 68, p. 102651, Jul. 2021, doi: 10.1016/j.bspc.2021.102651.

[233] M. L. Munoz *et al.*, “Validity of (Ultra-)Short Recordings for Heart Rate Variability Measurements,” *PLOS ONE*, vol. 10, no. 9, p. e0138921, Sep. 2015, doi: 10.1371/journal.pone.0138921.

[234] U. Fiore, A. De Santis, F. Perla, P. Zanetti, and F. Palmieri, “Using generative adversarial networks for improving classification effectiveness in credit card fraud detection,” *Inf. Sci.*, vol. 479, pp. 448–455, Apr. 2019, doi: 10.1016/j.ins.2017.12.030.

[235] J. C. Porcello, “Designing and Implementing SVMs for High-Dimensional Knowledge Discovery Using FPGAs,” in *2019 IEEE Aerospace Conference*, Big Sky, MT, USA: IEEE, Mar. 2019, pp. 1–8. doi: 10.1109/AERO.2019.8741916.

[236] Y. SONG and Y. LU, “Decision tree methods: applications for classification and prediction,” *Shanghai Arch. Psychiatry*, vol. 27, no. 2, pp. 130–135, Apr. 2015, doi: 10.11919/j.issn.1002-0829.215044.

[237] L. Breiman, “Random Forests,” *Mach. Learn.*, vol. 45, no. 1, pp. 5–32, Oct. 2001, doi: 10.1023/A:1010933404324.

[238] F. Murtagh, “Multilayer perceptrons for classification and regression,” *Neurocomputing*, vol. 2, no. 5, pp. 183–197, Jul. 1991, doi: 10.1016/0925-2312(91)90023-5.

[239]ANSYS, Inc, “Ansys Fluent - Fluid Simulation Software.” https://www.ansys.com/products/fluids/ansys-fluent (accessed Sep. 04, 2021).

[240] “Technical Data MQ-135 Gas Sensor.” HANWEI ELECTRONICS CO.,LTD. [Online]. Available: https://www.electronicoscaldas.com/datasheet/MQ-135_Hanwei.pdf

[241] A. V. Arundel, E. M. Sterling, J. H. Biggin, and T. D. Sterling, “Indirect health effects of relative humidity in indoor environments.,” *Environ. Health Perspect.*, vol. 65, pp. 351–361, Mar. 1986, doi: 10.1289/ehp.8665351.

[242] J. D. Schipke, M. Pelzer, and G. Arnold, “Effect of respiration rate on short-term heart rate variability,” *J. Clin. Basic Cardiol.*, vol. 2, pp. 92–95, 1999.

[243] C. Li, Q. Chang, J. Zhang, and W. Chai, “Effects of slow breathing rate on heart rate variability and arterial baroreflex sensitivity in essential hypertension,” *Medicine (Baltimore)*, vol. 97, no. 18, p. e0639, May 2018, doi: 10.1097/MD.0000000000010639.

[244] K. Hamunen, V. Kontinen, E. Hakala, P. Talke, M. Paloheimo, and E. Kalso, “Effect of pain on autonomic nervous system indices derived from photoplethysmography in healthy volunteers,” *Br. J. Anaesth.*, vol. 108, no. 5, pp. 838–844, May 2012, doi: 10.1093/bja/aes001.

[245] K. El Emam, L. Mosquera, and J. Bass, “Evaluating Identity Disclosure Risk in Fully Synthetic Health Data: Model Development and Validation,” *J. Med. Internet Res.*, vol. 22, no. 11, p. e23139, Nov. 2020, doi: 10.2196/23139.

[246] M. Jacob Rodrigues, O. Postolache, and F. Cercas, “Physiological and Behavior Monitoring Systems for Smart Healthcare Environments: A Review,” *Sensors*, vol. 20, no. 8, p. 2186, Apr. 2020, doi: 10.3390/s20082186.

[247] M. Jacob Rodrigues, O. Postolache, and F. Cercas, “Indoor Air Quality Monitoring System to Prevent the Triggering of Respiratory Distress,” in *2019 International Conference on Sensing and Instrumentation in IoT Era (ISSI)*, Aug. 2019, pp. 1–6. doi: 10.1109/ISSI47111.2019.9043669.

[248] J. Araujo, M. J. Rodrigues, O. Postolache, F. Cercas, F. F. Martín, and A. L. Martínez, “Heart Rate Variability Analysis in Healthy Subjects Under Different Colored Lighting Conditions,” in *2020 IEEE International Instrumentation and Measurement Technology Conference (I2MTC)*, May 2020, pp. 1–5. doi: 10.1109/I2MTC43012.2020.9129619.

[249] A. Linnemann, B. Ditzen, J. Strahler, J. M. Doerr, and U. M. Nater, “Music listening as a means of stress reduction in daily life,” *Psychoneuroendocrinology*, vol. 60, pp. 82–90, Oct. 2015, doi: 10.1016/j.psyneuen.2015.06.008.

[250] M. Hedblom *et al.*, “Reduction of physiological stress by urban green space in a multisensory virtual experiment,” *Sci. Rep.*, vol. 9, no. 1, p. 10113, Dec. 2019, doi: 10.1038/s41598-019-46099-7.

[251] H. Mojtabavi, A. Saghazadeh, V. E. Valenti, and N. Rezaei, “Can music influence cardiac autonomic system? A systematic review and narrative synthesis to evaluate its impact on heart rate variability,” *Complement. Ther. Clin. Pract.*, vol. 39, p. 101162, May 2020, doi: 10.1016/j.ctcp.2020.101162.

[252] E. Won and Y.-K. Kim, “Stress, the Autonomic Nervous System, and the Immune-kynurenine Pathway in the Etiology of Depression,” *Curr. Neuropharmacol.*, vol. 14, no. 7, pp. 665–673, Aug. 2016, doi: 10.2174/1570159X14666151208113006.

[253] L. K. McCorry, “Physiology of the Autonomic Nervous System,” *Am. J. Pharm. Educ.*, vol. 71, no. 4, p. 78, Sep. 2007, doi: 10.5688/aj710478.

[254]“Exposure of Europe’s population to environmental noise.” https://www.eea.europa.eu/ims/exposure-of-europe2019s-population-to (accessed Sep. 24, 2022).

[255] T. Carruthers, “Health effects of environmental noise pollution,” *Curious*, Nov. 30, 2017. https://www.science.org.au/curious/earth-environment/health-effects-environmental-noise-pollution (accessed Sep. 24, 2022).

[256] W. B. Davis, K. E. Gfeller, and M. Thaut, *An introduction to music therapy: theory and practice*, 3rd ed. Silver Spring, Md: American Music Therapy Association, 2008.

[257] G. Lu, F. Yang, J. A. Taylor, and J. F. Stein, “A comparison of photoplethysmography and ECG recording to analyse heart rate variability in healthy subjects,” *J. Med. Eng. Technol.*, vol. 33, no. 8, pp. 634–641, Nov. 2009, doi: 10.3109/03091900903150998.

[258] N. Selvaraj, A. Jaryal, J. Santhosh, K. K. Deepak, and S. Anand, “Assessment of heart rate variability derived from finger-tip photoplethysmography as compared to electrocardiography,” *J. Med. Eng. Technol.*, vol. 32, no. 6, pp. 479–484, Jan. 2008, doi: 10.1080/03091900701781317.

[259] “Relaxing Music with Nature Sounds - Waterfall HD - YouTube.” https://youtu.be/lE6RYpe9IT0 (accessed Sep. 24, 2022).

[260] M. J. Rodrigues, O. Postolache, and F. Cercas, “The Influence of Music Stimulation on Heart Rate Variability: Preliminary Results,” in *2022 IEEE International Symposium on Medical Measurements and Applications (MeMeA)*, Messina, Italy: IEEE, Jun. 2022, pp. 1–6. doi: 10.1109/MeMeA54994.2022.9856561.

[261] M.-C. Chiu and L.-W. Ko, “Develop a personalized intelligent music selection system based on heart rate variability and machine learning,” *Multimed. Tools Appl.*, vol. 76, no. 14, pp. 15607–15639, Jul. 2017, doi: 10.1007/s11042-016-3860-x.

[262] O. Postolache *et al.*, “Tailored Virtual Reality for Smart Physiotherapy,” in *2019 11th International Symposium on Advanced Topics in Electrical Engineering (ATEE)*, Bucharest, Romania: IEEE, Mar. 2019, pp. 1–6. doi: 10.1109/ATEE.2019.8724903.

[263] M. Malik, “Heart Rate Variability.: Standards of Measurement, Physiological Interpretation, and Clinical Use: Task Force of The European Society of Cardiology and the North American Society for Pacing and Electrophysiology,” *Ann. Noninvasive Electrocardiol.*, vol. 1, no. 2, pp. 151–181, Apr. 1996, doi: 10.1111/j.1542-474X.1996.tb00275.x.

[264] P. van Gent, H. Farah, N. van Nes, and B. van Arem, “HeartPy: A novel heart rate algorithm for the analysis of noisy signals,” *Transp. Res. Part F Traffic Psychol. Behav.*, vol. 66, pp. 368–378, Oct. 2019, doi: 10.1016/j.trf.2019.09.015.

[265] M. P. Tarvainen, J.-P. Niskanen, J. A. Lipponen, P. O. Ranta-aho, and P. A. Karjalainen, “Kubios HRV – Heart rate variability analysis software,” *Comput. Methods Programs Biomed.*, vol. 113, no. 1, pp. 210–220, Jan. 2014, doi: 10.1016/j.cmpb.2013.07.024.

[266] X. Wang, J. Ellul, and G. Azzopardi, “Elderly Fall Detection Systems: A Literature Survey,” *Front. Robot. AI*, vol. 7, p. 71, Jun. 2020, doi: 10.3389/frobt.2020.00071.
[267] A. Avci, S. Bosch, M. Marin-Perianu, R. Marin-Perianu, and P. Havinga, “Activity Recognition Using Inertial Sensing for Healthcare, Wellbeing and Sports Applications: A Survey,” in *23th International Conference on Architecture of Computing Systems 2010*, Feb. 2010, pp. 1–10.
[268] O. Steven Eyobu and D. Han, “Feature Representation and Data Augmentation for Human Activity Classification Based on Wearable IMU Sensor Data Using a Deep LSTM Neural Network,” *Sensors*, vol. 18, no. 9, p. 2892, Aug. 2018, doi: 10.3390/s18092892.
[269] V. K. Sinha, K. K. Patro, P. Pławiak, and A. J. Prakash, “Smartphone-Based Human Sitting Behaviors Recognition Using Inertial Sensor,” *Sensors*, vol. 21, no. 19, p. 6652, Oct. 2021, doi: 10.3390/s21196652.
[270] A. Leone, G. Rescio, A. Caroppo, P. Siciliano, and A. Manni, “Human Postures Recognition by Accelerometer Sensor and ML Architecture Integrated in Embedded Platforms: Benchmarking and Performance Evaluation,” *Sensors*, vol. 23, no. 2, p. 1039, Jan. 2023, doi: 10.3390/s23021039.
[271] “Pozyx | Multi Technology RTLS - Indoor & Outdoor.” https://www.pozyx.io/ (accessed Mar. 12, 2023).
[272]“3.2. Tuning the hyper-parameters of an estimator,” *scikit-learn*. https://scikit-learn/stable/modules/grid_search.html (accessed Mar. 14, 2023).
[273] H. Sak, A. Senior, and F. Beaufays, “Long Short-Term Memory Based Recurrent Neural Network Architectures for Large Vocabulary Speech Recognition,” 2014, doi: 10.48550/ARXIV.1402.1128.